

AD-A085 847

AIRSEARCH MFG CO OF CALIFORNIA TORRANCE
ELECTROMECHANICAL ACTUATION DEVELOPMENT.(U)

P/O 1/6

FEB 80 R A LEVIE, J GRAY, N E WOOD
80-16763

F33615-76-C-3043

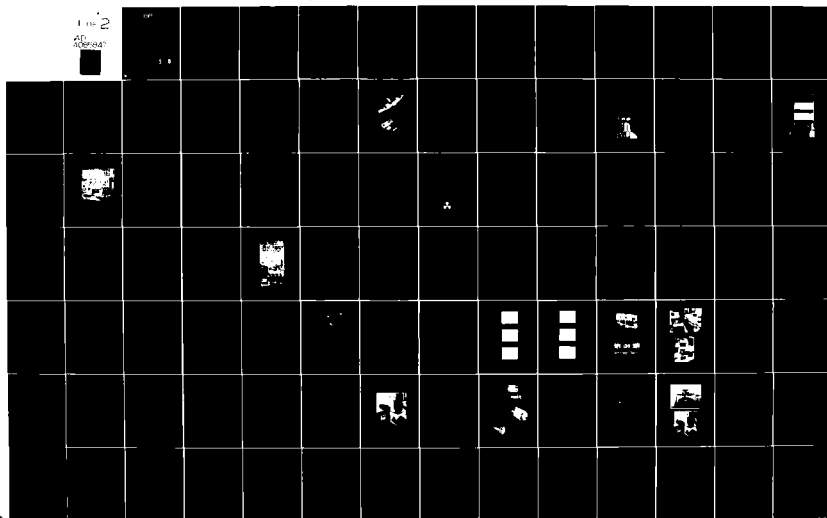
UNCLASSIFIED

AFWAL-TR-80-3024

ML

FIG 2

AD-A085 847



ADA 085847

LEVEL III

AFWAL-TR-80-3024

A065734

SC (2)

ELECTROMECHANICAL ACTUATION DEVELOPMENT

AiResearch Manufacturing Company of California
2525 W. 190th Street
Torrance, California 90509

February 1980

Final Report for period September 1978 - December 1979

Approved for public release
Distribution unlimited

DTIC
ELECTE
JUN 19 1980
S D E

Prepared for
Flight Dynamics Laboratory
Air Force Wright Aeronautical Laboratories
Air Force Systems Command
Wright-Patterson Air Force Base, Ohio 45433

80 6 19 125

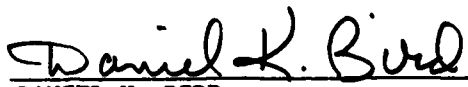
DOC FILE COPY

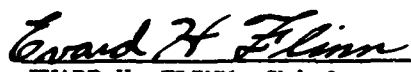
NOTICE

When Government drawings, specifications, or other data are used for any purpose other than in connection with a definitely related Government procurement operation, the United States Government thereby incurs no responsibility nor any obligation whatsoever; and the fact that the government may have formulated, furnished, or in any way supplied the said drawings, specifications, or other data, is not to be regarded by implication or otherwise as in any manner licensing the holder or any other person or corporation, or conveying any rights or permission to manufacture use, or sell any patented invention that may in any way be related thereto.


This report has been reviewed by the Office of Public Affairs (ASD/PA) and is releasable to the National Technical Information Service (NTIS). At NTIS, it will be available to the general public, including foreign nations.

This technical report has been reviewed and is approved for publication.


DANIEL K. BIRD
Project Engineer


EVARH H. FLINN, Chief
Control Systems Development Branch
Flight Control Division

FOR THE COMMANDER


RONALD O. ANDERSON
Acting Asst for Research & Technology
Flight Control Division

"If your address has changed, if you wish to be removed from our mailing list, or if the addressee is no longer employed by your organization please notify AFWAL/FIGL, W-PAFB, OH 45433 to help us maintain a current mailing list".

Copies of this report should not be returned unless return is required by security considerations, contractual obligations, or notice on a specific document.

SECURITY CLASSIFICATION OF THIS PAGE (When Data Entered)

19 REPORT DOCUMENTATION PAGE		READ INSTRUCTIONS BEFORE COMPLETING FORM	
1. REPORT NUMBER (18) AFWAL-TR-80-3024	2. GOVT ACCESSION NO. AD-A085847	3. RECIPIENT'S CATALOG NUMBER	
4. TITLE (and Subtitle) (6) ELECTROMECHANICAL ACTUATION DEVELOPMENT		5. TYPE OF REPORT & PERIOD COVERED FINAL REPORT 9/78 to 12/79	
7. AUTHOR(s) (10) ROBERT A. LEWIS, JOHN GRAY, NEAL E. WOOD		8. PERFORMING ORG. REPORT NUMBER (14) 80-16763	9. CONTRACT OR GRANT NUMBER(s) (15) F33615-76-C-3043 AMENDMENT 1
9. PERFORMING ORGANIZATION NAME AND ADDRESS AiResearch Manufacturing Company, A Division of The Garrett Corporation, 2525 W. 190th St., Torrance, California 90509		10. PROGRAM ELEMENT, PROJECT, TASK AREA & WORK UNIT NUMBERS	
11. CONTROLLING OFFICE NAME AND ADDRESS AIR FORCE WRIGHT AERONAUTICAL LABORATORIES UNITED STATES AIR FORCE WRIGHT-PATTERSON AFB, OHIO 45433		12. REPORT DATE (11) Feb 1980	13. NUMBER OF PAGES 107
14. MONITORING AGENCY NAME & ADDRESS (if different from Controlling Office) (12) 119		15. SECURITY CLASS (of this report) Unclassified	
16. DISTRIBUTION STATEMENT (of this Report) Approved for public release; distribution unlimited. (9) Final rept. 20 Sep 78 - 15 Dec 79			
17. DISTRIBUTION STATEMENT (of the abstract entered in Block 20, if different from Report)			
18. SUPPLEMENTARY NOTES			
19. KEY WORDS (Continue on reverse side if necessary and identify by block number) Power-by-wire Rare earth samarium Fly-by-wire Brushless dc motor 270-vdc high power control Permanent magnet rotor Pulse width modulation Cobalt magnets			
20. ABSTRACT (Continue on reverse side if necessary and identify by block number) Electromechanical actuation of primary flight control surfaces has been demonstrated by the development of an integrated rotary hinge-line dual-redundant actuation unit. The controller power level of 30 amp at 270 vdc was demonstrated. Thermal characteristics of the motor and actuator were evaluated at ambient temperatures ranging from -65°F to 250°F.			

DD FORM 1473 EDITION OF 1 NOV 68 IS OBSOLETE

SECURITY CLASSIFICATION OF THIS PAGE (When Data Entered)

327343

PREFACE

This report was prepared by AiResearch Manufacturing Company of California, a division of The Garrett Corporation, for the Air Force Wright Aeronautical Laboratories, Wright-Patterson Air Force Base, under Amendment 1 to Contract F33615-76-C-3043, Integrated Hinge (Rotary) Electromechanical Actuation Development. The final report (AFFDL-TR-78-150) presented the results of the design, fabrication, and laboratory test of an electromechanical actuation unit developed under the basic contract. This report documents the additional effort authorized by the amendment, which was to extend the data base of electromechanical actuation by performing temperature environmental tests on the unit, and to increase the power output level of the controller to 30 amp at 270 vdc. The technical effort was performed from September 20, 1978 to December 15, 1979 by the AiResearch mechanical power systems product line, with Mr. Neal Wood as principal investigator. Mr. Daniel K. Bird (FGL), the Air Force technical monitor for the program, provided direction, technical support, and discussion on actuation principles.

Although many individuals have made significant contributions to the organization and content of this report, the efforts of several key personnel merit special recognition. E. F. Echolds was responsible for the development of the electric powered servomotor; J. Ashmore, J. Cleek, J. Gray, and W. Beck were responsible for the electronic design and breadboard controller power uprating; M. Yang provided specialized technical support in the development of the computerized thermal simulation program and analysis of the motor and actuator characteristics in various environments; and S. Rowe provided technical support with the duty cycle evaluation analysis.

Accession For	
NTIS GRA&I	<input checked="checked" type="checkbox"/>
DDC TAB	<input type="checkbox"/>
Unannounced	<input type="checkbox"/>
Justification	
By _____	
Distribution/	
Availability Codes	
Dist	Avail and/or special
A	

CONTENTS

<u>Section</u>	<u>Page</u>
1. INTRODUCTION AND SUMMARY	1
1.1 Program Objective and Scope	2
1.2 Program Technical Summary	3
1.3 Test Summary	5
2. TECHNICAL APPROACH	6
2.1 Actuation Unit Description	6
2.2 Actuator	7
3. CONTROLLER DESIGN IMPROVEMENT	14
3.1 Design of the Original Controller	14
3.2 Controller Modification and Improvements	35
3.3 New Power Switch Design	47
4. DETAILED ANALYSES	56
4.1 Thermal Prediction	56
4.2 Mission Duty Cycle Determination	60
4.3 Figure of Merit Determination	62
5. TEST EQUIPMENT	63
5.1 Special Test Equipment and Fixtures	63
5.2 Facilities	65
6. TESTING	67
6.1 Extended Temperature Test	67
6.2 Extended Current Limit Test	70
6.3 Power Supply Voltage Variation Test	70
6.4 Motor/Actuator Duty Cycle Capability Test	70
7. TEST RESULTS	74
7.1 Frequency Response Test	74
7.2 Extended Current Limit Test	74
7.3 Power Supply Voltage Variation Test	74
7.4 Thermal Evaluation	77
	79

CONTENTS (Continued)

<u>Section</u>	<u>Page</u>
8. CONCLUSIONS AND RECOMMENDATIONS	84
9. REFERENCES	86
<u>Appendix</u>	
ACTUATOR DUTY CYCLE EVALUATION ALGORITHMS	88

ILLUSTRATIONS

<u>Figure</u>		<u>Page</u>
1	Electromechanical Actuation Unit Block Diagram	1
2	Program Task Definition	3
3	Program Schedule	4
4	Actuation Unit	6
5	Hingeline Actuator Motors	8
6	Rare-Earth Permanent Magnet Motor Parts	8
7	Motor Performance	9
8	Actual and Predicted Motor Performance Comparison	11
9	Hingeline Actuator Gearing Components	12
10	Control Console Breadboard Configuration	15
11	Voltage Control Servo Breadboard	17
12	Position Error and Compensation Amplifiers, Pulse-Width Modulators, and Direction Sense Circuitry	18
13	Pulse-Width-Modulation Idealized Timing Diagram	19
14	Triangle Wave Generator	20
15	Triangle Waveform	20
16	Surface Position Decoding Circuitry	21
17	Rotor Position Outputs	23
18	Motor Rotor Position Detection Circuitry	24
19	Sequence, Control, and Inhibit Logic	25
20	Sequencer Timing Diagrams	27
21	Schematic of Driver Switches	28
22	Typical Turnoff Locus	29
23	Current Limit Circuitry	30

ILLUSTRATIONS (Continued)

<u>Figure</u>		<u>Page</u>
24	Power Supply	32
25	Tachometer Feedback Control Block Diagram	33
26	Tachometer Feedback Servo Control Breadboard	34
27	Tachometer Control Circuitry	35
28	Rotor Speed Detection Circuit	36
29	Rotor Detection Circuit	37
30	Controller Block Diagram	39
31	Control Circuitry	41
32	Triangle Wave Generator	42
33	Baseline Control Current Limit Waveforms	42
34	Typical Current Waveforms for Improved Controller in Current Limit	43
35	Sequence, Control, and Inhibit Logic	44
36	Current Limit Forward and Plug Reverse	45
37	Power Switch Circuitry	47
38	Surface Position Sensing Circuit	48
39	Transistor Comparison	49
40	Power Transistor Current and Voltage Waveform	51
41	Transition of Top Transistor, B Phase, 10 Amp per Division	52
42	Transition of Bottom Transistor, B Phase, 10 Amp per Division	53
43	Power Switch Unit, Side View	54
44	Power Switch Unit, Front View	54

ILLUSTRATIONS (Continued)

<u>Figure</u>		<u>Page</u>
45	Power Switch Assembly, During Checkout	55
46	Two-Channel, Rack-Mounted Controller Breadboard	55
47	Actuator Motor Thermal Model	56
48	Rotor Thermal Model	57
49	Simplified Thermal Model of Gearbox	57
50	Motor Stator Windings Thermal Model for Transient Analysis	58
51	Predicted Hot Spot Motor Winding Temperatures for Hingeline Actuator Motor (Node 10)	59
52	Predicted Hot Spot Motor Winding Temperatures for Hingeline Actuator Motor (Node 10)	60
53	Load Spectrum for Full Time Maneuvering Leading Edge Systems	61
54	Block Diagram of the Power Supply	63
55	Thermal Chamber	64
56	Arrangement of Thermal Instrumentation	65
57	Thermal Instrumentation Placement	66
58	Detail Placement Views	66
59	Extended Temperature Test	68
60	Actuator Installed in Environmental Enclosure	69
61	Actuator During Temperature Testing	69
62	Extended Current Limit Test	71
63	Power Supply Voltage Variation Test	72
64	Motor/Actuator Duty Cycle Capability Test	73
65	Frequency Response Temperature Comparison, Full Gain	75
66	Frequency Response Temperature Comparison, Half Gain	75

ILLUSTRATIONS (Continued)

<u>Figure</u>		<u>Page</u>
67	Frequency Response Temperature Comparison, Half Gain, 20 Percent Load	76
68	Frequency Response Temperature Comparison, Half Gain, 10 Percent Load	76
69	Frequency Response Current Limit Comparison, Half Gain, No Load	77
70	Temperature Profile Motor Hot Spot	80
71	Data Comparison Between Predicted Hot Spot Motor Winding Temperatures and Hingeline Actuator Motor Winding Temperatures	80
72	Motor Winding and Motor Brake Coil Temperature Profile, 250°F Ambient	81
73	Motor Winding and Motor Brake Coil Temperature Profile, -65°F Ambient	82

TABLES

<u>Table</u>		<u>Page</u>
1	Motor Characteristics	10
2	Summary of Controller Improvements	40
3	Power Loss for WPAFB Hingeline Actuator Motor Thermal Analysis	59
4	Actuator Response Summary for 2 Hz	78
5	Actuator Response Summary for 4 Hz	78
6	Nodal Temperature Profiles	83

1. INTRODUCTION AND SUMMARY

This final report presents the results of a design and testing effort that was devoted to strengthening the evaluation data base of electromechanical actuation for primary flight control. The effort described herein is authorized through an amendment to Air Force Contract F33615-76-C-3043, which sponsored the design and development of an electromechanical actuation system for aircraft primary flight control. The original contract (F33615-76-C-3043) is described in Air Force document AFFDL-TR-78-150, Electromechanical Actuation Development, dated December 1978.

The amended program was based upon the electromechanical actuation unit baseline shown schematically in Figure 1. This unit, developed and evaluated under the original contract, provides dual redundancy in the electronic control, motor drive, and mechanical elements. The actuator was designed to be in a flight configuration to illustrate hingeline structural interface capability, thermal management considerations, and servo feedback mounting and design considerations. The controller was fabricated as an engineering breadboard with two separate, rack-mounted servocircuits and power switch assemblies. This arrangement provided maximum flexibility to incorporate design improvements. Major actuation unit features are described on the following page.

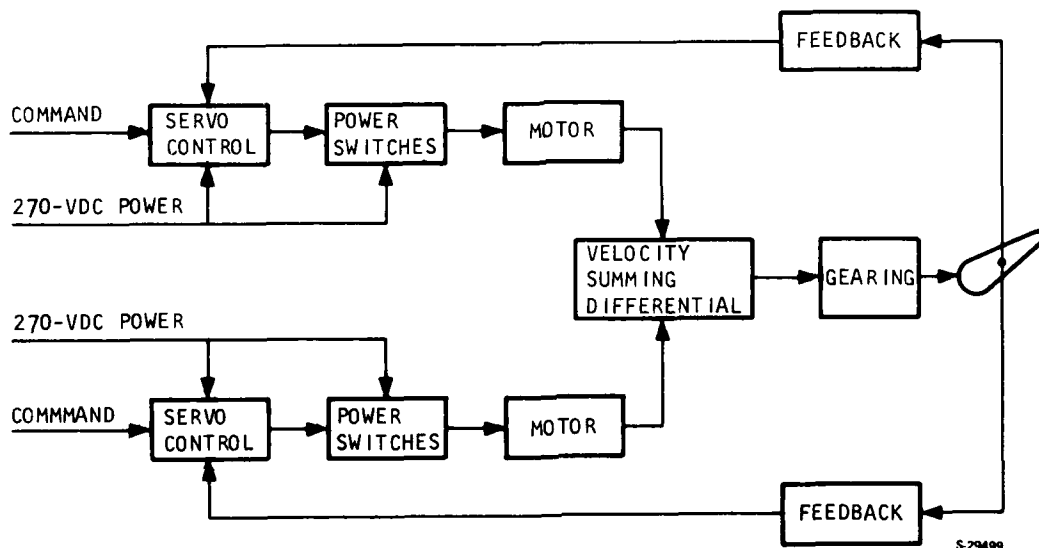


Figure 1. Electromechanical Actuation Unit Block Diagram

- (a) Closed-loop position servo circuits were implemented using both analog and digital techniques to demonstrate versatility for interfacing with various aircraft flight control systems. Optical, digital encoders, and analog potentiometers were used to monitor control surface position and are used in the servo feedback loop. Transistorized electric power switch circuits provides motor torque-rate and commutation control.
- (b) Permanent-magnet, 270-vdc motors using brushless commutation and rare-earth cobalt magnets in the rotor assembly are used to achieve high acceleration and torque in minimum space and weight. Samarium cobalt and other high-energy, rare-earth-magnet materials are being used to reduce servomotor size and weight while maintaining high performance output. As a result, dc electric motors are competitive with the hydraulic motors used in primary flight control systems. The selection of 270-vdc power was based upon rectification of a standard 115/200-v, 400-Hz aircraft power source.
- (c) Torque multiplication and speed reduction are accomplished through a rotary hingeline actuator that implements dual redundant drive channels, using a velocity summing planetary differential and planetary gear stages to the rotary output. The rotary actuator gear ratio matches the torque and speed requirements of the control surface to the motor output. Improved materials and manufacturing processes make use of high-strength alloys to achieve high fatigue strength, high stiffness, and loss of producibility.

This hardware has demonstrated the capability of using low-level electric signals (fly-by-wire) to control high-power electrical servomotors (power-by-wire). Previous testing was limited to a laboratory demonstration of capability and versatility at room temperature. The following tests were performed under the basic contract:

- Component acceptance and functional testing
- Mechanical and electrical interface compatibility verification
- System performance (frequency response, dynamic stiffness, velocity, position resolution, and efficiency)
- System demonstration (reliability redundancy management)

1.1 PROGRAM OBJECTIVE AND SCOPE

The design and testing effort described in this report was conducted by AiResearch Manufacturing Company of California under an amendment to USAF Contract F33615-76-C-3043 to further evaluate the unit designed for application as an aircraft primary flight control. The program objective is to supply additional performance information for final evaluation of the hardware demonstration unit in the following areas of operation:

- Temperature extremes
- Increased current limit

- Low supply voltage
- Various duty cycles

To accomplish these objectives, the program has been divided into five discrete tasks as shown in Figure 2.

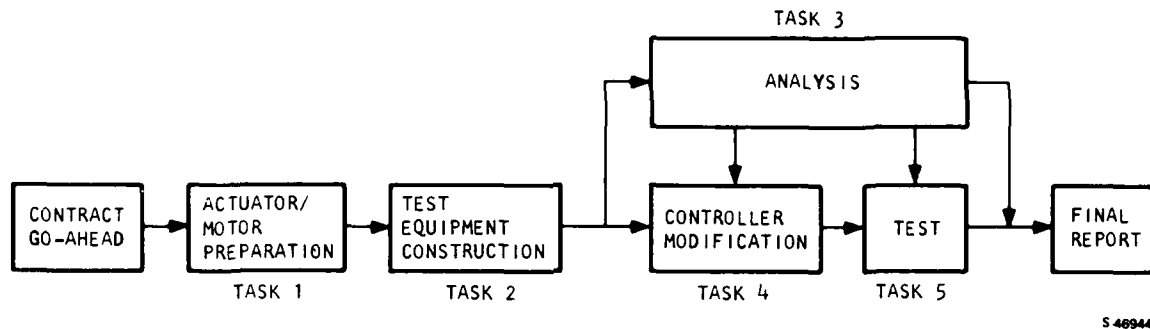
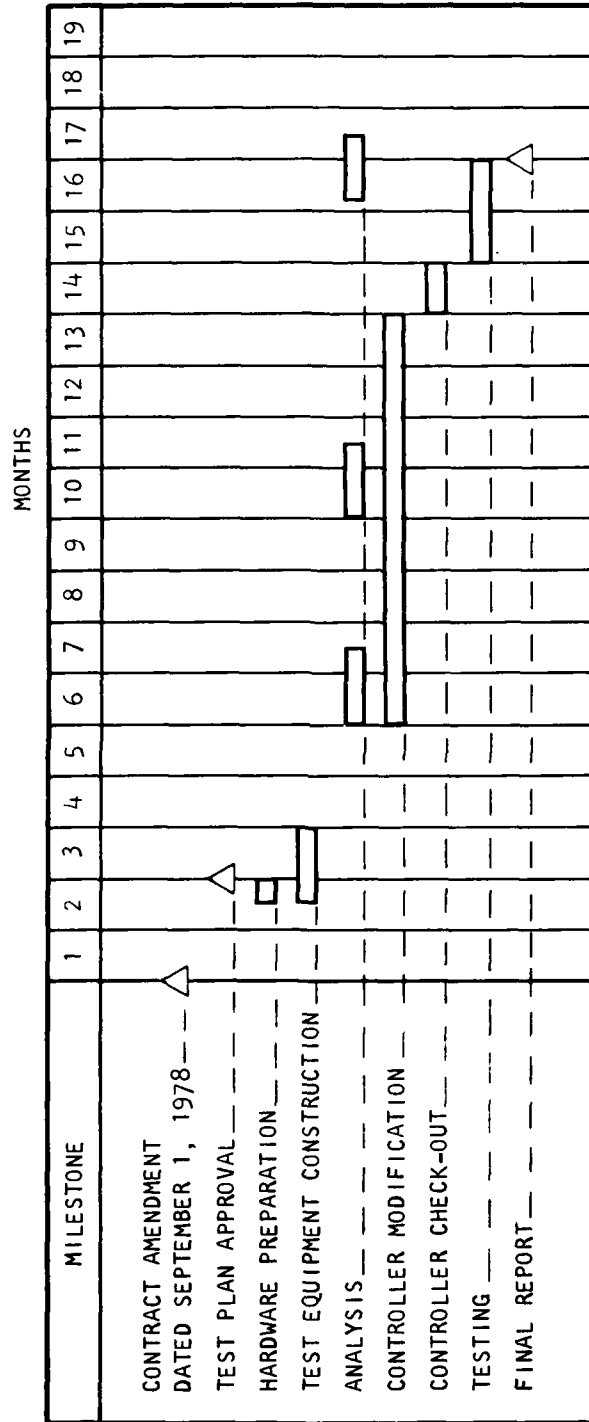


Figure 2. Program Task Definition

1.2 PROGRAM TECHNICAL SUMMARY

AiResearch Manufacturing Company of California was awarded a contract in 1976 for the design, development, fabrication, and limited test of an electro-mechanical actuation unit for aircraft primary flight controls. This program was successfully completed at the beginning of 1979.

It was then recognized that there was a need to further strengthen the data base of electromechanical actuation. On September 1, 1978, the contract was amended to include (1) a substantial increase of the current applied to the motors, and (2) a comprehensive test program. This amendment is the subject of this report. The schedule for this amended program is presented in Figure 3.



S-46914

Figure 3. Program Schedule

1.3 TEST SUMMARY

The testing effort covered by this amendment was divided into four discrete areas. The significant results of these tests are summarized as follows:

- Extended Temperature Test--Performance of the actuation unit was essentially unaffected over an ambient temperature range of -65°F to $+250^{\circ}\text{F}$.
- Increased Current Limit Test--The inverter current limit can easily be adjusted to any value. This feature makes the actuation unit extremely versatile since it can be tailored to any particular application requiring up to 30-amp current per motor.
- Voltage Variation--Significant reduction in line voltage has a minimal effect on actuation unit performance at frequencies up to 4 Hz.
- Temperature Evaluation--Correlation of test data and analysis has verified the thermal model, which is now available as a valuable analytical tool.

2. TECHNICAL APPROACH

The amended contract effort to demonstrate the power uprating of the solid-state power controller was based on the use of the motors and actuator that were previously developed.

This section presents a brief summary of the hardware characteristics as fabricated and tested during the original contract effort. It also describes any modifications or improvements to the mechanical hardware that were deemed necessary to support evaluation of the controller.

2.1 ACTUATION UNIT DESCRIPTION

The actuation unit consists of two controllers, two motors, an actuator, and an output position feedback. The arrangement of these elements is shown in Figure 4.

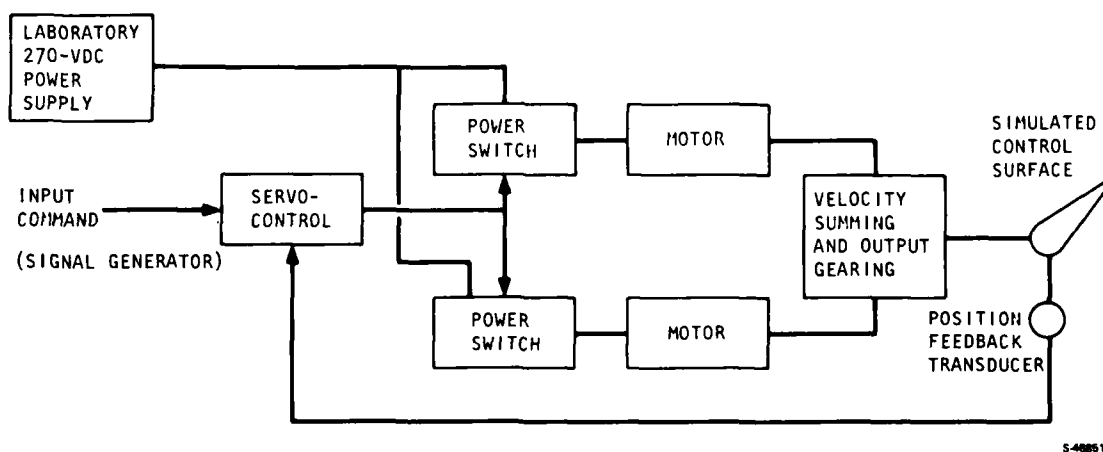


Figure 4. Actuation Unit

The arrangement of elements remained unchanged during the contract amendment, although the mechanization of the power switch, servocontrol, and selection of the position feedback transducer was changed. The background of each of the principal components is presented in the following text.

2.2 ACTUATOR

The actuator shown in Figure 5 is comprised of two motors operating into a velocity summing differential, the output of which drives a planetary geared output with structural attachments, all of which serves as a rotary hinge for the control surface. The gearing assembly serves as the structural mounting for the two redundant motors and as the structural interface between the control surface and mating aircraft structure.

2.2.1 Motor Description

The motor in an electromechanical actuation unit functions to convert electrical current and voltage to mechanical torque. The assembled permanent-magnet rotor, which consists of high-energy-density, samarium cobalt magnets, arranged in a 6-pole configuration, allows high-speed operation with low rotor inertia.

The wound stator (see Figure 6) is designed with a large copper cross-section to provide low electrical losses (I^2R), high current, and high torque capabilities. Improved thermal control of the motor is a result of winding locations in the stator. Heating that occurs in the windings can be easily transferred to the finned motor housing.

The motor assembly includes a rotor shaft position sensor. Commutation (putting current in the proper direction through the stator windings) is accomplished by using variable reluctance pickups. The rotor position information is input to the controller switching network to develop the commutation logic.

A parking brake is included as a part of the motor. Its only purpose within the present configuration is to lock a failed drive channel. Without this lock, the operating motor could back-drive the failed motor through the high efficiency differential gearing.

2.2.2 Motor Performance

The motor, which was unchanged from the original contract effort, was mounted in a laboratory dynamometer. The improved (30 amp) controller assembly was connected to it to drive as a motor in both the clockwise and counter clockwise direction. Figure 7 shows the relationship of motor speed, torque, and the input motor current. One important characteristic is shown in this figure; a nonlinear torque speed curve. For current levels up to approximately 20 amps, the torque speed relationship is linear as expected. At current levels of above 20 amp, the speed drops off as torque increases.

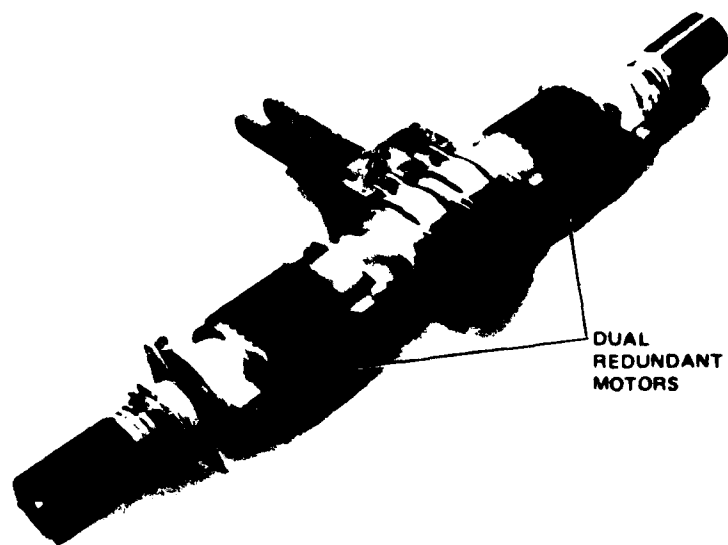


Figure 5. Hingeline Actuator Motors

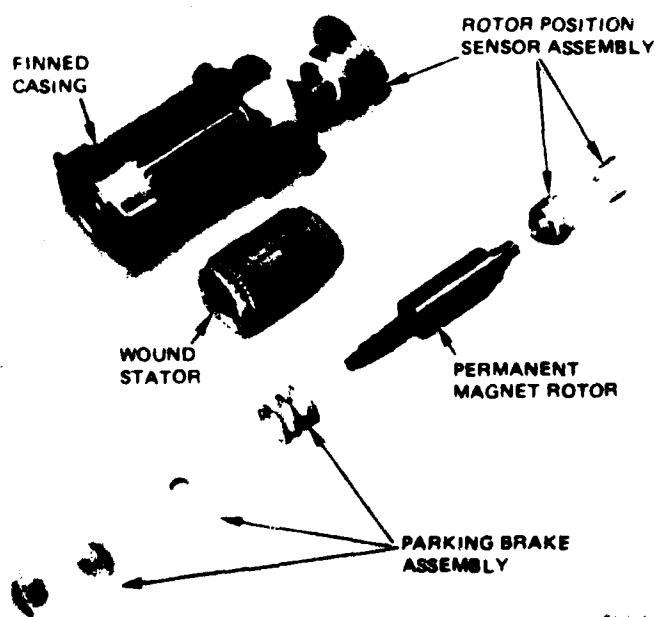


Figure 6. Rare-Earth Permanent Magnet Motor Parts

F-31362

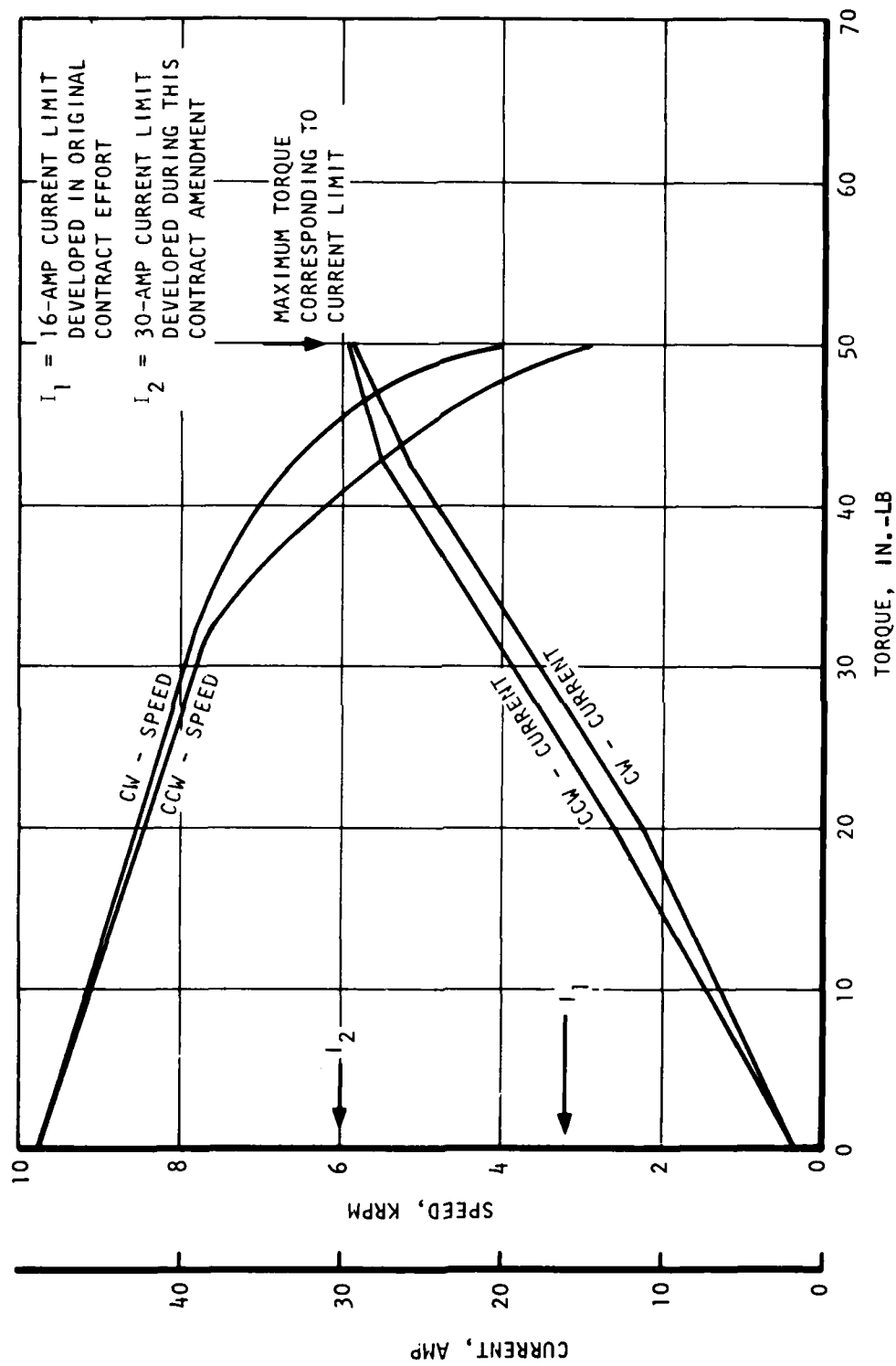
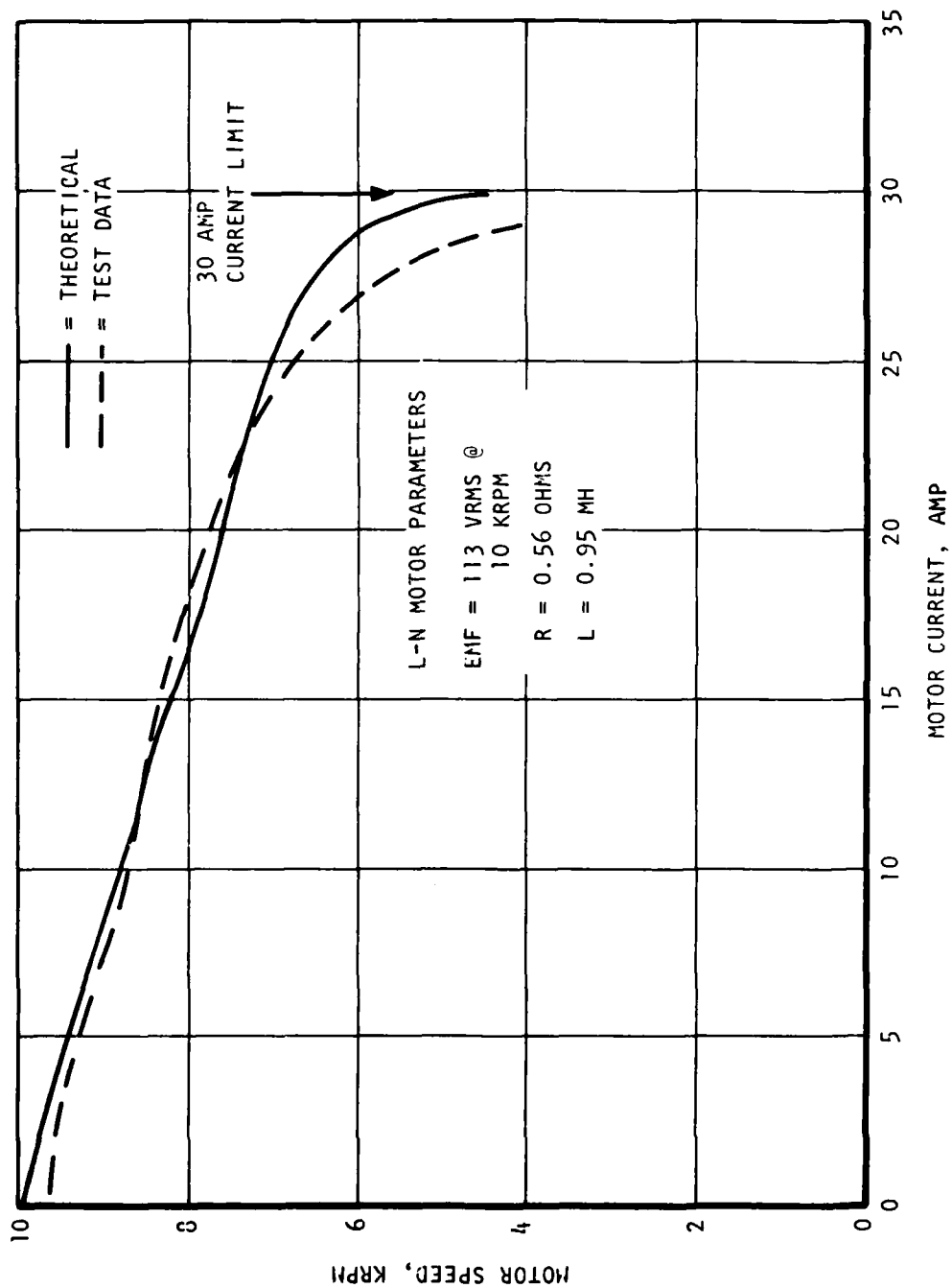


Figure 7. Motor Performance

An analysis was initiated to determine the reason for this effect. The motor had originally been designed to operate at 16 amp and to exhibit a linear relationship of torque to speed. The nonlinear torque speed plot was judged to be related to the increase in current and the inductance of the motor windings. Using the motor characteristics shown in Table 1, the analysis was conducted on an AiResearch computer program to develop the maximum motor performance at current levels of 30 amp as opposed to the original design value of 16 amp. Figure 8 shows the results of the analytical prediction of motor performance compared to the test data. The correlation is good. This figure shows that the motor can operate at stall (30 amp limit) current for speeds of 0 to approximately 3500 rpm. At that speed, the back emf, in combination with the stator winding inductance, begins to reduce the amount of current that can be forced into the windings from the available line voltage supply. A smooth transition is experienced to the point of 8000 rpm and 20 amp, where the torque-speed-current relationships become linear and remain linear up to full speed.

TABLE 1
MOTOR CHARACTERISTICS

Rated voltage	265 vdc
No-load speed	9600
Stator resistance (68°F)	0.74 ohm (line to line)
Rotor inertia	9.95×10^{-4} lbf-in.-sec ²
Time constants	0.002 sec, electrical 0.015 sec, mechanical
Back emf	28.13 per 1000 rpm
Brake voltage	270 vdc
Brake torque	75 lbf-in. (minimum)
Weight	9.65 lb



S-46852

Figure 8. Actual and Predicted Motor Performance Comparison

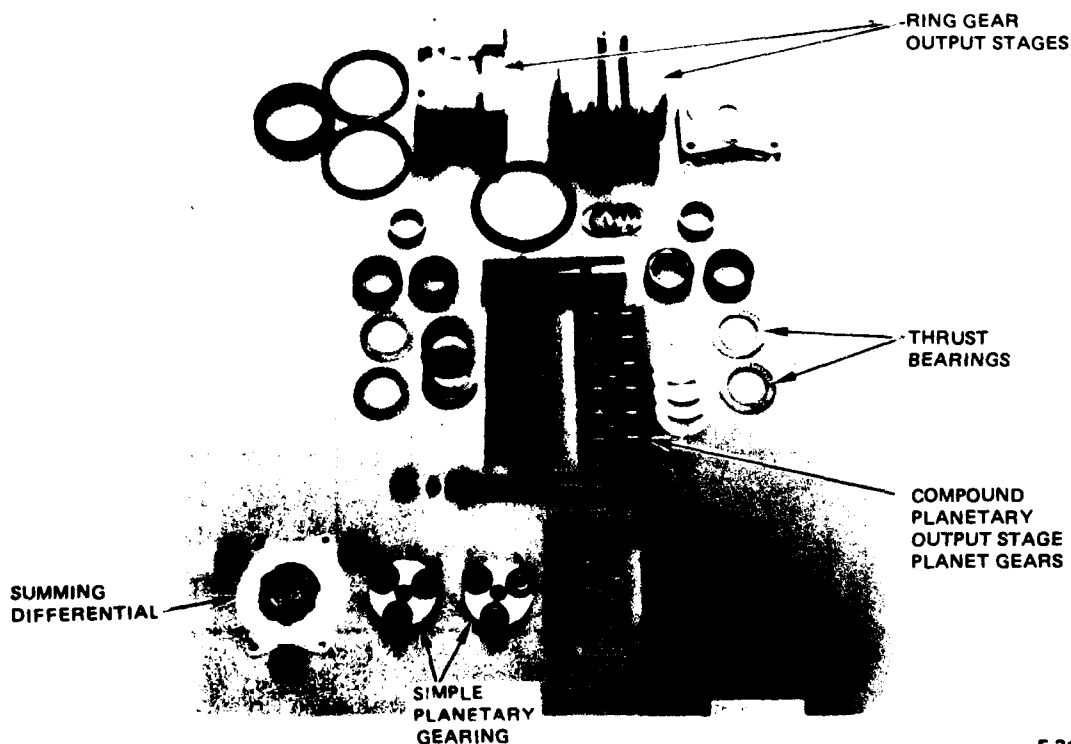
2.2.3 Actuator Gearing

The actuator gearbox design was based upon contract and program ground rules representative of future aircraft actuation system requirements. The following list of parameters formed the basis of the gearbox design:

- Rotary hingeline design
- 4 in. depth
- 37,575 in.-lb maximum hinge moment torque
- 80 deg/sec no-load rate

The dual redundant motors operate into the velocity summing differential (Figure 9), followed by two stages of simple planetary reduction. The output of the second stage operates into the compound planetary gearset, which consists of two identical load sharing slices.

For this contract amendment, the gearing was used without modification. The exterior of the actuator was cleaned and painted to prevent corrosion during repeated temperature cycling. The actuator was painted with baked on FP73 B04 gloss white paint, which has sufficient properties to adequately protect the exterior of the actuator throughout the testing effort.



F-31363

Figure 9. Hingeline Actuator Gearing Components

2.2.4 Position Feedback

Two control surface position feedback transducers were demonstrated under the original contract testing. A digital, optical encoder was used to provide direct interfacing with the early microprocessor controller. Later, a rotary potentiometer was used to simplify interfacing with an analog servocontrol. No actuator performance difference could be identified when switching from one transducer to the other.

For this test program, the rotary potentiometer was used due to the simplicity of interfacing with the analog servo circuits.

2.2.5 Controller

The major part of the amended contract effort was in the design, bread-board fabrication, and performance verification of the high power controller. Because of the extensive nature of this activity, Section 3 describes (1) the original controller circuits as a baseline, and (2) the modified and new controller circuits.

3. CONTROLLER DESIGN IMPROVEMENT

The major effort of this amendment was centered on design improvements in the power servo control area. The improvements were required for two reasons: (1) to increase the controlled output power, and (2) to simplify and redesign specific circuits and functions.

To accommodate the increase in output power, new higher-power solid-state switching devices were considered. After selection of the power switch, specific drive circuits were designed, tested, and integrated into the existing controller breadboard. During fabrication of the uprated breadboard, some circuitry was found to be marginal or obsolete because of modifications made in the power switch section. These circuits were then redesigned or eliminated as necessary.

This section details the method by which the controller current limit was increased by a factor of approximately four, from an average of 8 amps to an average of 30 amps. The material is organized in two parts: (1) the design of the controller developed under the original contract (the discussion serves as a baseline for part two), and (2) the modifications and improvements to the power servo controller that were made under the amended contract.

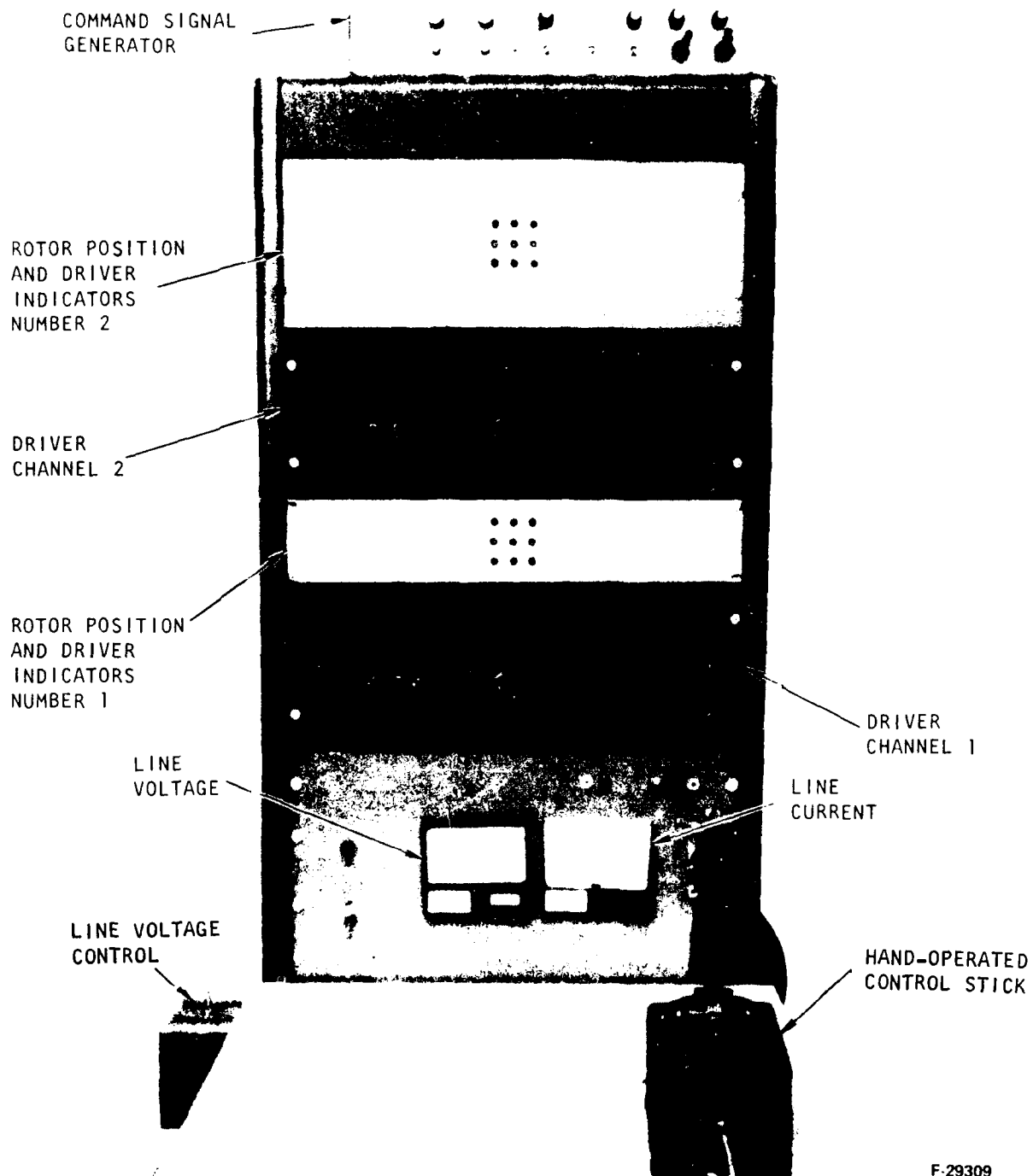
3.1 DESIGN OF THE BASELINE CONTROLLER

The controller for the electromechanical actuation unit consists of the servo and power switch assemblies, which are the two major functional elements. The servo circuits provide the proper logic to accomplish the desired high current switching of the power switch assemblies. These assemblies are further divided and described as follows:

- (a) Analog servo assembly, comprised of the control circuitry; surface position sensing; rotor position detectors; and the sequence control and inhibit logic.
- (b) Power switch, comprised of the driver switches; current limit; and the power supplies.
- (c) Servo circuits for tachometer feedback configuration, comprised of the tachometer feedback control loop and the rotor speed detection.

3.1.1 Analog Servo Assembly

The analog servo assembly was packaged within a standard instrument rack as shown in Figure 10. Various standard laboratory power supplies were also used to support operation of the unit. These were located in the bottom of the console.



F-29309

Figure 10. Control Console Breadboard Configuration

3.1.1.1 Control Circuitry

The control circuitry is shown in Figure 11 for the voltage servo breadboard; the schematic for the control circuitry is shown in Figure 12. The control circuitry is comprised of the command buffer, position error, loop dynamic compensation, pulse width modulators, and error direction detectors. Amplifier U1 combines the following functions: buffering the command input; summing the command and feedback position signals to produce a position error; and providing dynamic compensation for the position feedback signal. Amplifier U2 integrates the position error and provides the additional dynamic compensation required for position loop stability. The zener diodes VR1 and VR2 provide a clamp for the integrator to limit its range in corresponding to the range of the pulse-width modulator.

Pulse-width modulation is accomplished by comparators U3 and U4. The pulse width is generated for positive errors by comparing the error voltage with a 3-kHz triangle wave, which is offset so that the bottom tip of the waveform is at zero. When the error is greater than the triangle wave, the output is energized, which applies the line voltage to the motor. When the error is less than the triangle, the line voltage is turned off. For negative errors, the error is added to the triangle wave and the sum is compared with zero, which produces the same pulse widths as for positive errors. The pulse width produced is proportional to the error voltage, as shown in Figure 13. The average motor voltage is therefore the V_{line} times duty cycle, where duty cycle = t/T , t = pulse width, and T = period of the triangle wave. Therefore, the gain of the pulse-width modulator is a direct function of the line voltage. To keep the gain constant, the line voltage is monitored and used as the reference for the triangle wave. The triangle wave is, therefore, amplitude-modulated as a function of line voltage. For a given error voltage, the pulse width is increased or decreased in inverse proportion to line fluctuations, ensuring a fixed motor voltage and gain.

The schematics of the triangle wave generator and its resulting waveform are shown in Figures 14 and 15. Comparators U5 and U6 are used to detect the motor drive direction. The two detectors are cross-coupled, with a 10-sec delay between turnoff of one and turn-on of the other. This ensures that the drive transistors for one direction have time to turn off before the transistors for the other direction are turned on; this prevents transistors in series across the 270-vdc line from being on at the same time, thus ensuring that they are not damaged.

3.1.1.2 Surface Position Sensing

The control surface position is sensed by a 12-bit digital rotary shaft encoder. The encoder output is in a digital gray code and must be decoded to binary format by a cascaded series of exclusive OR gates. The decoded binary number is then converted to an analog voltage level by an analog-to-digital converter that is offset to provide bipolar output corresponding to positive and negative surface positions. A filter is included in the output buffer to smooth the bit-to-bit transitions of the converter. A schematic is shown in Figure 16.

ERROR DIRECTION
DETECTION

PULSE WIDTH
MODULATOR

DECOUPLING
NETWORK

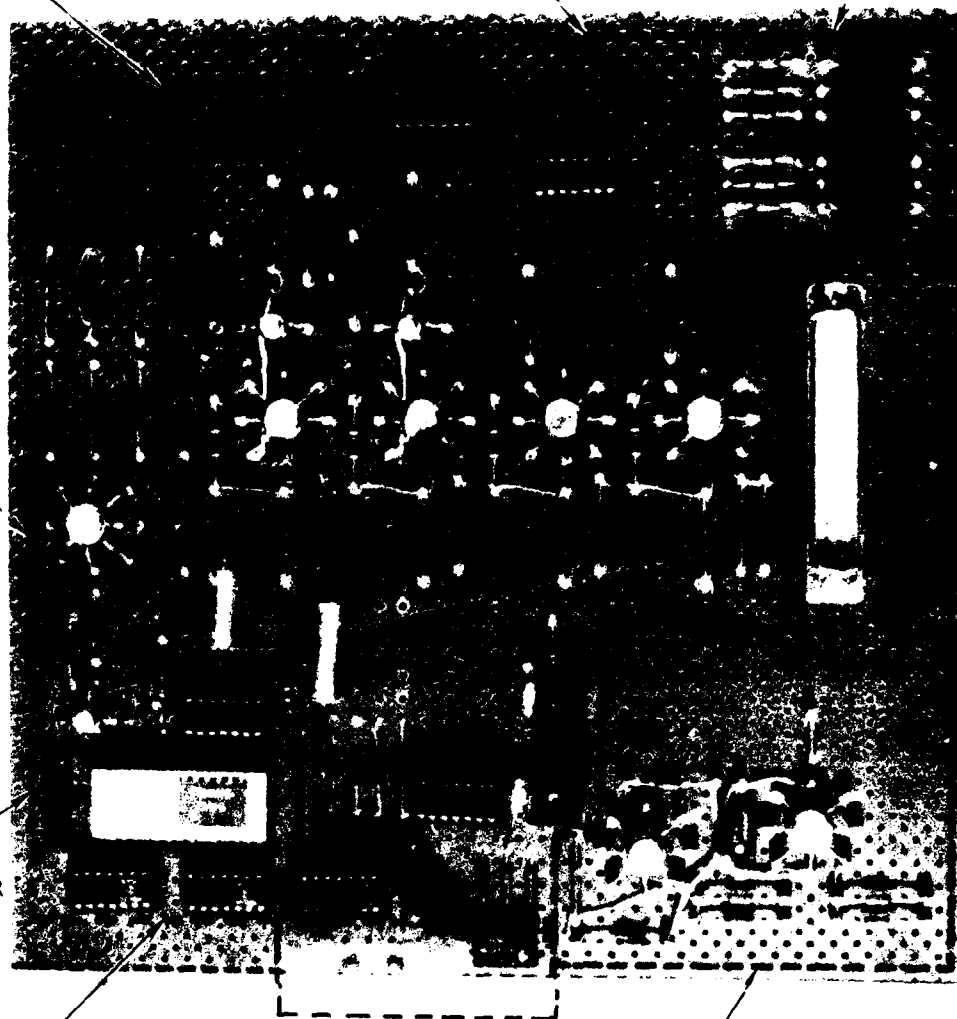
VOLTAGE
REFERENCE

D/A CONVERTER
AND BUFFER

GREY-BINARY
DECODER

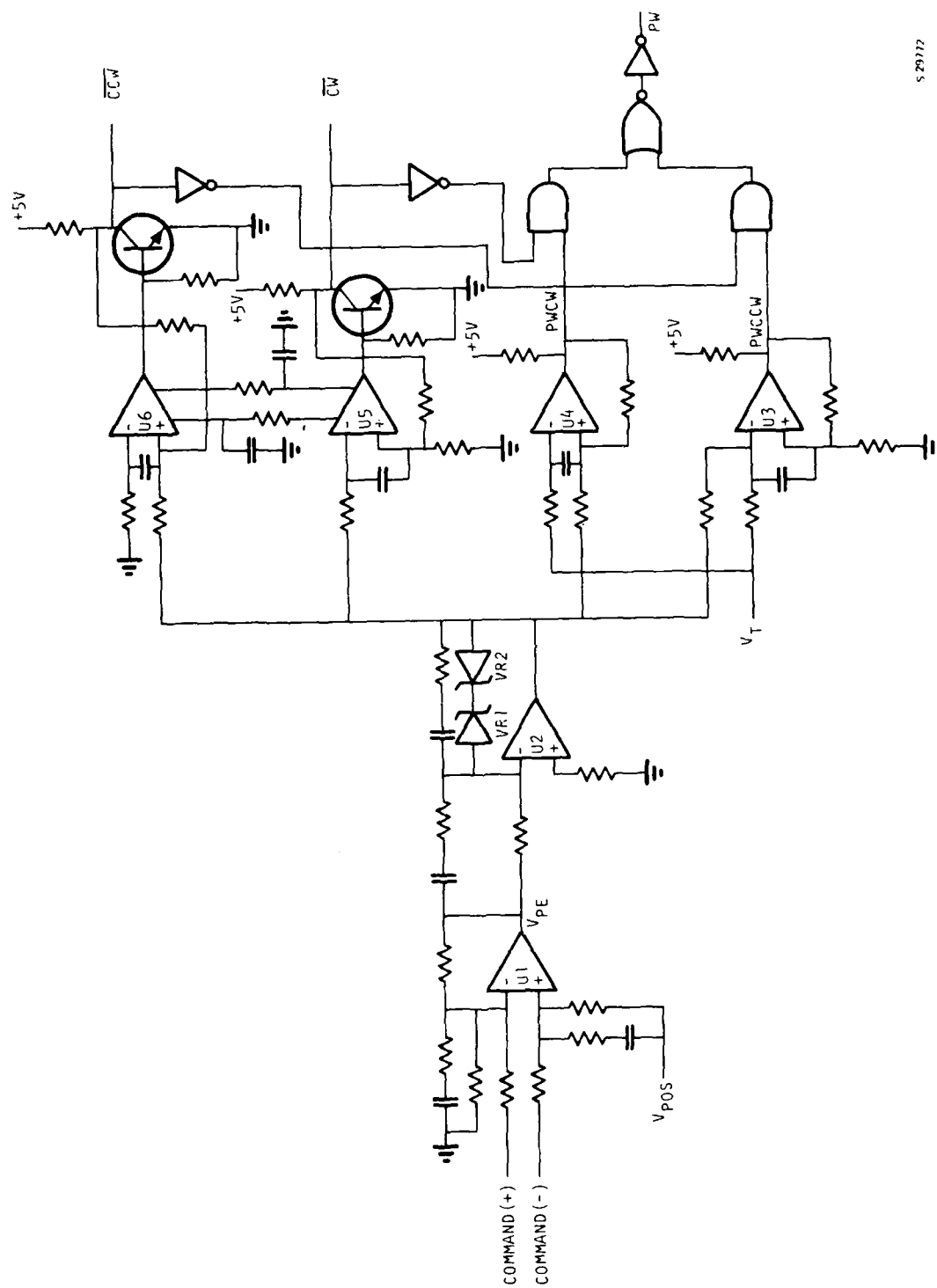
POSITION ERROR
AMPLIFIER AND
INTEGRATOR

TRIANGLE WAVE
GENERATOR



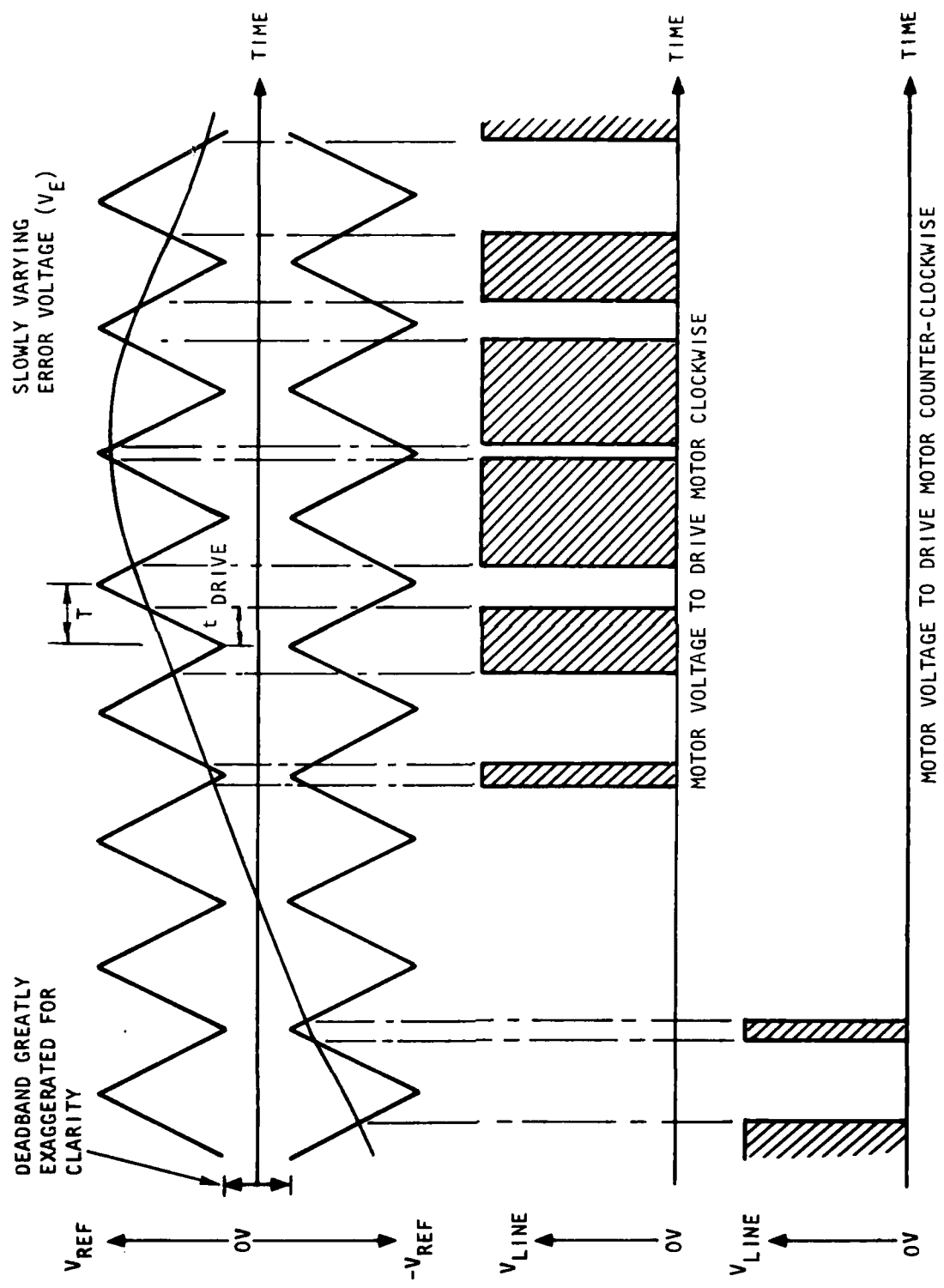
F.29310

Figure 11. Voltage Control Servo Breadboard



S 29172

Figure 12. Position Error and Compensation Amplifiers, Pulse-Width Modulators, and Direction Sense Circuitry



S-78017-B

Figure 13. Pulse-Width-Modulation Idealized Timing Diagram

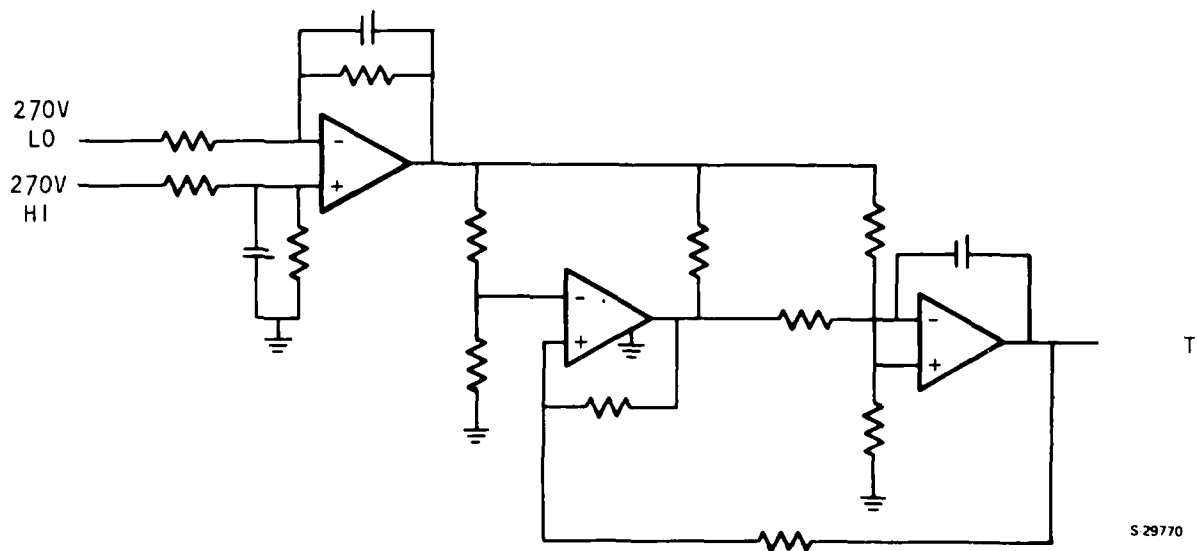


Figure 14. Triangle Wave Generator

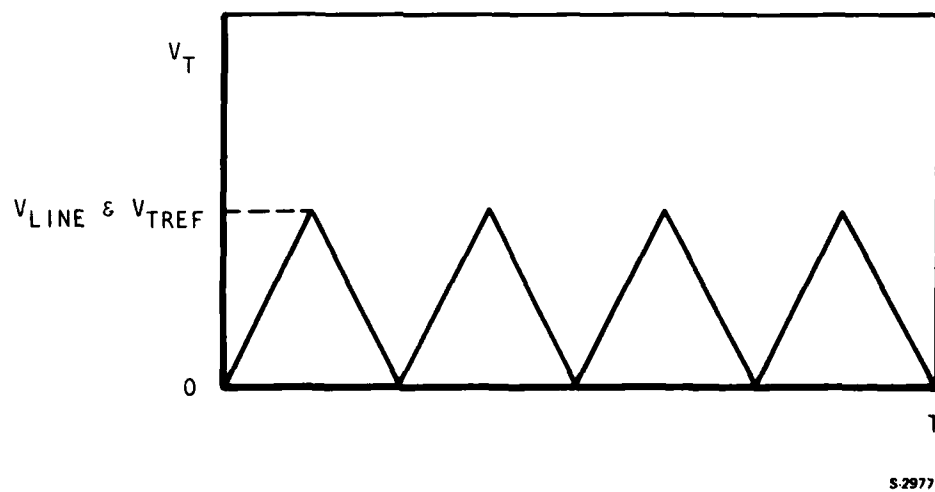


Figure 15. Triangle Waveform

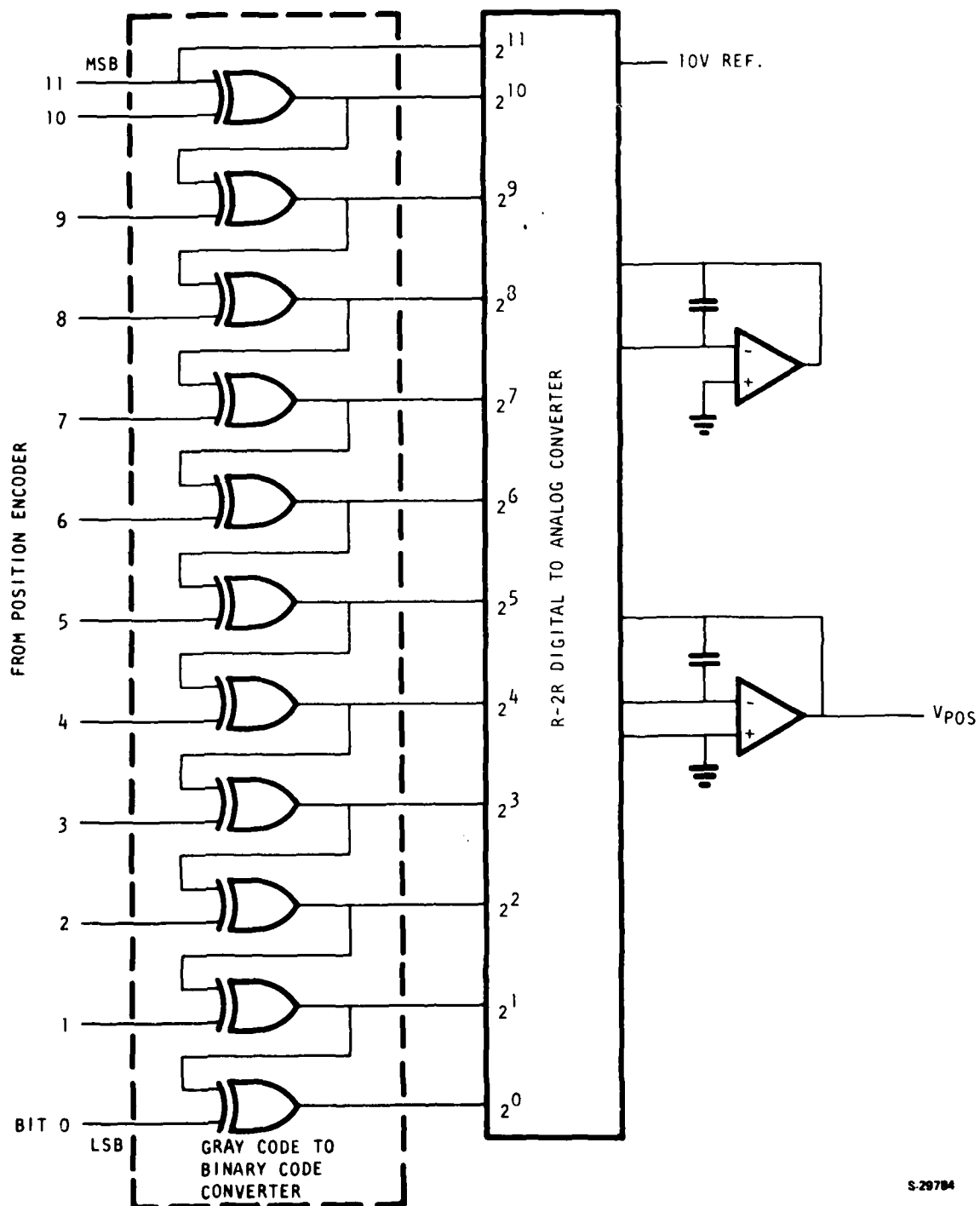


Figure 16. Surface Position Decoding Circuitry

The precision 10-v reference is used for the D/A conversion, which gives an output scaling of 0.2489 v/deg. The 12-bit encoder gives two discrete states for 80.36 deg of travel, which provides a resolution of 0.0196 deg.

3.1.1.3 Rotor Position Detectors

To synchronize the stator voltage with the rotor for efficient torque transfer, the position of the rotor must be known. To sense this position, three variable reluctance position sensors are mounted in the motor frame at 40-deg intervals. These sensors are transformers with a mechanical shutter mounted on the motor shaft, which varies the coupling between the primary and secondary. This coupling change varies the amplitude of the voltage in the sensor secondary. A diagram of the idealized position outputs is shown in Figure 17.

The position detection circuitry is shown in Figure 18. There are three identical detector circuits. The primaries of the sensors are driven with a 50-kHz, 18-v peak-to-peak square wave. This frequency is generated by timer U1, which is connected as a square-wave oscillator; the frequency is amplified to the proper level by Q1 and Q2. The sensor output is demodulated by U2 and U3, which amplify and full-wave rectify the signal. The signal is then filtered and level detected to eliminate the 50-kHz reference frequency, and to give the position output.

3.1.1.4 Sequence, Control, and Inhibit Logic

The schematic of the drive logic is shown in Figure 19. The drive logic sets the sequence in which the drive transistors are turned on as a function of the rotor position (as indicated by \emptyset_1 , \emptyset_2 , and \emptyset_3) and the commanded direction signals CW and CCW. The upper switches (indicated by a +) are turned on as a function of direction and rotor position, whereas the power switches (indicated by a -) are modulated as a function of the pulse-width modulation signal. The logic equations for the switches are as follows:

- Upper switches

$$A + = (\overline{\emptyset_1} \cdot \emptyset_3 \cdot CW + \emptyset_1 \cdot \overline{\emptyset_3} \cdot CCW) \cdot \overline{INHIBIT} \cdot \overline{AM}$$

$$B + = (\emptyset_2 \cdot \overline{\emptyset_3} \cdot CW + \overline{\emptyset_2} \cdot \emptyset_3 \cdot CCW) \cdot \overline{INHIBIT} \cdot \overline{BM}$$

$$C + = (\emptyset_1 \cdot \overline{\emptyset_2} \cdot CW + \overline{\emptyset_1} \cdot \emptyset_2 \cdot CCW) \cdot \overline{INHIBIT} \cdot \overline{CM}$$

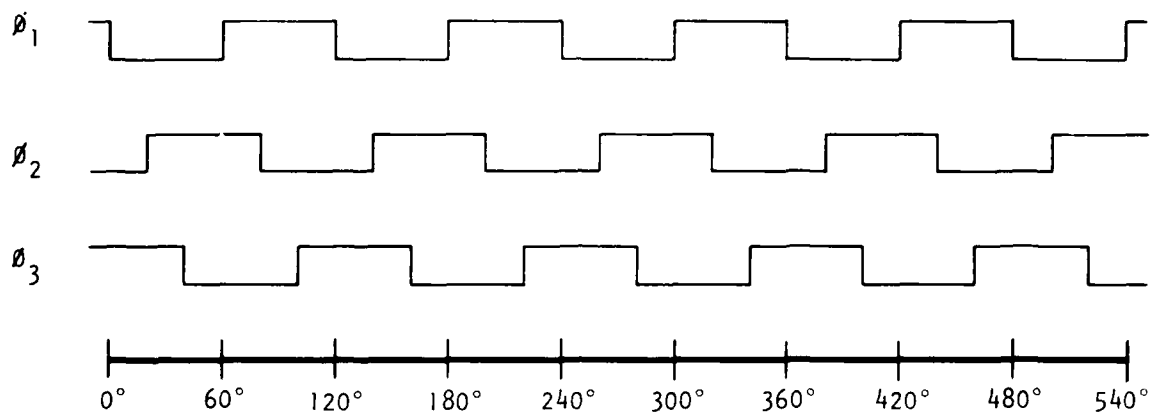
- Lower switches

$$A - = (\emptyset_1 \cdot \overline{\emptyset_3} \cdot CW + \overline{\emptyset_1} \cdot \emptyset_3 \cdot CCW) \cdot ENABLE \cdot \overline{AP}$$

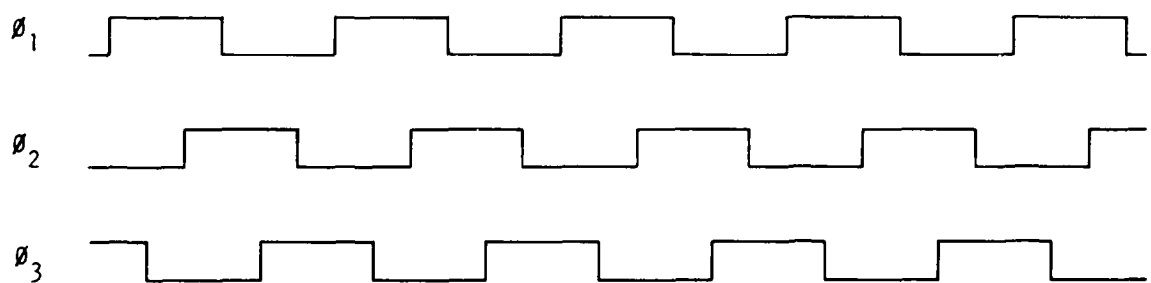
$$B - = (\overline{\emptyset_2} \cdot \emptyset_3 \cdot CW + \emptyset_2 \cdot \overline{\emptyset_3} \cdot CCW) \cdot ENABLE \cdot \overline{BP}$$

$$C - = (\overline{\emptyset_1} \cdot \emptyset_2 \cdot CW + \emptyset_1 \cdot \overline{\emptyset_2} \cdot CCW) \cdot ENABLE \cdot \overline{CP}$$

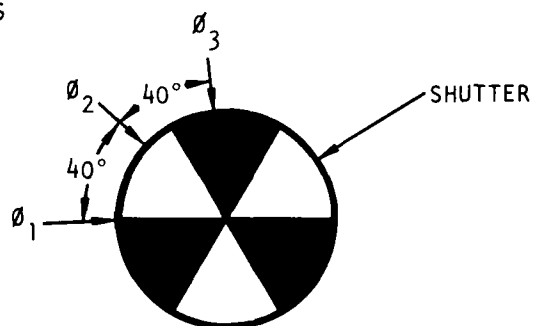
COUNTER CLOCKWISE



CLOCKWISE



POSITION
SENSORS



S-29788

Figure 17. Rotor Position Outputs

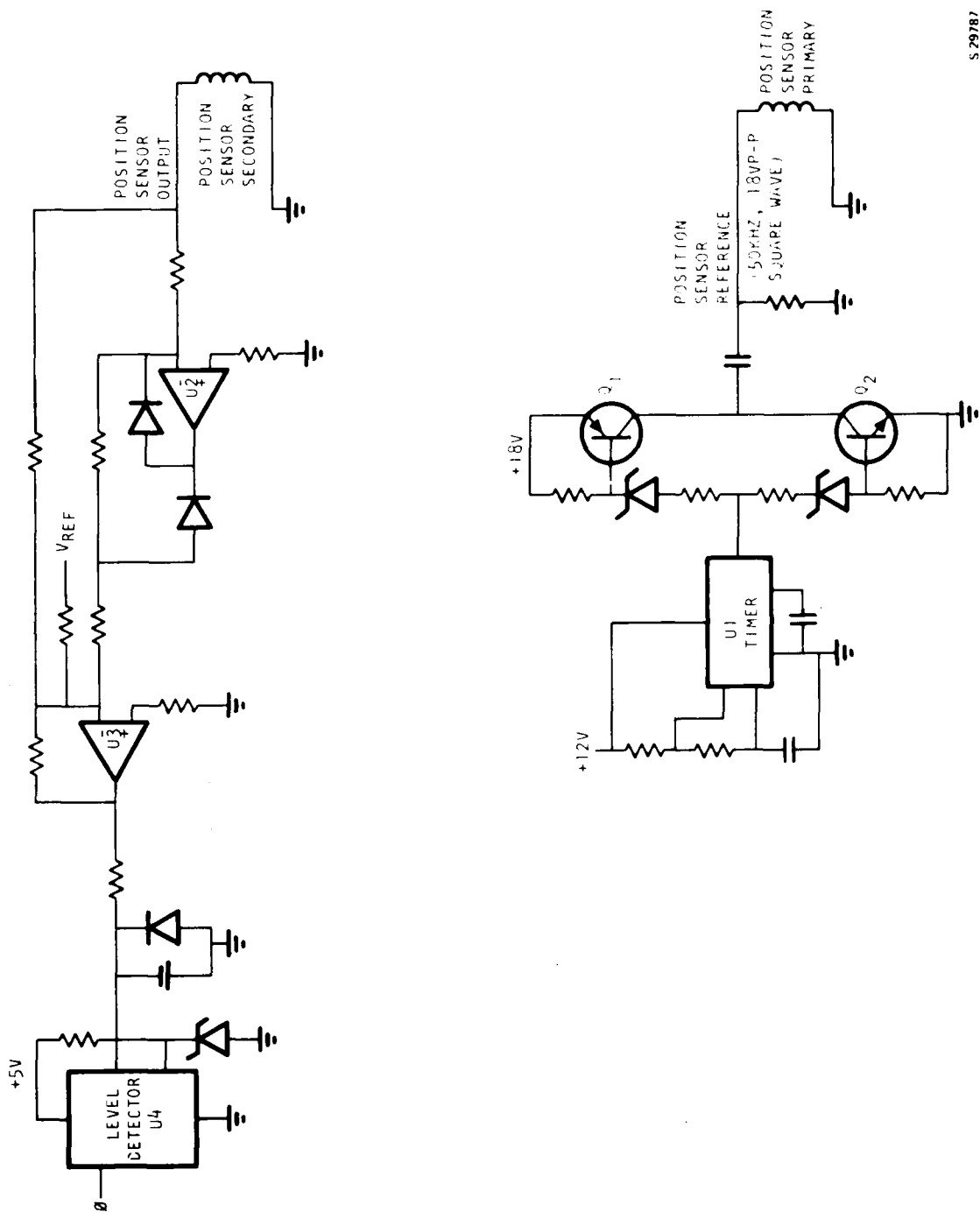


Figure 18. Motor Rotor Position Detection Circuitry

S 29787

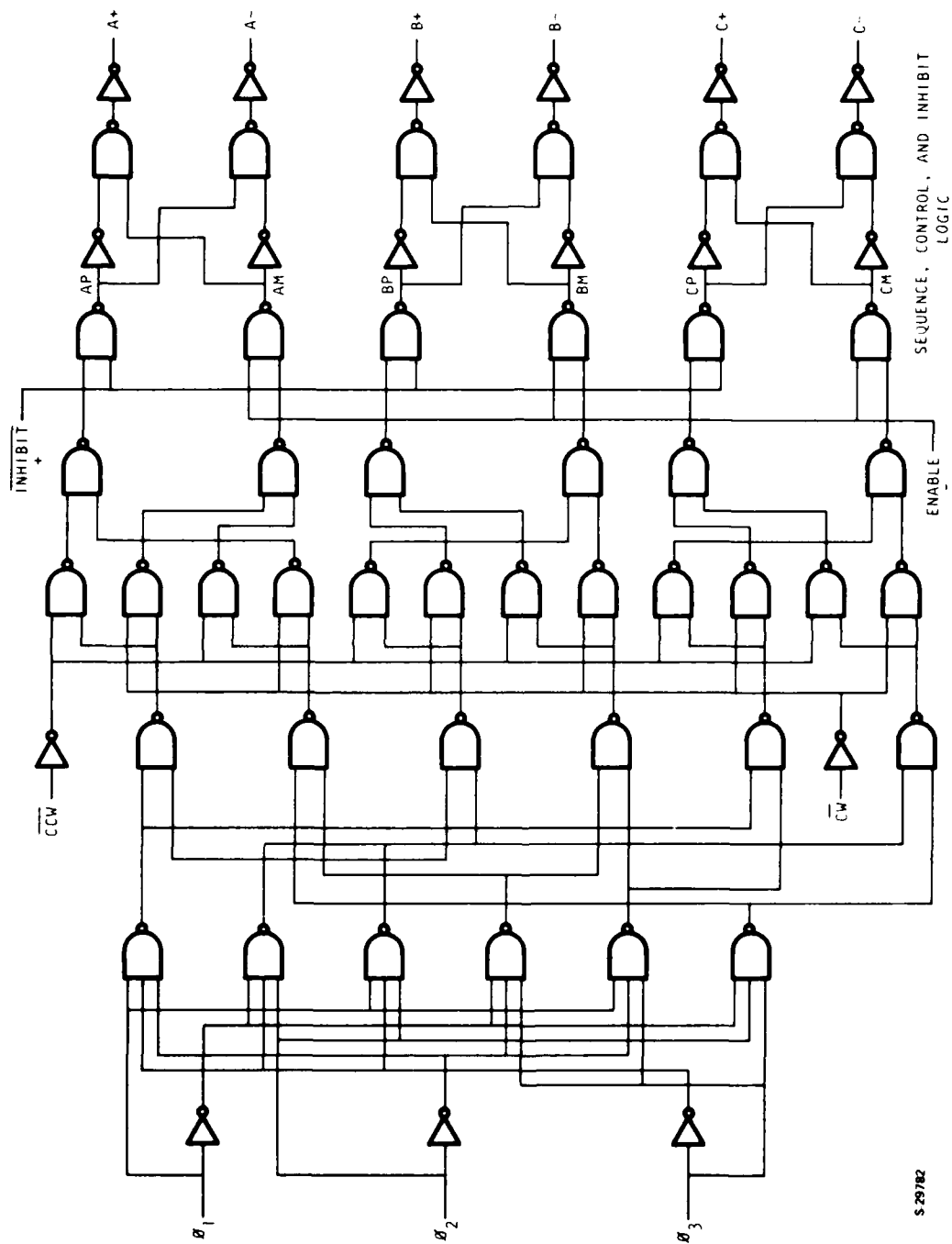


Figure 19. Sequence, Control, and Inhibit Logic

S 29782

where: $\overline{\text{INHIBIT}} = \overline{\text{CLH}} \cdot \overline{\text{DELH}}$

CLH = Plug current limit

DELH = Plug 140 sec delay

ENABLE = $\text{PW} \cdot \overline{\text{CLL}} \cdot \overline{\text{DELL}}$

PW = Pulse width modulation

CLL = Lower current limit

DELL = Lower 140 sec delay

Timing diagrams of the drive logic are shown in Figure 20.

The AP, BP, CP, AM, BM, and CM signals are used to ensure that two of the switches (for example, A+ and A-) are never enabled at the same time. This would cause a short across the line, damaging the transistors.

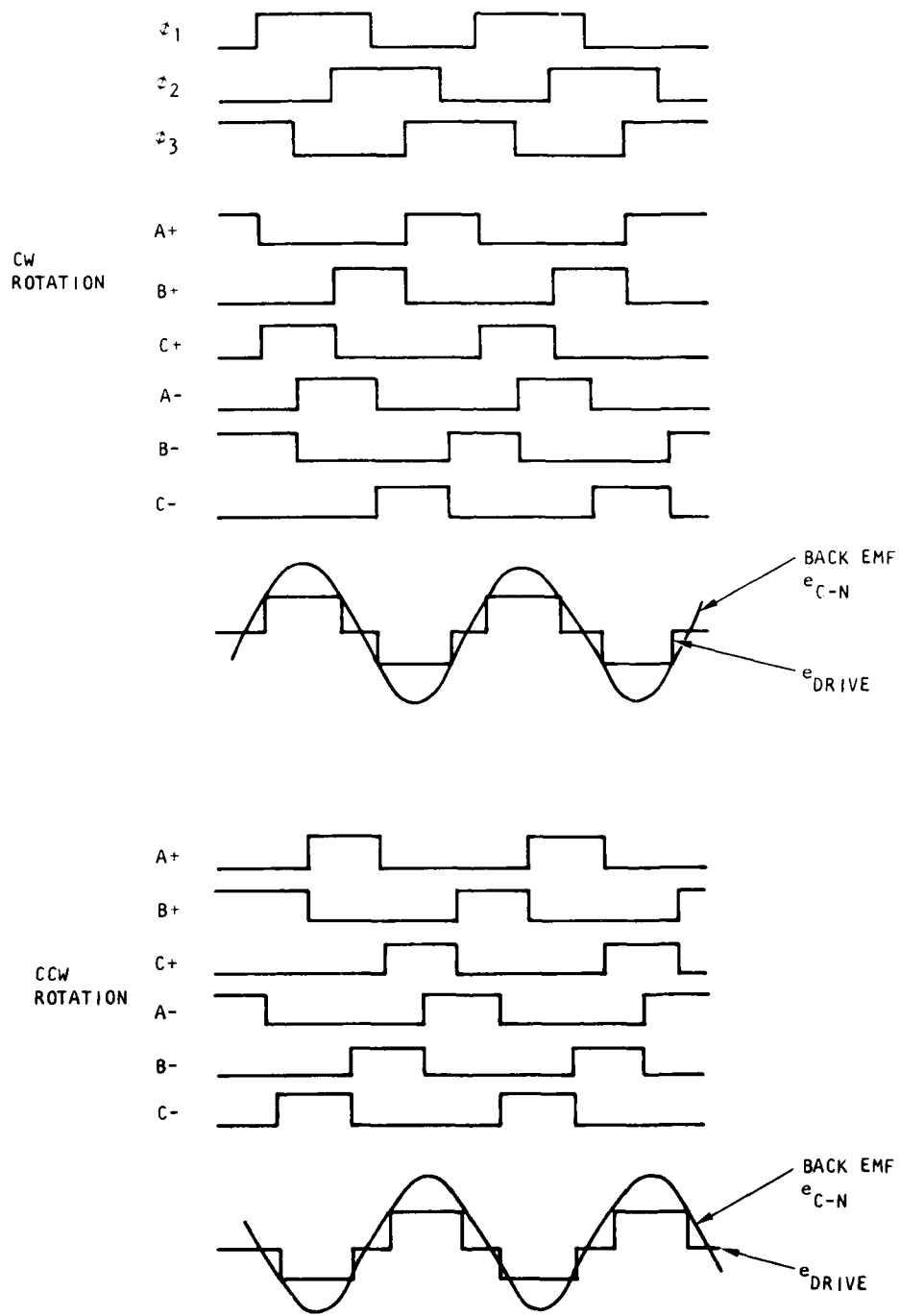
3.1.2 Power Switch Supply

3.1.2.1 Driver Switches

The schematic of the driver switches is shown in Figure 21. The operation of a switch (for example, switch A+) is typical for all of the power switches. When logic signal A+ is high, optical coupler Q₃ is off, making the level detector output low. This turns on Q₁ and energizes switch A+, causing current to flow in one leg of the motor. When logic signal A+ goes low, optical coupler Q₃ is energized, forcing the level detector output high. This turns off Q₁ and turns on Q₂, which pulls current out of the base of switch A+, thus turning it off. Since the motor has inductance, the current cannot be interrupted; the voltages go low and forward bias diode CRA-, giving a path for the motor current.

The bias for the power switches is obtained from a floating power supply PSA, which is referenced to the motor terminal A. The optical couplers isolate the logic signals from the 270-v power.

The network R, C, and CR is a snubber network to shape the transistor current-voltage turnoff locus. Without the snubber, the transistor turns off with an inductive load, and the current continues to flow in the transistor until the flyback diode starts to conduct. This means it has full current and full line voltage across it at the same time. This produces a very high power spike in the transistor that can cause damage or failure. With the snubber, capacitor C charges through the diode CR when the voltage across the transistor increases, therefore sharing the current with the transistor. A typical curve of this operation is shown in Figure 22.



S-29748

Figure 20. Sequencer Timing Diagrams

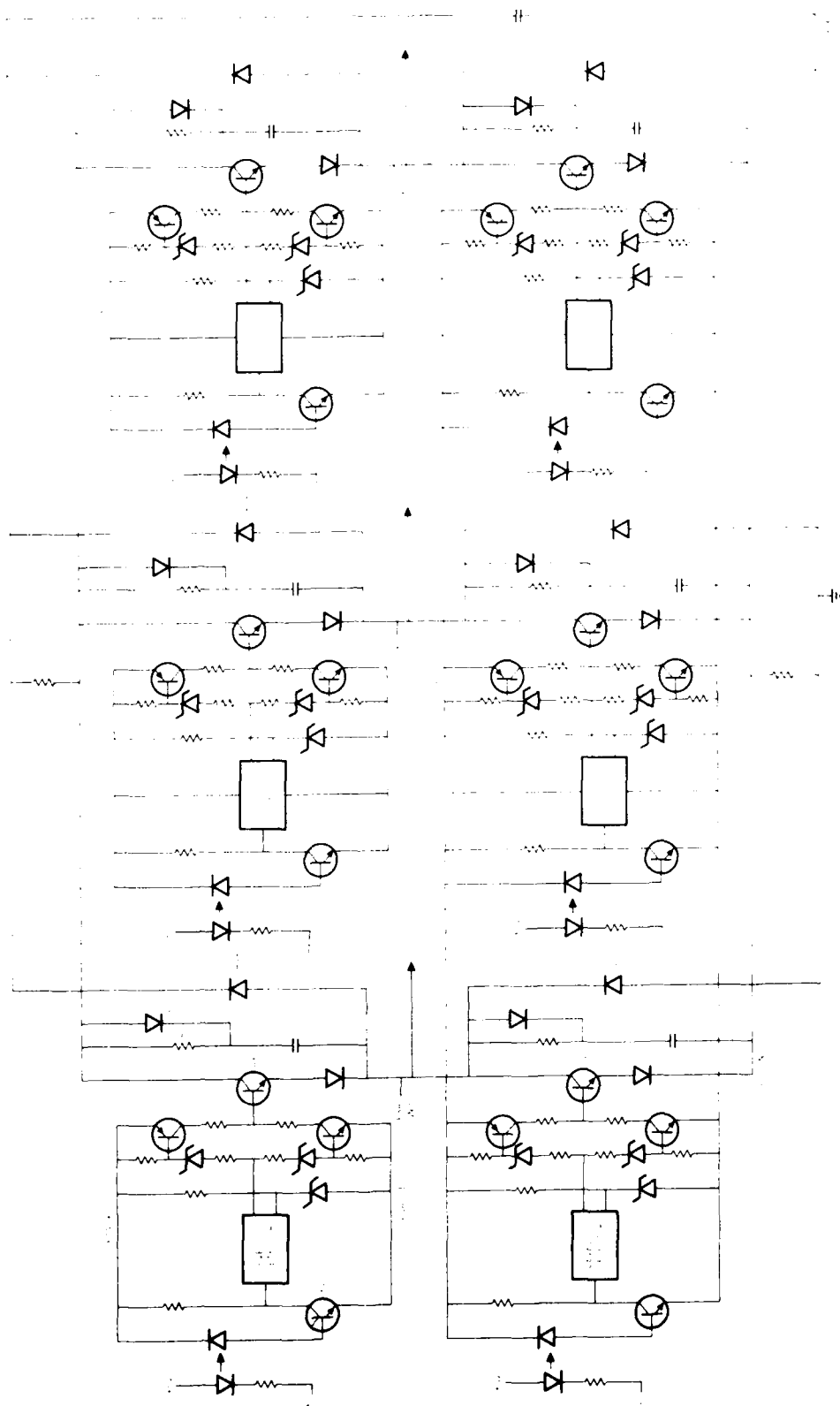


Figure 21. Schematic of Driver Switches

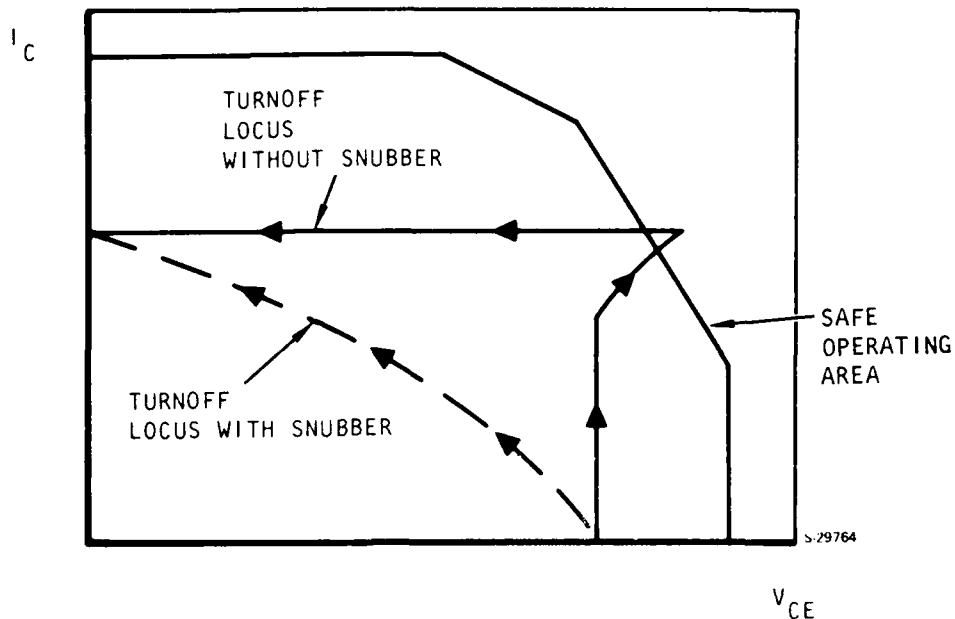


Figure 22. Typical Turnoff Locus

3.1.2.2 Current Limit

The current limit circuitry is shown in Figure 23. There are two current limits for controlling motor and transistor currents. The primary function of the lower current limit is to limit the motor torque and power in normal operation. The upper limit is used in the plugging mode of operation when the motor is rotating in one direction and the inverter is driving in the other. This condition occurs during braking and reversing. Under these conditions, both the back emf and the applied voltage cause current to flow in the same direction, which can cause high currents. This upper limit is primarily to protect the transistors from possible damage.

For normal operation with one upper and one lower switch on (for example A+ and B-), the current flow is from the line through R_{SH} , switch A+, motor windings A - B, switch B - R_{SL} , and into ground. The voltage across R_{SH} and R_{SL} is proportional to motor current. When the motor current reaches the limit level of 16 amp, U2 goes low, which starts one shot U3 and forces the ENABLE low; this turns the B- switch off. Due to the motor inductive flyback, the current path is now changed to the line R_{SH} , switch A+, motor winding A - B, diode CRB+, and back to the line. In this condition, the current loop does not include the line, and the current is not taken out of the supply. The current in the motor decays in this condition. Since no current flows in R_{SL} , U2 returns high. The ENABLE remains low until the one-shot period of 140 μ sec is over; the ENABLE then returns high, depending on the level of PW. Switch B- is again turned on and current increases in the motor until it reaches the current limit, and the sequence is then repeated.

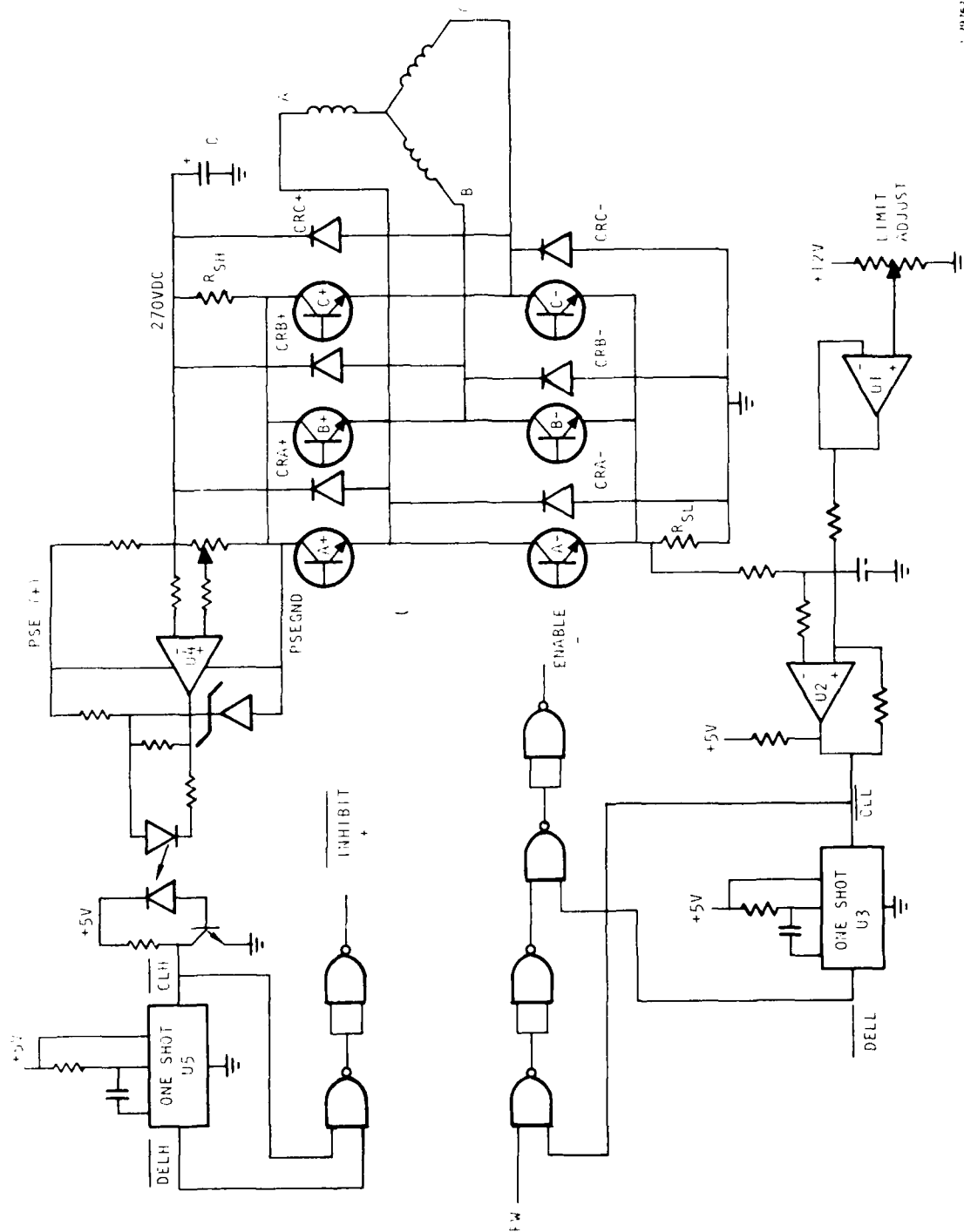


Figure 23. Current Limit Circuitry

In the plugging mode, the current rapidly rises in the motor due to the addition of the back emf and the applied voltage. The lower limit is reached first, and the operation is as described above. Due to the back emf, the current continues to rise until the upper limit of 18 amp is reached. At this time, U4 goes low, starting one shot U5 and forcing INHIBIT low, thus turning off A+. The current path is now from ground, diode CRA-, motor winding A - B, diode CRB+, and into capacitor C to ground. Since current cannot flow back into the supply, the capacitor is charged with the current. In this condition, the motor current decays. The INHIBIT is held low until the one-shot period of 140 sec ends, when it again goes high, turning on A+. The current again increases, repeating the process until the motor speed is reduced to a point where the back emf and the applied voltage will not drive the limit current.

3.1.2.3 Power Supplies

The power supplies are shown in Figure 24. Power supplies A, B, C, D, and E are commercial and are used to (1) bias the power switches, and (2) provide a floating supply for the upper current limit circuitry. A precision 10-v reference is created for the D/A converter reference and for other circuits in the system. The +12 v and -12 v supplies are derived from the +18 v and -18 v supplies for use as references and as supplies for lower voltage circuits.

3.1.3 Servo Circuits for Tachometer Feedback Configuration

3.1.3.1 Tachometer Feedback Control Loop

For additional dynamic compensation of the position control loop, the speed of the motor rotor is sensed and used as a secondary control loop. A block diagram of this control is shown in Figure 25, and the breadboard layout is shown in Figure 26. The control loop electronics have been changed to accommodate this addition, and the circuitry associated with rotor speed and direction detection have been added. The pulse-width modulators, sequence control logic, current limiting, drive switches, rotor position, and fin position circuitry are the same as previously described.

The schematic of the control loop circuitry is shown in Figure 27. Amplifier U1 sums the command input, fin position, and rotor speed, and provides an error output. This error is integrated by U2. Zener diodes VR1 and VR2 limit the output to prevent integrator windup. U3 sums an additional speed input with the integrator to provide a voltage signal that is compared with the triangle wave in the pulse-width modulator.

Amplifier U4 and U5 provide speed signal scaling and phase compensation required for loop stability. Zener diodes VR3 and VR4 limit the authority of the secondary speed loop.

3.1.3.2 Rotor Speed Detection

To determine the rotor speed, a tachometer winding was added in parallel with each of the three rotor windings. This provides a 3-phase sine wave signal with the amplitude proportional to the rotor speed.

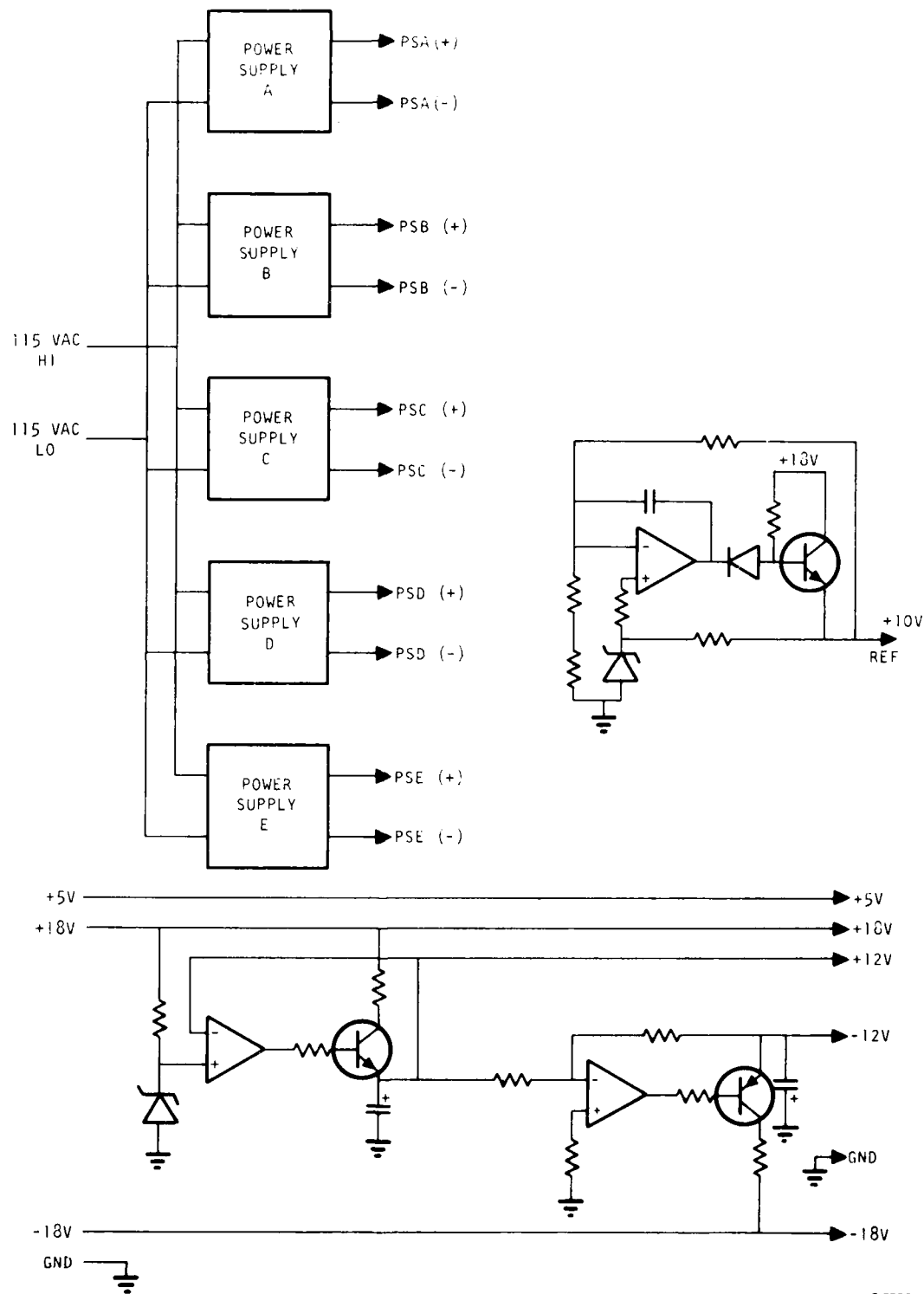
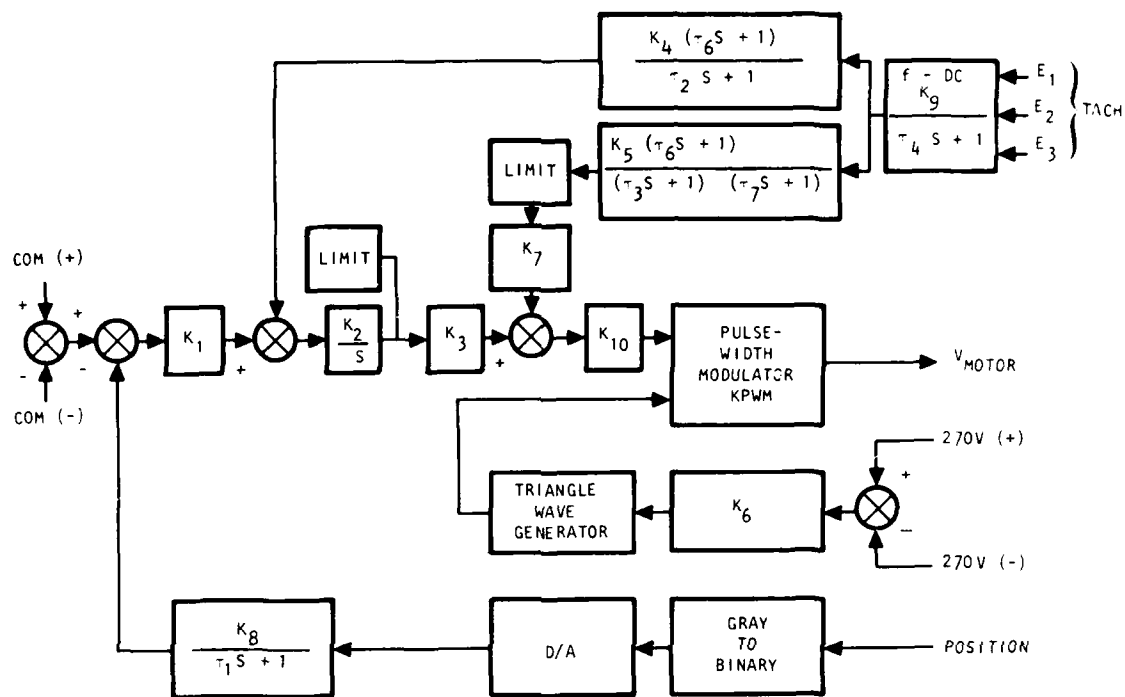


Figure 24. Power Supply

S 29773



S 32432

Figure 25. Tachometer Feedback Control Block Diagram

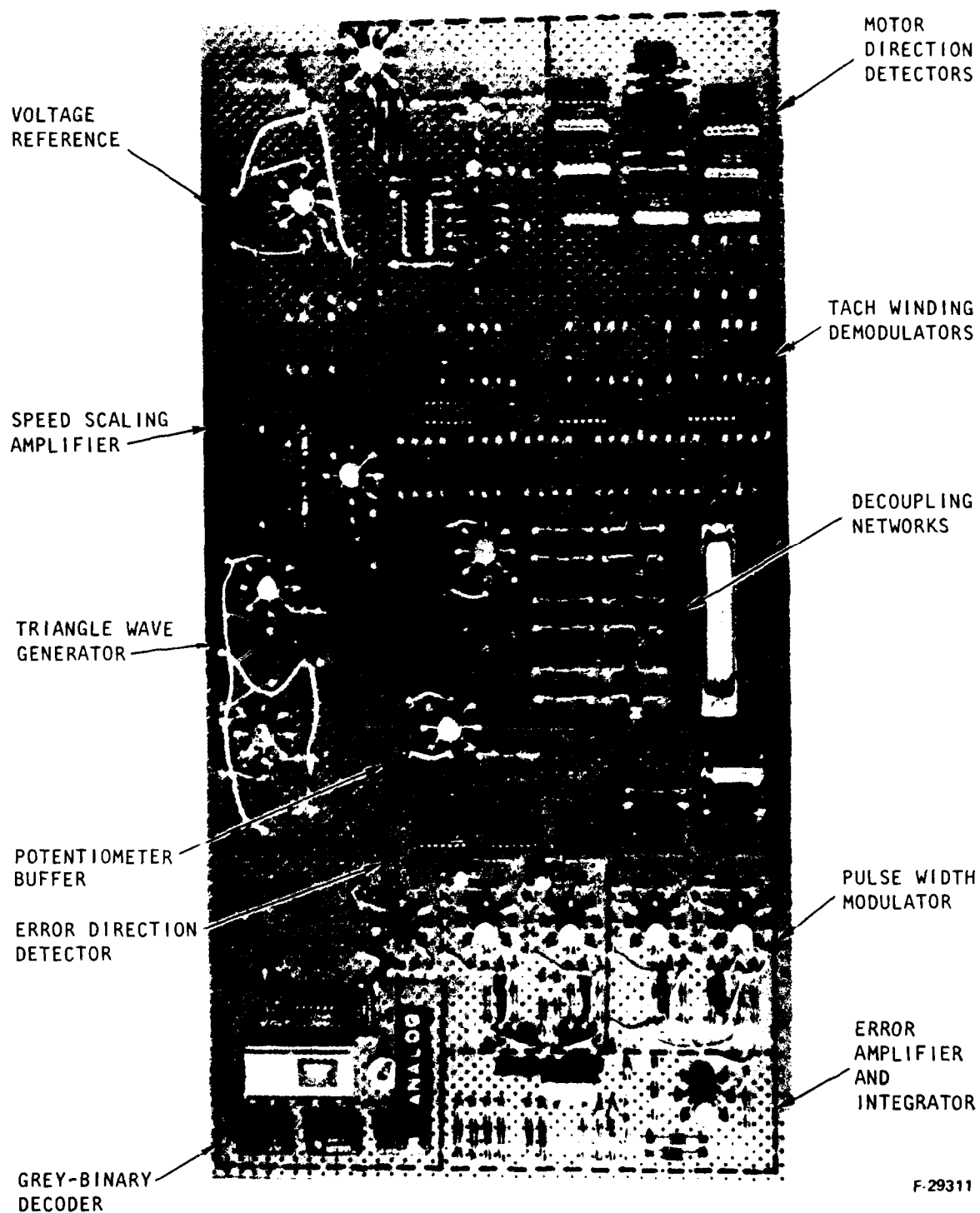


Figure 26. Tachometer Feedback Servo Control Breadboard

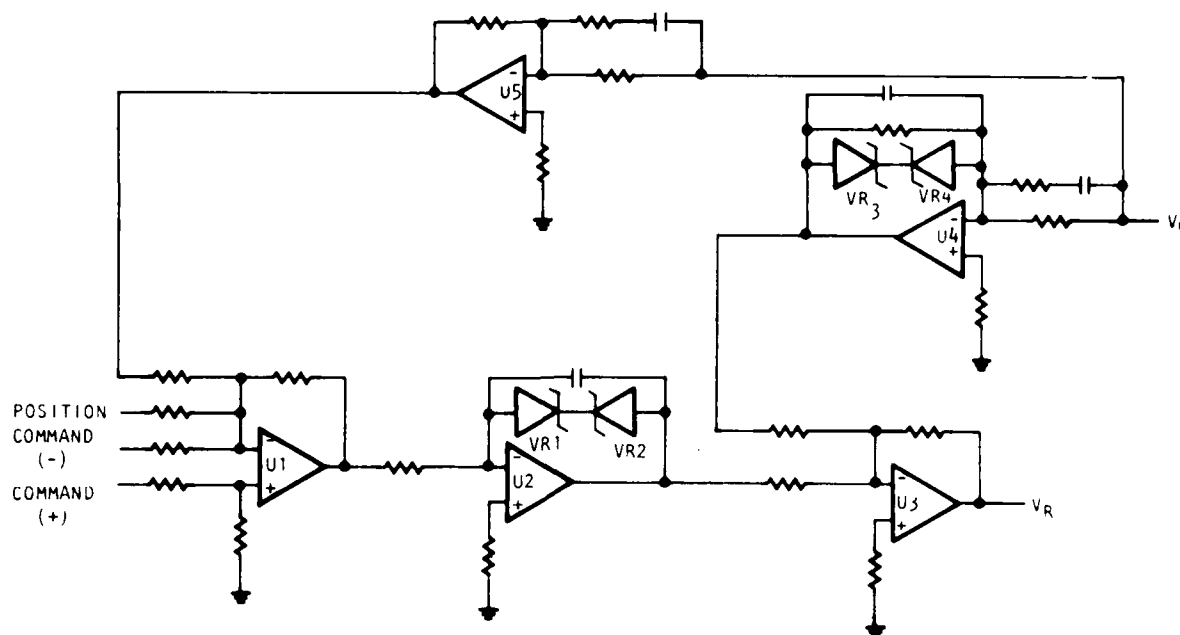


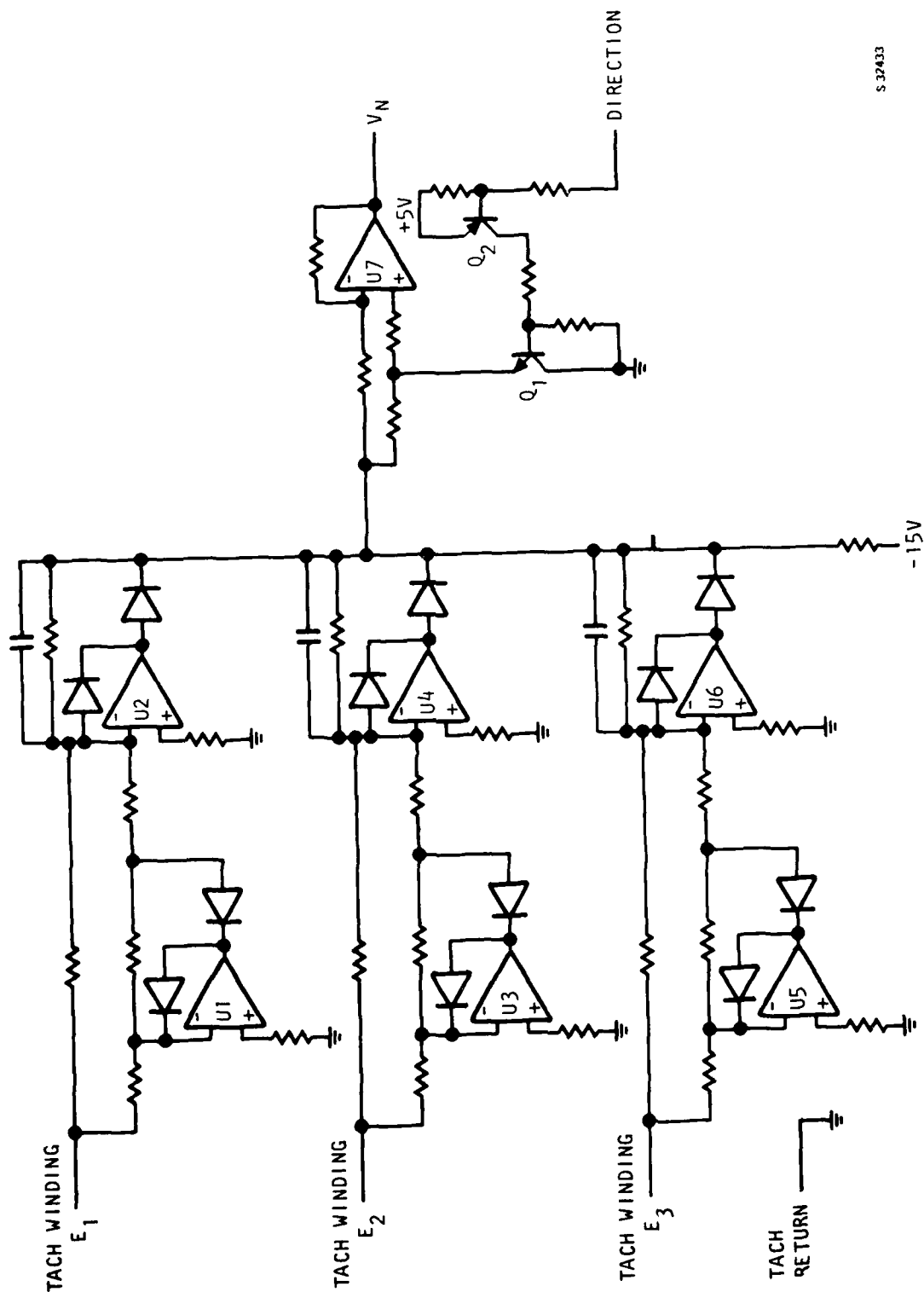
Figure 27. Tachometer Control Circuitry

The schematic of the speed detection circuitry is shown in Figure 28. The 3-phase speed signal is converted to dc by a precision full-wave rectifier circuit, U1 through U6, which does not have the voltage losses because of diodes that are usually associated with rectifier circuits. This gives a continuous signal from zero to full amplitude. Because this signal has the same sign for both directions of rotation, the signal must be inverted for the reverse direction. This is accomplished by amplifier U7 and transistor Q1. When Q1 is off, the sign of U7 is positive. When Q1 is on, the sign is negative. The state of Q1 is determined by the rotor direction detection circuit.

The schematic diagram for the motor rotor direction circuit is shown in Figure 29. The direction of rotation is sensed by the output of the three rotor position detectors: θ_1 , θ_2 , and θ_3 . On each transition of these outputs, a pulse is generated. The previous state of rotor position, which has been stored in flip-flops 1 and 2, is compared with the present state and a direction is determined. A transition occurs every 60 deg of electrical cycle. There are 3 electrical cycles for each complete rotation; therefore, a direction change can be determined within 20 deg of rotation.

3.2 CONTROLLER MODIFICATION AND IMPROVEMENTS

As a result of the controller development described above, a number of areas were identified as candidates for further improvement. Some were related to the contract amendment requiring increased power output from the controller, and some were simply deficiencies in the design that were revealed as the development progressed.



S 32433

Figure 28. Rotor Speed Detection Circuit



Figure 29. Rotor Detection Circuit

The following paragraphs describe the circuits that were modified. Figure 30 shows the controller block diagram, with emphasis on those circuit functions where major modifications were made. These modifications included the control circuits, logic circuits current limit, and control surface position sensing. Table 2 summarizes the aspects of the baseline controller that were found deficient; describes the problem area; and shows the selected approach to circuit improvement.

3.2.1 Control Circuitry

Two improvements were made on the control circuitry (see Figure 31). The first improvement is to maintain constant loop gain with either one or two motors operating. The PWM gain is increased when only one motor is operating to compensate for the loss of mechanical gain in the velocity summing differential.

Loop gain is also affected by fluctuations in the 270-vdc line voltage. For example, an increase in the 270-vdc line voltage would provide additional power to the motor. To compensate for the additional motor power available from the higher line voltage, the PWM gain is reduced in proportion to the increased voltage detected on the 270-vdc line.

One modification was adding the 270-v signal from channels 1 and 2 to make V_{Tref} (see Figure 32). V_{Tref} then adjusts the triangle wave peak voltage to keep the loop gain constant for small signals.

The second improvement is to generate individual pulse width modulation (PWM) control for channel 1 and channel 2. Therefore, individual pulse width modulators can adjust each of the motors characteristic differences. In addition, separate PWM control is necessary to implement two-channel redundancy.

Each control channel provides individual motor current limits for the individual pulse width modulators and can change the pulse width modulation of that channel to the respective motor. Reducing the pulse width to the motor reduces the average applied voltage and current of the motor. The reason for this reduction is discussed in para. 3.2.3.

3.2.2 Sequence, Control, and Inhibit Logic

In the baseline controller, current sense information is provided to the sequence, control, and inhibit logic function block, as INHIBIT and ENABLE shown in Figure 19. The baseline controller arrangement operated to limit peak current, not average current. For example, when motor current reached a predetermined level, it completely turned off the transistors in the bottom leg of the circuit shown in Figure 23. The transistors were turned back on after a set time period of 140 μ sec. Figure 33 shows the waveforms that result from using only peak current for a current limit concept. It is clear from the comparison of high and low speed motor operation that extreme variation in average current can result according to motor speed. Since output torque is directly proportional to average motor current, the control of peak current limit results in wide variations in average motor torque depending upon the motor operating speed.

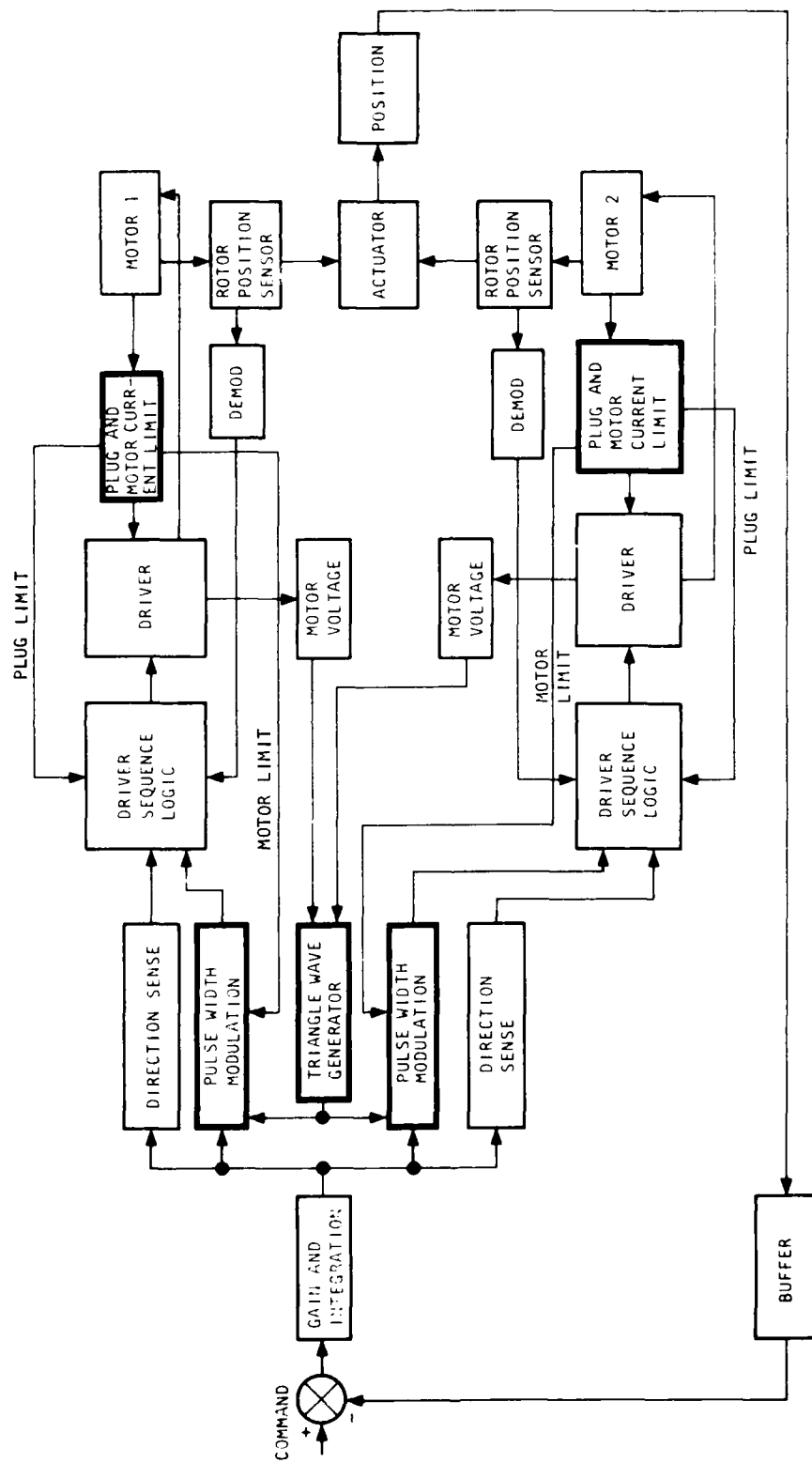


Figure 30. Controller Block Diagram

TABLE 2

SUMMARY OF CONTROLLER IMPROVEMENTS

Baseline Controller	Problem Area	Circuit Modification and Improvements
Control Circuit	<p>Loop gain affected by fluctuations in 270-vdc line and by number of motors operating.</p> <p>Control of 2 motors with a single PWM circuit; (1) reliability, and (2) motor current limiting limiting deficiencies.</p>	<p>Summing of line voltages of channels 1 and 2 for control of output voltage of the triangle wave generator</p> <p>Separate PWM generators, each with separate current limit provisions</p>
Sequence, control, and inhibit logic	Discontinuity of motor current control	Control circuit improvements described above
Current limit	<p>(a) Contract amendment-required demonstration of significant increase in power control capability</p> <p>(b) Previous 16-amp current limit achieved only as a peak value, resulting in a 8-amp average current applied to motor</p>	<p>(a) Use of D60T power transistors</p> <p>(b) Improve efficiency of predrive circuits using VFET devices</p> <p>(c) New current limit control to limit average current as opposed to peaks</p>
Control surface position sensing	Complex interfacing of digital encoder with analog control	Replace optical digital encoder with a rotary potentiometer.

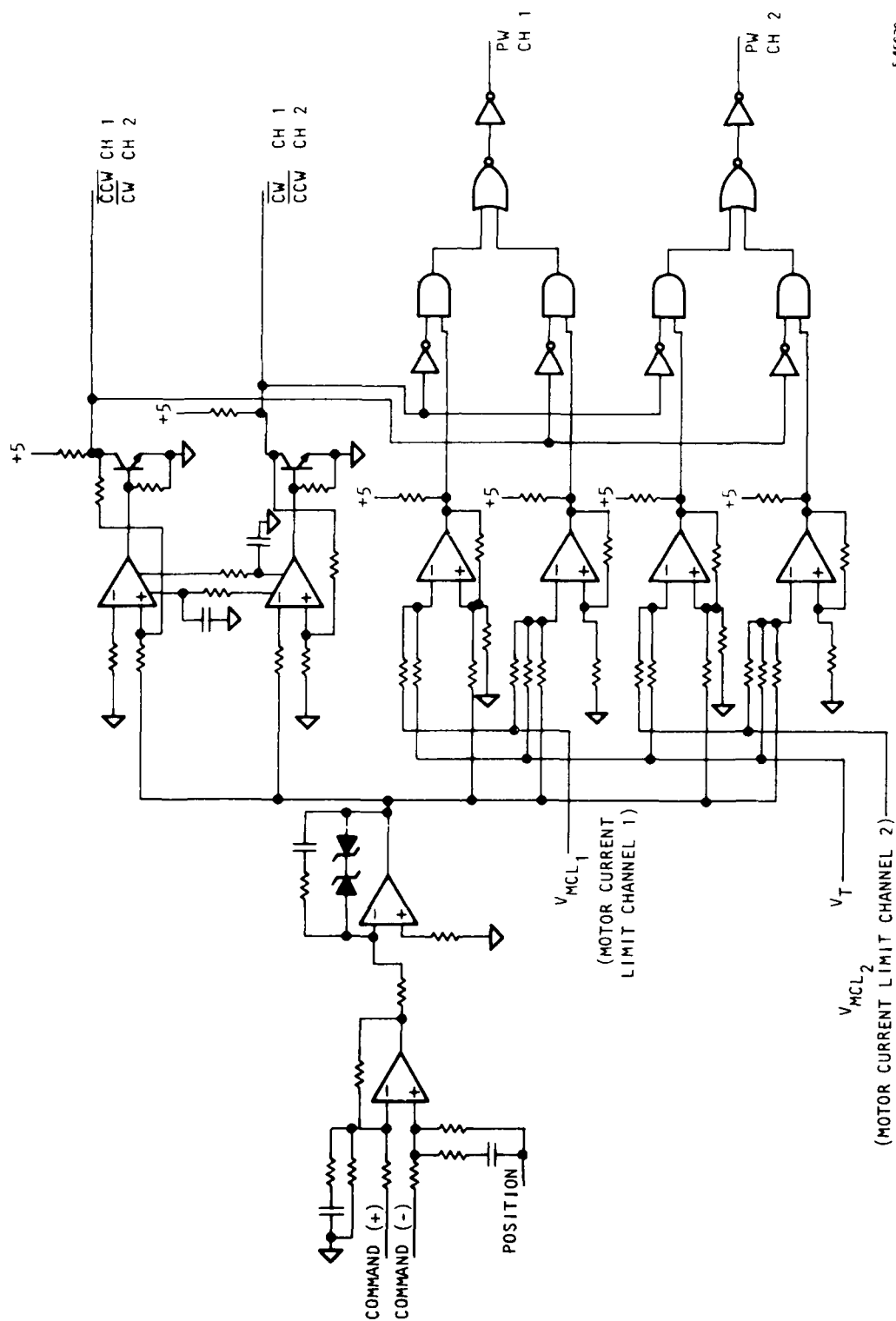


Figure 31. Control Circuitry

S-45630

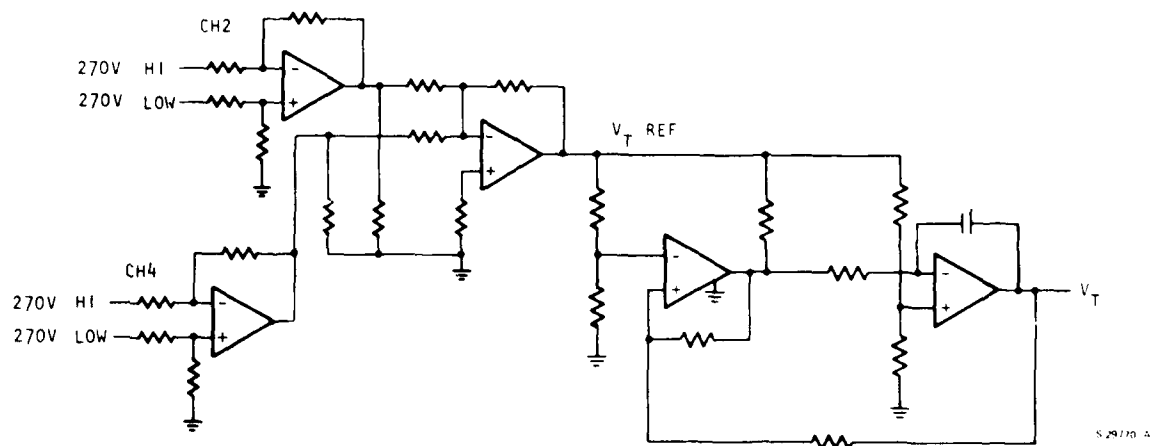
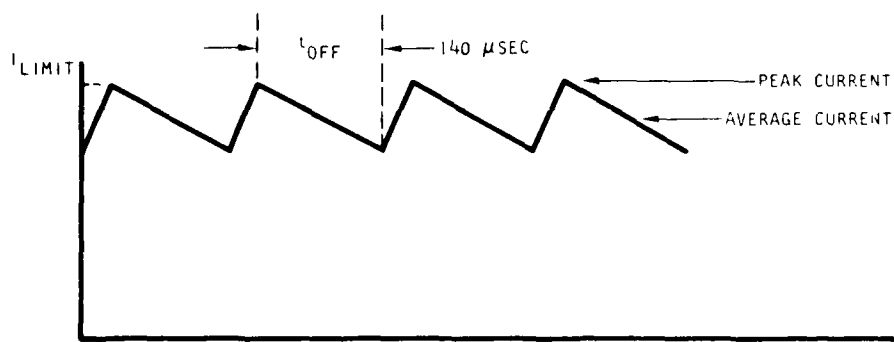
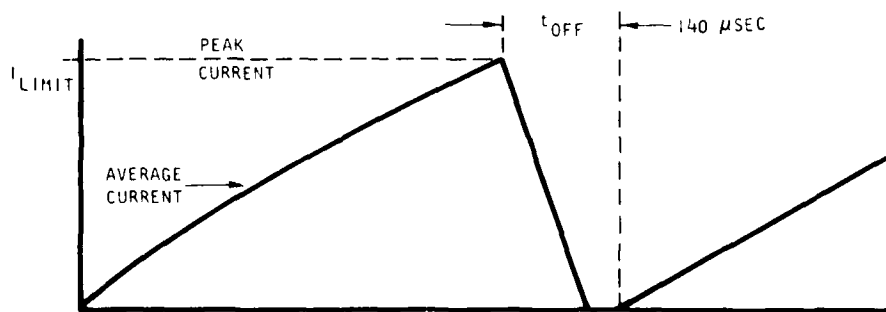


Figure 32. Triangle Wave Generator



a. CURRENT LIMIT AT LOW MOTOR SPEED



b. CURRENT LIMIT AT HIGH MOTOR SPEED

S 48283

Figure 33. Baseline Control Current Limit Waveforms

Circuits were redesigned to operate from the average motor current (average motor torque). The average motor current (motor current limit) information is now directed to the PWM block, shown in Figure 30. This information is used to control on average current through the top transistors. Figure 34 shows the typical waveforms for the improved current limit control. This figure shows that the average current (average torque) at current limit is approximately the same for either high or low motor speed operation.

The current limit information for a motor operating in the plug mode is still directed to the sequence, control, and inhibit logic block shown in Figure 35.

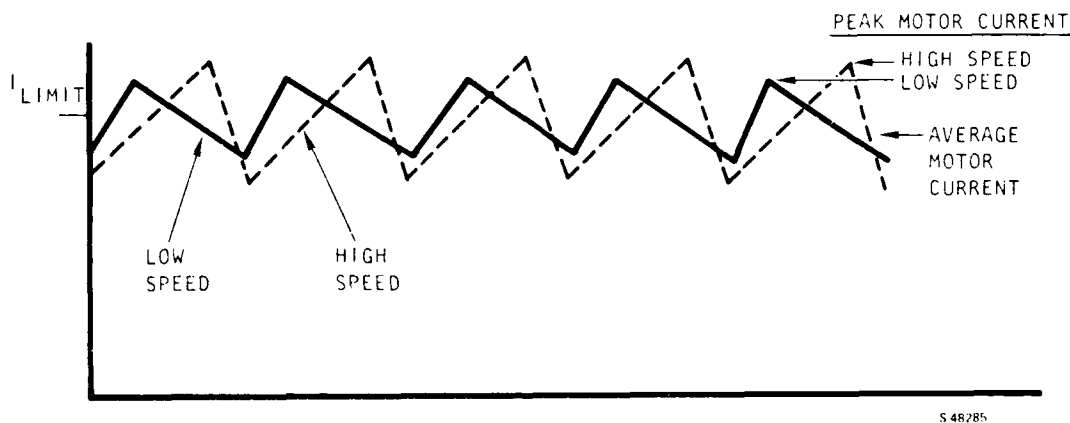


Figure 34. Typical Current Waveforms for Improved Controller in Current Limit

The PWM information is directed to the top transistor control logic (INHIBIT), and the plug limit information is directed to the bottom transistor control logic (ENABLE). This was done to provide low common mode voltage for the plug current sense resistor, as shown in Figure 36. This required that the functions of the top and bottom transistors be exchanged.

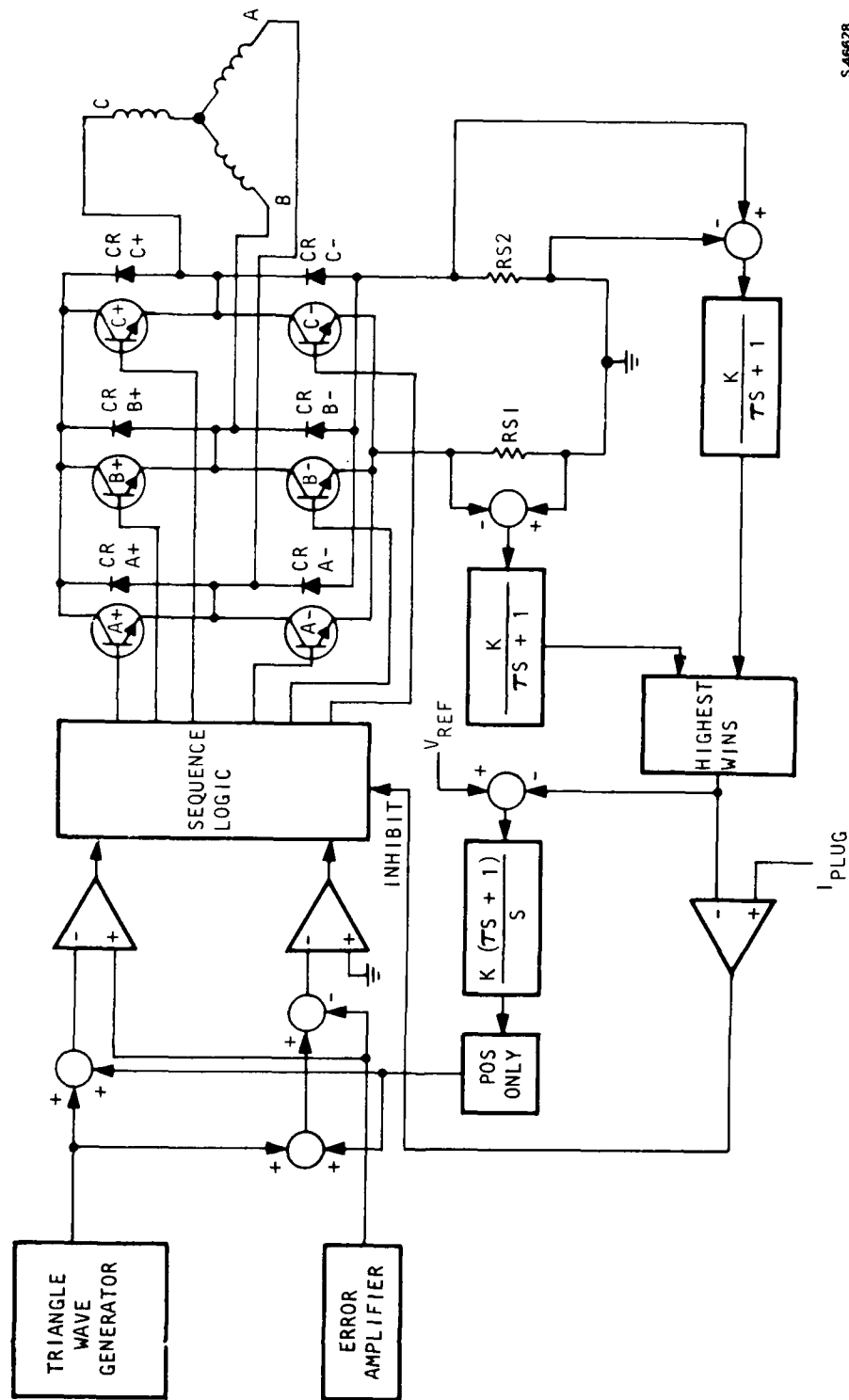
3.2.3 Current Limit

The controller includes two current limits--one for the condition of the actuator moving toward the commanded position (normal drive mode), and one for the braking and reversing of the actuator (plug mode).

Figure 36 presents the current limit block diagram. For normal operation of the transistor bridge, one pair of transistors is used at a time. The upper transistor (+) is pulse width modulated and the lower transistor (-) is



Figure 35. Sequence, Control, and Inhibit Logic



S 46628

Figure 36. Current Limit Forward and Plug Reverse

turned on to provide a return path to ground. For example, if A+ is modulated and B- is turned on (see Figure 36), the current path is from V supply through A+, through the motor windings A-B, through switch B-, and through RS1 to ground. When A+ is switched off, the current path changes. Current flows from ground through RS2, diode CRA-, motor windings A-B, switch B-, and through RS1 back to ground. The current in RS1 is the current that flows through the motor. Therefore, the voltage across RS1 is proportional to motor current.

During normal operation, the voltage across RS1 (motor current) is sensed, filtered, and compared with a reference. When the sensed current is greater than the reference, the result is integrated and subtracted from the error voltage in the PWM block of Figure 30, reducing the pulse width and therefore the motor current.

The effect of this action is to limit the average motor current to the reference level by reducing the applied motor voltage by lowering the duty cycle of the pulse width. The peak motor current and current ripple around the average level will depend on the motor load and motor speed (Figure 34).

For operation of the transistor bridge during plug mode, one pair of transistors is used at a time. Again, as for the normal drive mode, the upper transistor (C+) is controlled in a PWM mode and the bottom transistor (B-) is turned on to provide a return path to ground. The voltage across the motor winding is the sum of the 270-vdc line and the generated motor voltage. The high voltage causes a rapid rise in current in the motor, which also goes through RS1. The sensed voltage across RS1 is used to turn off the top transistor, as previously described.

The current path, after C+ is turned off, is from motor winding C through motor winding B, through transistor B-, through RS1 and RS2, and returns through diode (CR) C- to motor winding C.

When the current through RS2 is greater than a reference value, transistor B- is turned off. The current path is then modified as follows. From motor winding C, the current follows through winding B, through diode (CR) B+, through the 270-vdc source to ground, through RS2, and through diode (CR) C- to return to winding C. Therefore, the current flow in RS2 is the motor current in the plug mode.

The voltage across RS2 is sensed, filtered, and compared with a reference. When the current is greater than the reference, the result is to switch a comparator low, which turns off the bottom transistor and reduces the flow of motor current. When the current goes below the reference, the comparator then switches high, turning the transistor back on. This effectively causes the motor winding to be shorted, which increases the current and the braking torque.

3.2.4 Surface Position Sensing

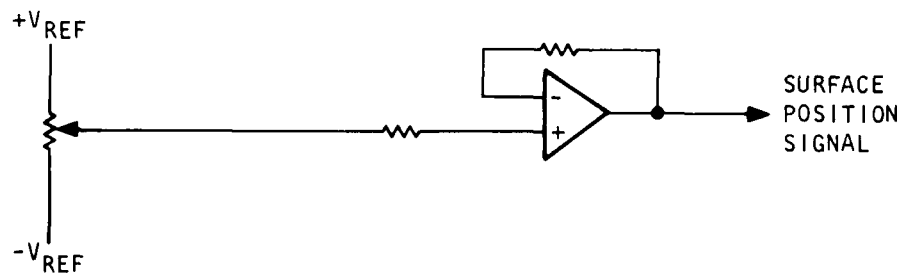
To simplify sensor to controller interfaces, the 12-bit digital rotary shaft encoder and D/A converter were replaced with a potentiometer and buffer (see Figure 37). The potentiometer is mechanically connected to the actuator in a manner similar to that used for the encoder.

3.3 NEW POWER SWITCH DESIGN

The following text describes the modifications for 30-amp (average) operation for the power switch. Figure 38 shows the power switch circuitry. The following circuits were modified in the power switch circuitry: power transistors, predriver circuit, and voltage clamp network.

3.3.1 Power Transistors

The new power switch design was based upon achieving an average current load of 30 amp to the motor. The transistors used in the original design (Motorola MJ10016) were rated at 50 amp and approximately 500 v. A new transistor was selected that provided additional margin for current capacity and thermal power dissipation. Selection was based on known availability of solid-state devices; AiResearch testing of devices; and previous experience in this area by NASA-JSC during sponsorship of contract NAS 9-14952 for the electromechanical flight control actuator. Figure 39 presents candidate power switching devices evaluated by AiResearch during this and other development programs. The Westinghouse D60T, which was used by NASA, was selected primarily because of availability and the satisfactory experience of NASA in the development of similar power service applications. Power VMOS devices also were considered, but were rejected because the available devices did not have both high voltage and high current capability needed to satisfy this application.



S 46626

Figure 38. Surface Position Sensing Circuit

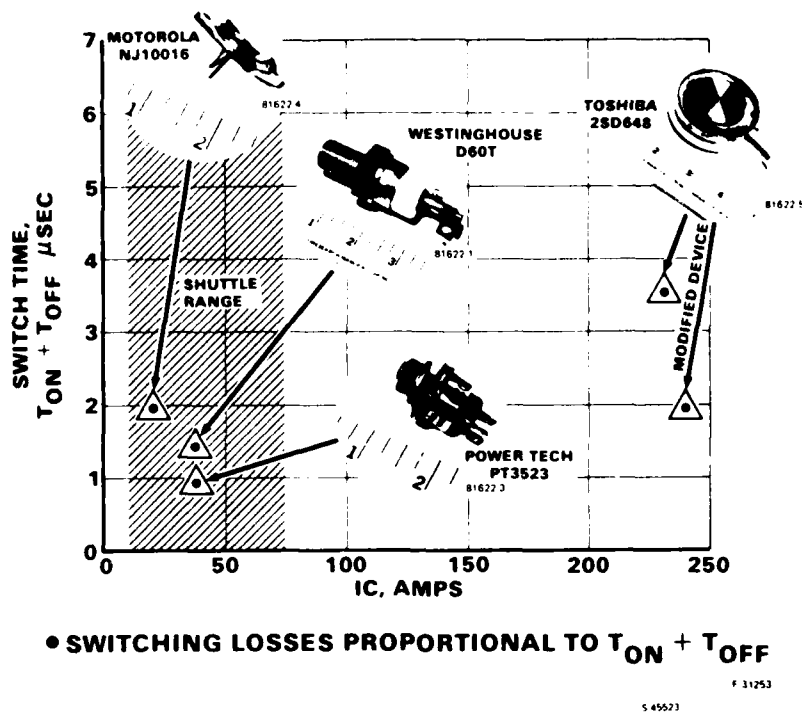


Figure 39. Transistor Comparison

The 2N6547 transistor was combined to make a discrete darlington with the Westinghouse transistor. This increased the gain and reduced power loss in the predriver section.

3.3.2 Predriver Circuit

The predriver section has been redesigned, providing faster transitions and improved efficiency. Vmos transistors are used where bipolar transistors were used to switch the power transistors. Cmos open collector logic can operate the Vmos transistors, and small power signals can operate Cmos logic. With the Cmos and Vmos technology in the predriver section, the circuits operate faster and more power efficiently than the ones developed under the original contract.

The logic performed by the predriver section has also been improved. In the original predriver section, the light-emitting diode (LED) in the opto-decoupler must be turned on to turn the power switch off. In the improved predriver section, the LED in the opto-decoupler must be turned off to turn the power switch off. The power switch will therefore be off if the input lines to the predriver section are disconnected.

3.3.3 Design

The flyback diodes (see Figure 37) protect the power transistors from voltage spikes caused by the inductive load of the motor windings. These

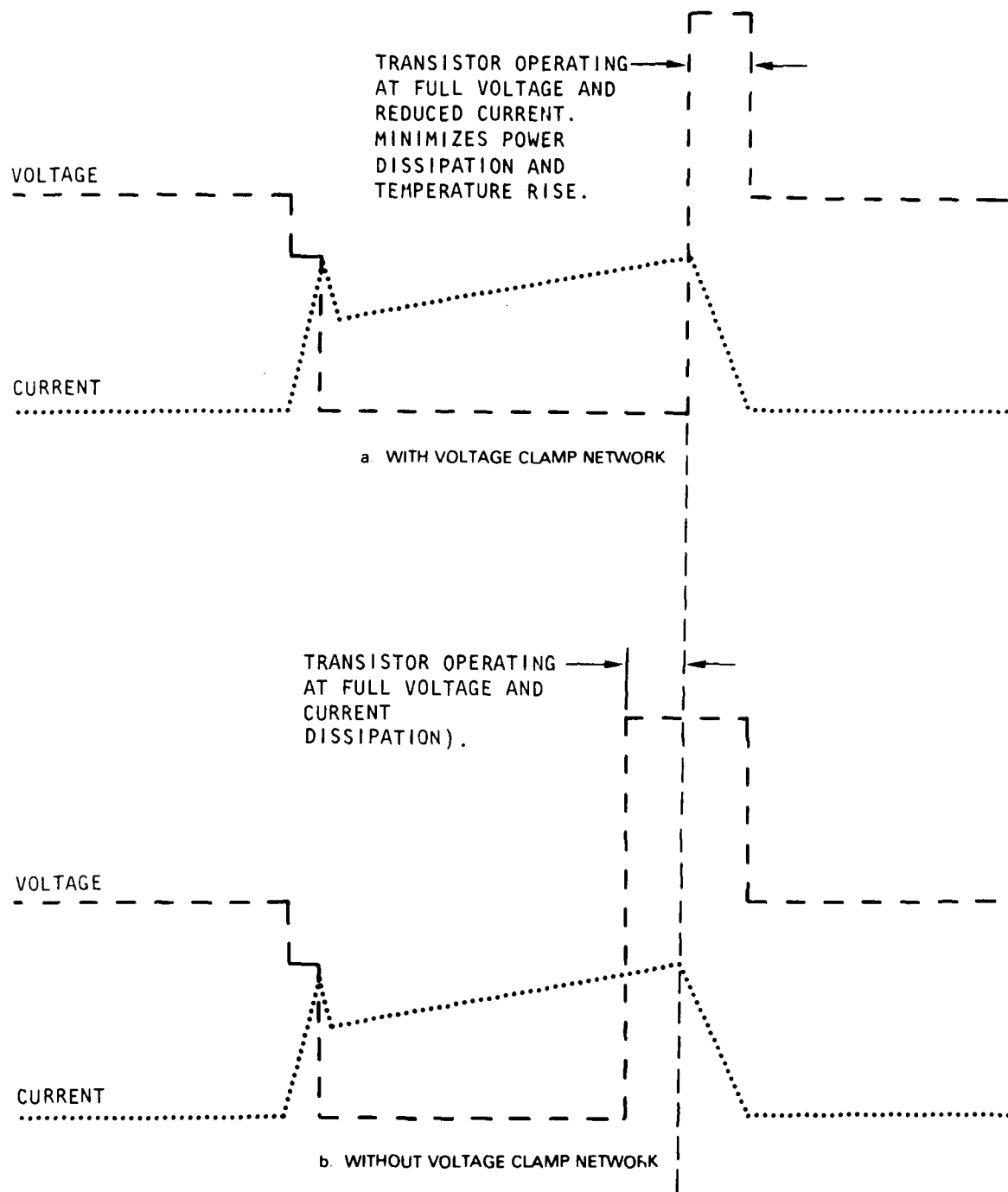
transient voltages can exceed the high side of the 270-v line or be below the low side of the 270-v line, which could result in destroying the power transistors. The flyback diodes limit the motor winding voltage to seven tenths of a volt above the high side of the 270-v line, or seven tenths of a volt below the low (or ground) side of the 270-v line. There is a suppression circuit (see Figure 37) across the flyback diode that stores transient energy during the time it takes to turn the flyback diode on. Once the flyback diode turns on, the energy in the suppression circuit is dissipated across the flyback diode.

When the power transistor is being turned off, a voltage clamp network slows the voltage rise across the power transistor until the current through the transistor starts to decay. If this network was not there, the voltage across the transistor would go to full line voltage (270 vdc) before the current through the transistor was turned off. This is shown by comparing the two voltage/current waveforms in Figure 40. This would result in a large power loss in the transistor that would cause eventual destruction of the transistor through overheating. If the voltage across the transistor were delayed until the current starts to decay, the power loss in the transistor is significantly lower (see Figure 40). Figures 41 and 42 are actual pictures of the power transistor turnoff and turnon characteristics.

Figures 43 and 44 present views of one of the power switch assemblies used to drive one servomotor. The D60T transistors are mounted on each of the finned aluminum heat sinks. Predriver circuits and power supplies complete the assembly. The predriver and power supplies are located close to the switches to minimize lead length.

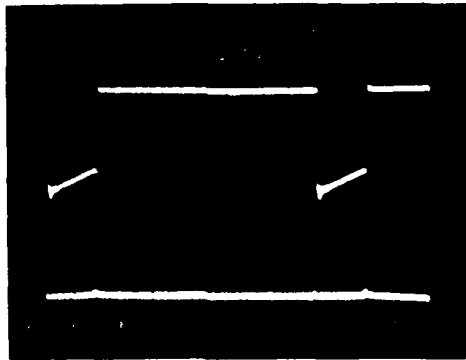
Figure 45 shows the assembled power switch being tested in the laboratory prior to interfacing with the servomotor. This tester can evaluate transistor performance over wide ranges of voltage, current, and switching speed.

Figure 46 shows the modified 2-channel, rack mounted, controller breadboard. The 2-power switch assemblies are located in the upper rear portion of the console.

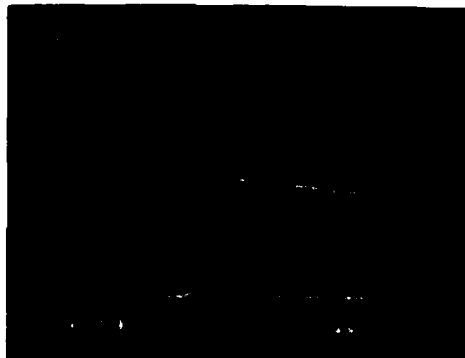


S 48284

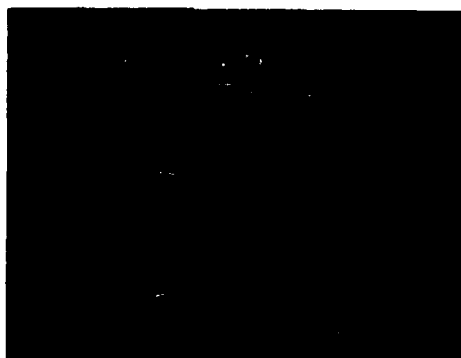
Figure 40. Power Transistor Current and Voltage Waveform



a. OVERALL PERIOD



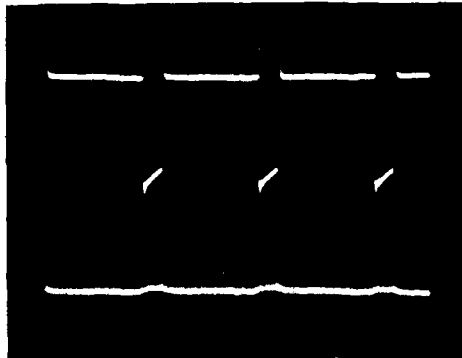
b. TURN-ON



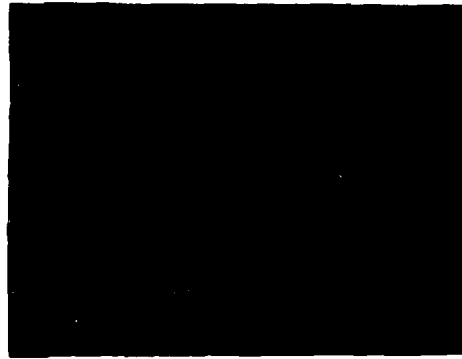
c. TURN-OFF

Figure 41. Transition of Top Transistor,
B Phase, 10 Amp per Division

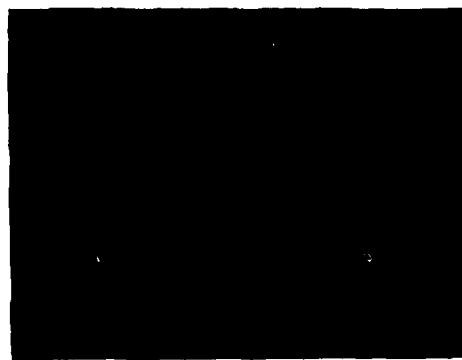
F-31360



a. OVERALL PERIOD



b. TURN-ON



c. TURN-OFF

F-31361

Figure 42. Transition of Bottom Transistor,
B Phase, 10 Amp per Division

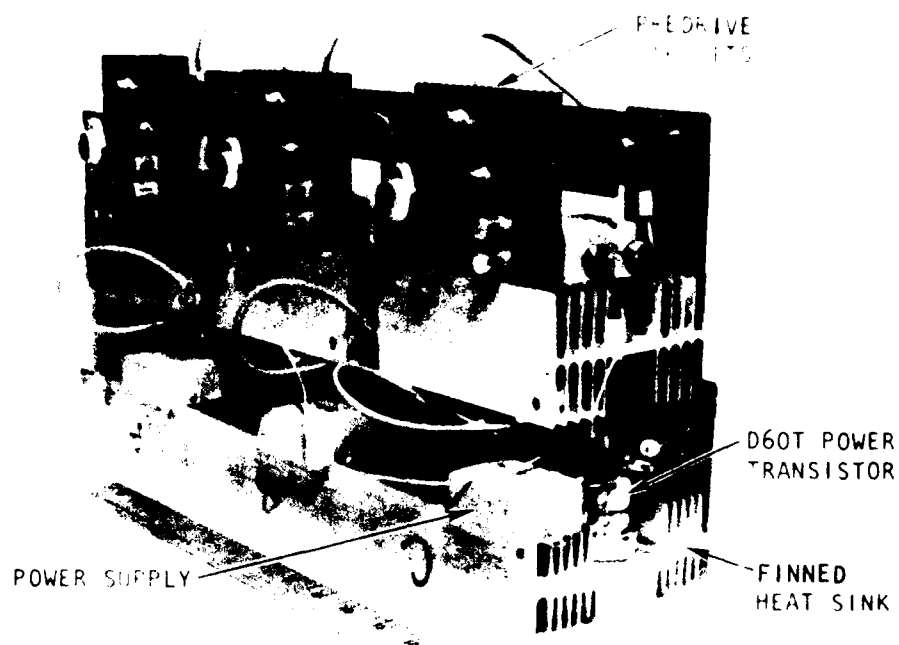


Figure 43. Power Switch Unit, Side View

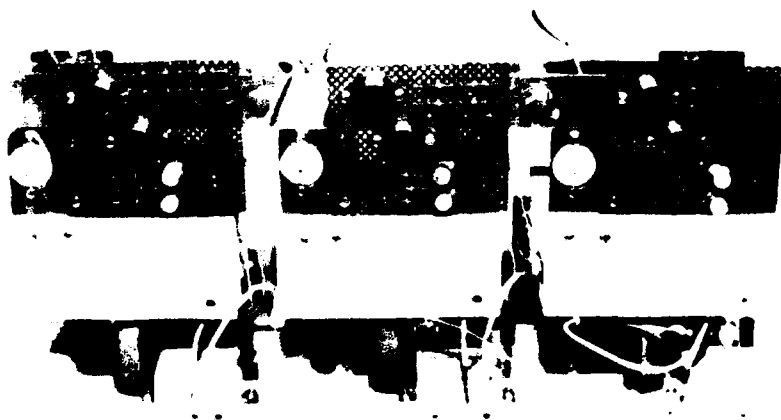


Figure 44. Power Switch Unit, Front View

F-31366

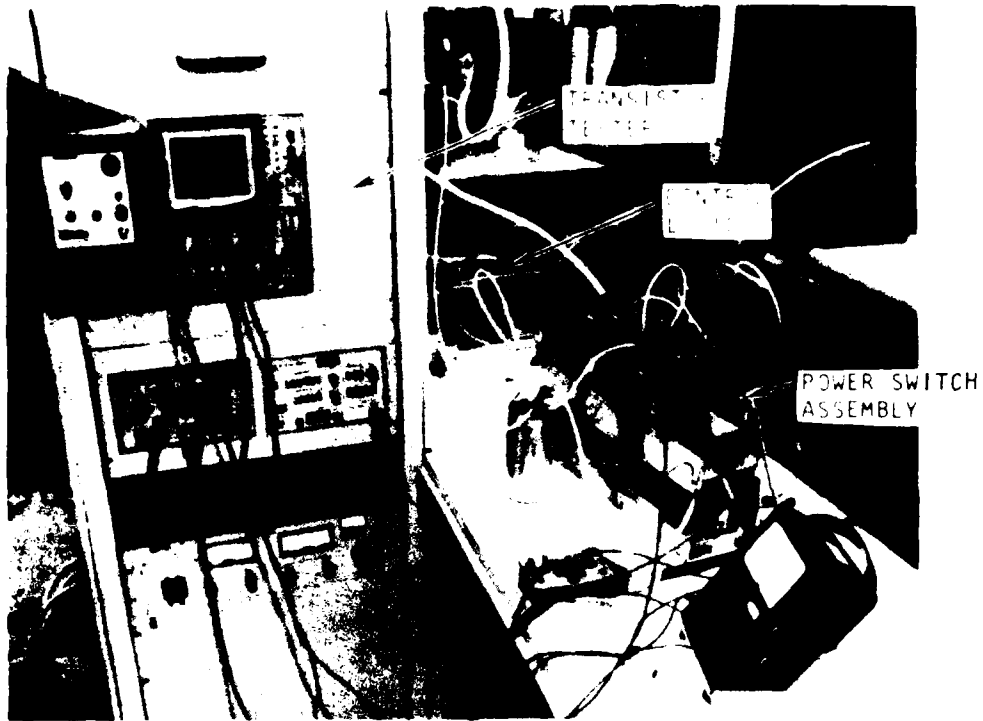


Figure 45. Power Switch Assembly, During Checkout

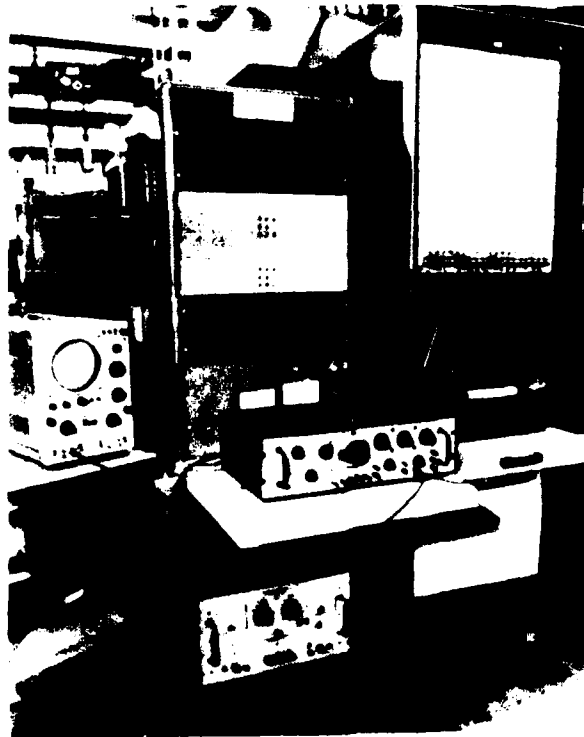


Figure 46. Two-Channel, Rack-Mounted Controller Breadboard

4. DETAILED ANALYSES

The analysis required for this program was divided into three categories: (1) thermal prediction; (2) mission duty cycle determination; and (3) figure of merit determination. The following text will discuss these categories in detail.

4.1 THERMAL PREDICTION

Transient and steady-state thermal analyses of the hingeline actuator motor presented in Reference 1* were performed. The original thermal model was modified to reflect the as-built configuration of the components. The model was used to predict the thermal performance of the motor at various operating conditions.

The purpose of this analysis is to evaluate the thermal capability of the motor. The thermal model used in the computer analyses is presented in Figures 47 through 50.

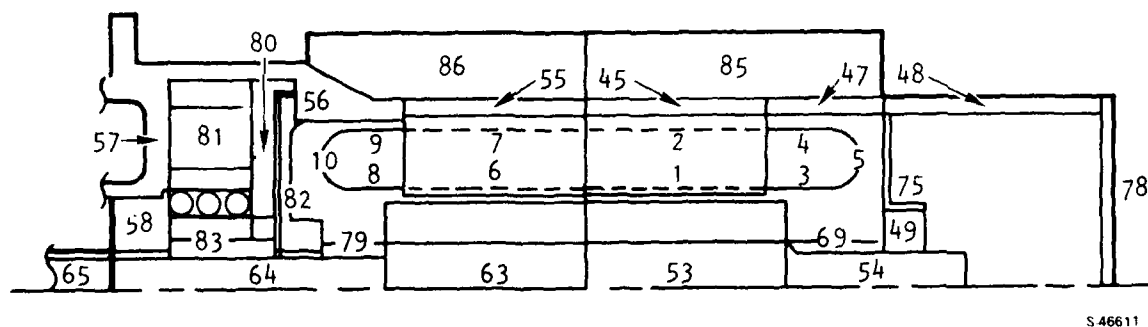
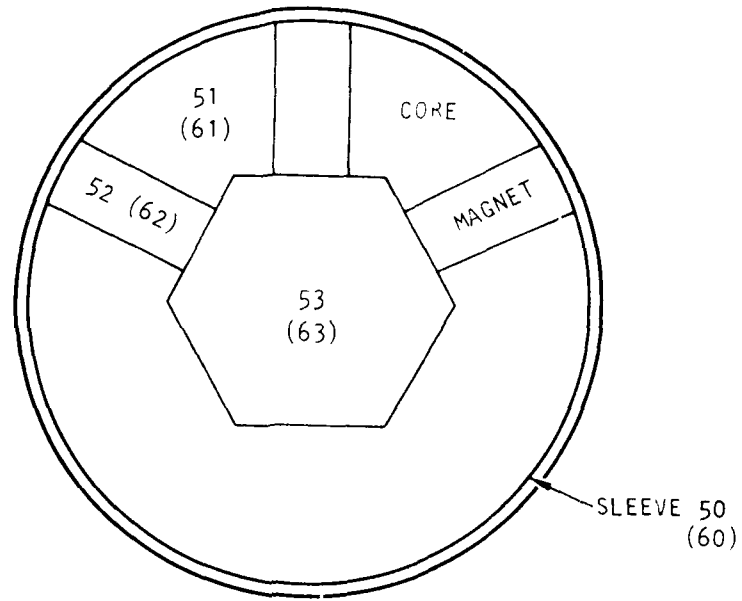


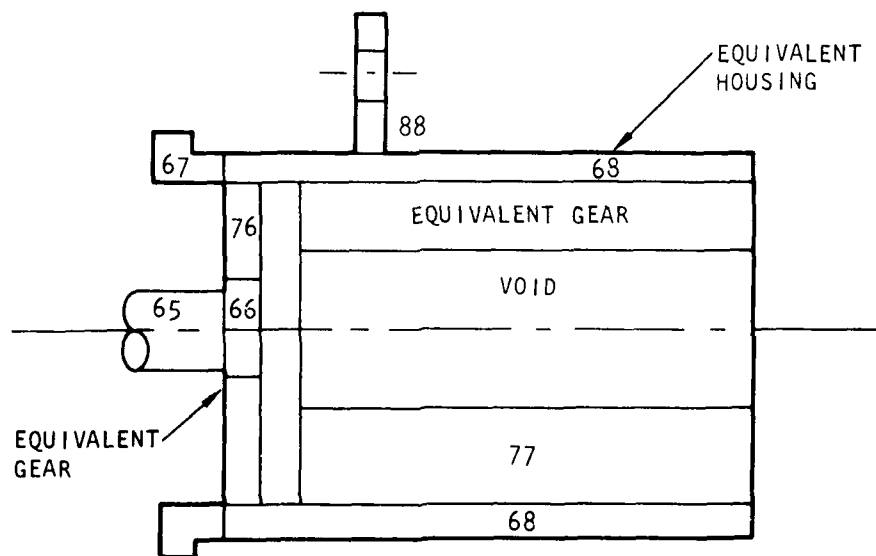
Figure 47. Actuator Motor Thermal Model

*Electromechanical Actuation Development, AFFDL-TR-78-150, December 1978, pp. 229 through 236.



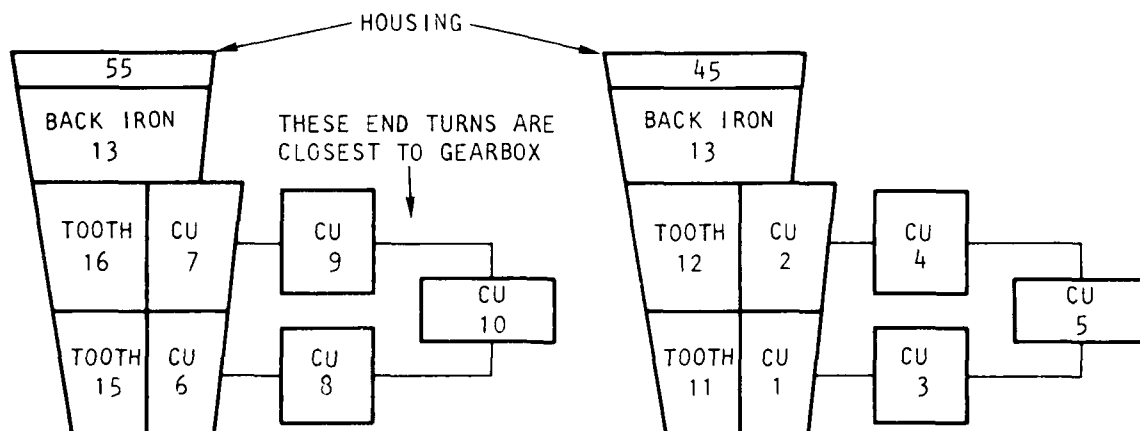
S 46904

Figure 48. Rotor Thermal Model



S 46612

Figure 49. Simplified Thermal Model of Gearbox



S 46613

Figure 50. Motor Stator Windings Thermal Model for Transient Analysis

4.1.1 Thermal Conditions

The operating conditions used in the analysis are:

- Ambient temperature = 80°F.
- 270 volts, 8,000 rpm. Resistance = 0.967 ohms at 200°F.
- Brake coil loss = 15.2 w at 100 v and 200°F.

The detailed electrical losses and gearbox loss are tabulated in Table 3. The gearbox loss at continuous duty cycle was assumed to be approximately 15 percent of the motor input power ($I \times V$). This is consistent with the torque efficiency determined by test from the earlier development effort (Reference 1). The copper loss is given at 200°F, and the computer program adjusts the copper loss as a function of the predicted temperature.

4.1.2 Results

The predicted motor hot spot temperatures are summarized in Figures 51 and 52. As expected, the hot spot temperatures occur at the stator end turn near the gearbox. The steady-state motor hot spot temperatures, as function of current and gearbox loss, are presented in Figure 51. Figure 52 shows the transient hot spot temperature response at different current levels with maximum gearbox loss (15 percent of $I \times V$).

TABLE 3

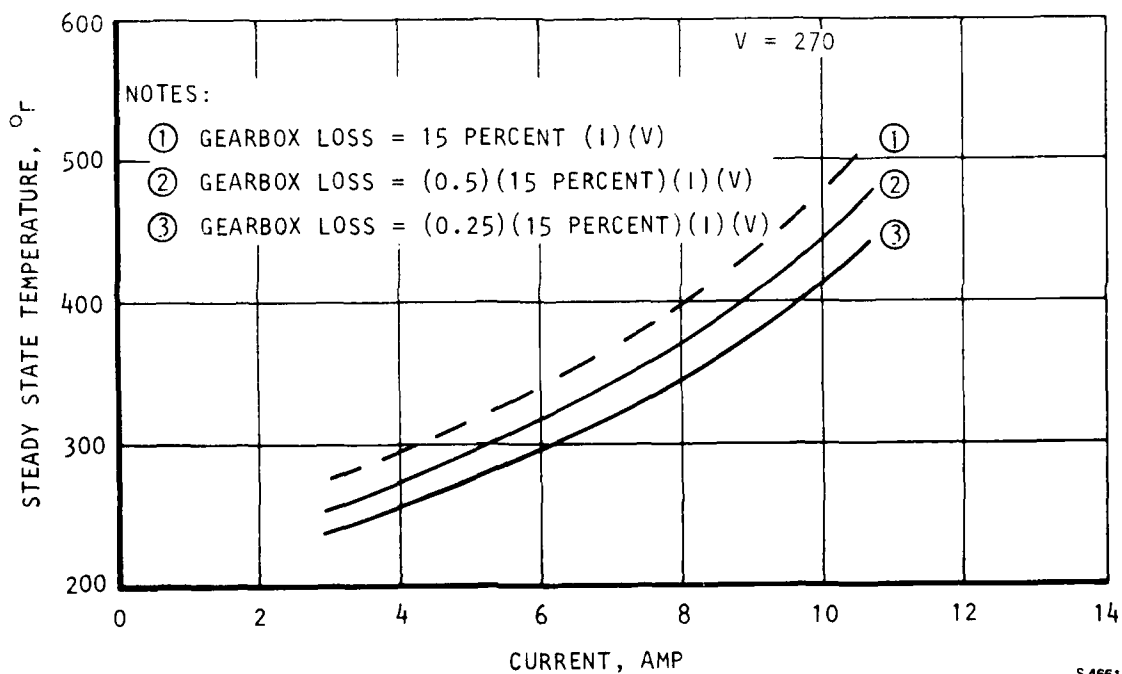
POWER LOSS FOR WPAFB HINGELINE ACTUATOR MOTOR THERMAL ANALYSIS

I Amp	Q1 I ₂ R at 200°F	Stray 10 percent, Q1	Tooth	Back Iron	Rotor 2.5 percent, Q1	Gearbox 15 percent, V
4	15.5 w	1.6 w	47 w	33 w	0.4 w	162 w
6	34.8	3.5	47	33	0.87	243
8	62.0	6.2	47	33	1.5	324
10	96.7	9.7	47	33	2.4	405
15	217.0	21.7	47	33	5.4	608
20	387.0	38.7	47	33	9.7	810

NOTE: V = 270 v; 8,000 rpm

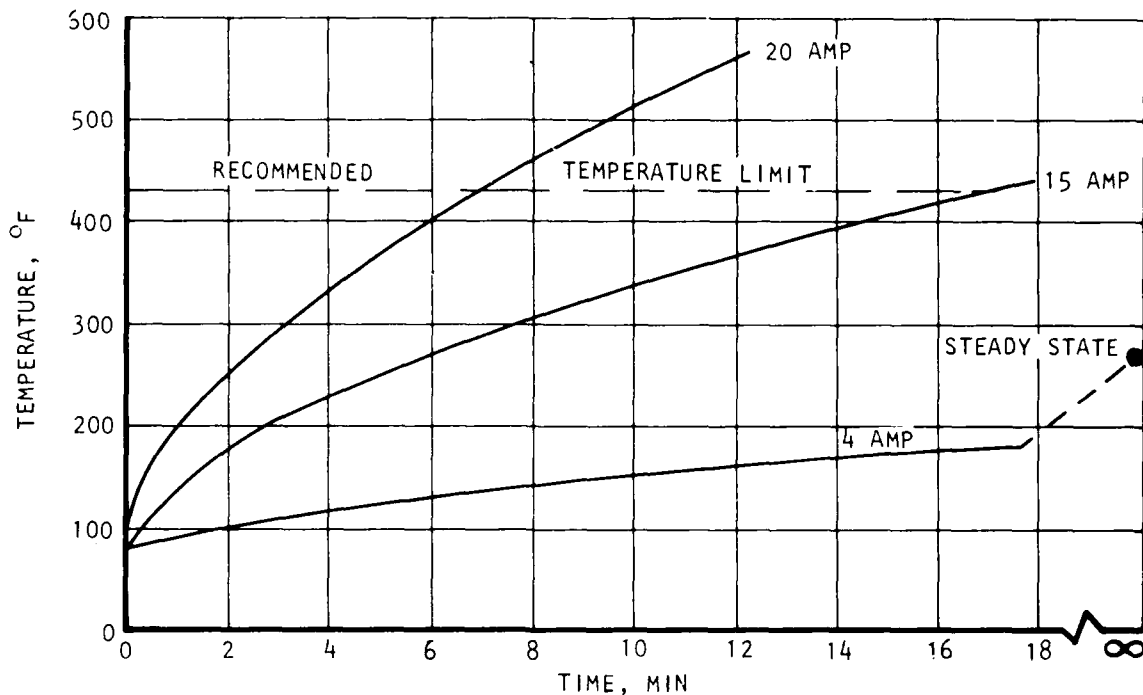
Brake Coil Loss = 15.2 w at 100 v, 200°F

R Winding = 0.967 ohms at 200°F



S46617

Figure 51. Predicted Hot Spot Motor Winding Temperatures for Hingeline Actuator Motor (Node 10)



S 46615

Figure 52. Predicted Hot Spot Motor Winding Temperatures for Hingeline Actuator Motor (Node 10)

4.1.3 Computer Analyses Conclusions

It can be concluded from the computer analysis that Figures 51 and 52 can be used as guidelines to optimize the operating conditions on the existing unit.

4.2 MISSION DUTY CYCLE DETERMINATION

Three representative duty cycles, typical for an aircraft hingeline actuation system, have been synthesized. The following is a discussion of each duty cycle. These duty cycles were input to the thermal model.

Figure 53 shows the load spectrum for a full-time maneuvering leading edge system. This data was derived from the F-16 and F-18 maneuvering leading edge programs. Based on the present demonstration system, 100 percent load is equivalent to 37,575 lb-in. Therefore, the approximate root mean load (see Figure 53) of 25 percent is equivalent to 9400 lb-in.

Since the 37,575 in.-lb torque corresponds to 16-amp maximum current to the motor, the equivalent motor current required to provide 25 percent level is equal to 4 amp. The hot spot temperature history for this level condition is shown in Figure 52. The steady-state maximum temperature is 270°F, well below the maximum allowable motor winding temperature of 430°F.

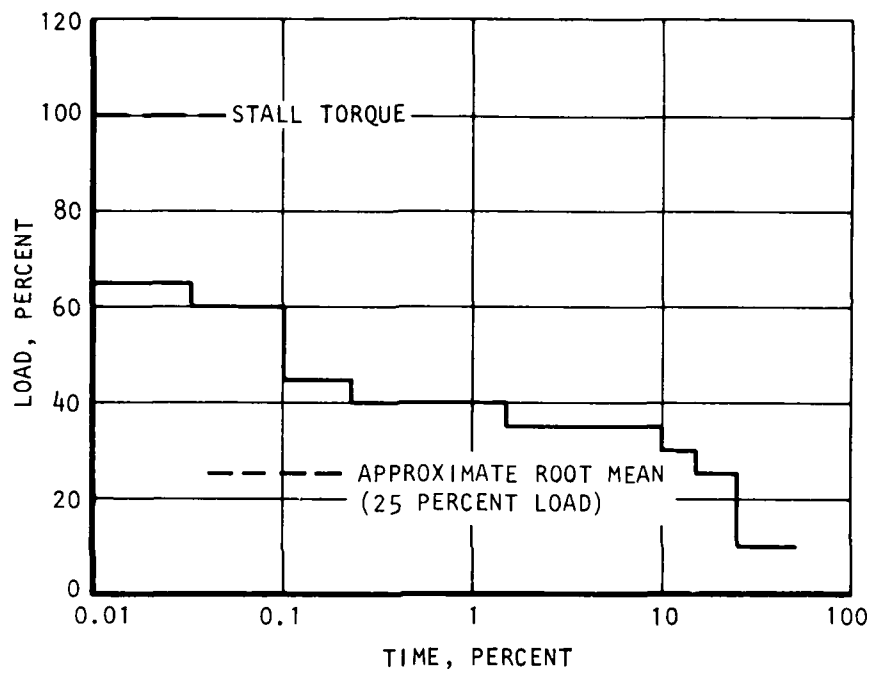


Figure 53. Load Spectrum for Full Time Maneuvering Leading Edge Systems

4.3 FIGURE OF MERIT DETERMINATION

An analysis was conducted to provide a simple yet complete method of relating control surface operating requirements to motor current required to operate into the loads. The analysis approach includes both aiding and opposing aerodynamic loads, inertias of the control surface and motor, gear ratio, and definition of a probable duty cycle. The analytical approach is described in detail in the Appendix. Using the procedure presented in this Appendix, the following problem statement is analyzed.

Problem Statement

Load spring rate, K_L (in.-lb-deg ⁻¹)	130
Load inertia, J_L (in.-lb-sec ²)	2.5
Input amplitude, A (deg)	± 1
Gear ratio, GR	605
Forward efficiency, η	0.78
Reverse efficiency, η	0.70
No. of motors, n	2
Motor inertia, J_m (in.-lb-sec ²)	9.95×10^{-4}
Torque constant, K_T (in.-lb-amp ⁻¹)	1.625
Current limit, I_{LIM} (amp)	30

Three frequencies (2, 4, and 8 Hz) were input into the analyses to determine the corresponding motor currents.

The results of analysis are as follows:

<u>Duty Cycle, Hz</u>	<u>Motor Current, Amp</u>
a. 2	2.0
b. 4	7.4
c. 8	23.1

The 23.1-amp current required to provide 8-Hz frequency correlates with test data gathered at 8 Hz while monitoring temperature histories of motor components. The analysis can therefore be verified.

5. TEST EQUIPMENT

5.1 SPECIAL TEST EQUIPMENT AND FIXTURES

The hingeline actuation unit was tested using a test stand to support the actuator and to simulate the aircraft structural interfaces. The test stand also included a spring load to simulate aerodynamic loading of the actuator. An electric supply was set up to provide 270-vdc power to the controller and the motor. To accommodate environmental testing, (1) a thermal chamber for the actuator was constructed, and (2) the motor and actuator were instrumented to monitor external temperatures. These test and support hardware items are described below.

5.1.1 Test Stand

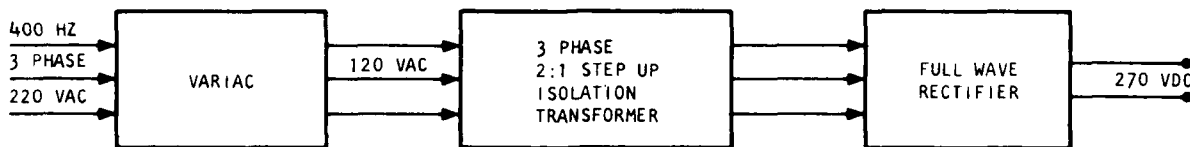
The test stand was designed to interface with the actuator assembly in a manner similar to an aircraft installation. The test stand provides for mounting of the position feedback device (potentiometers) at the extreme end of the simulated control surface interface.

The output of the actuator mates to a 10-in.-long arm, which allows interface with the load spring assembly. The springs simulate linear aerodynamic loading.

5.1.2 Power Supply

The electrical power distribution system is comprised of a primary power source, a 3-phase setup isolation transformer, and a full-wave rectifier. The power supply is shown in Figure 54.

The dc voltage output of the power supply is sensitive to the output demand. Variations as high as 20 percent were observed under loaded conditions. Although this fluctuation is a large one, frequency response and performance requirements were met. Standardization of test conditions would be improved, however, if a power source was used that did not exhibit the voltage variation as a function of power demand. A reduction in the power supply voltage may reduce the maximum actuator output rate.



S 25911

Figure 54. Block Diagram of the Power Supply

5.1.3 Thermal Chamber

A thermal chamber was constructed to enclose the actuator/motor portion of the hardware unit. The thermal chamber shown in Figure 55 is comprised of an insulated sheet metal box that is parted on opposing sides to allow circulation of heated or cooled air. The temperature extremes of the chamber were -65°F and $+250^{\circ}\text{F}$.



Figure 55. Thermal Chamber

5.1.4 Actuator/Motor Temperature Monitoring

The thermal model developed under the original contract (see Section 4) was reviewed and updated to fully evaluate the actuator/motor assembly when exposed to high ($+250^{\circ}\text{F}$) and low (-65°F) temperature environments.

Preliminary results of the thermal analysis defined the placement of temperature instrumentation installed on one of the motors. Figure 56 illustrates the arrangement of the thermal instrumentation that was installed. Thermal testing results are presented in Section 7.

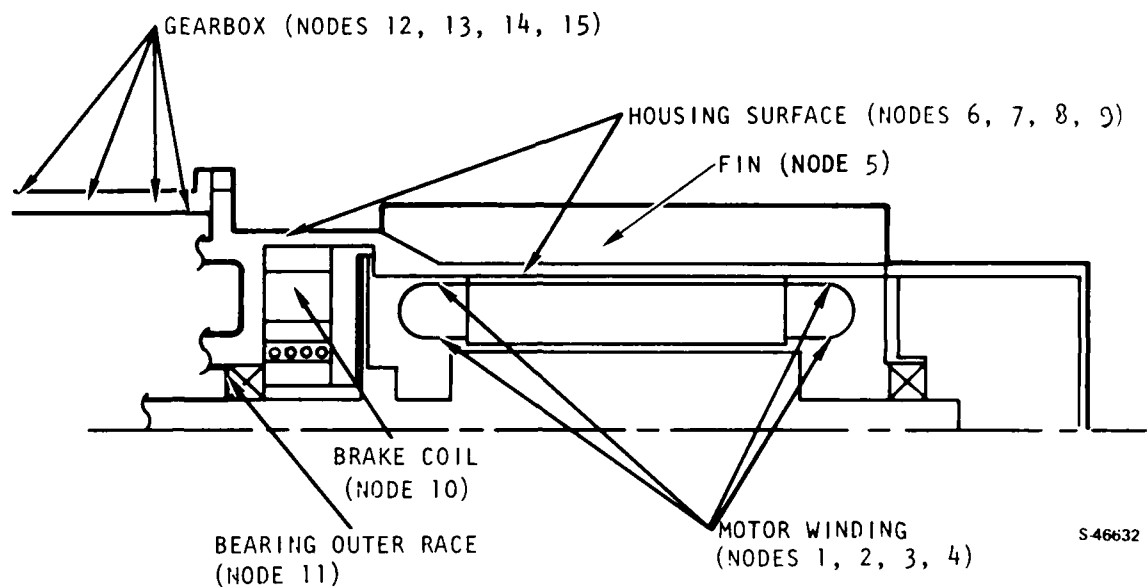


Figure 56. Arrangement of Thermal Instrumentation

Figure 57 is a photograph showing the placement of the thermal instrumentation. Detail views of these placements are shown in Figure 58 as follows: motor end bell (a); stator assembly (b); and rotor assembly (c).

5.2 FACILITIES

AiResearch Manufacturing Company of California provided all engineering and testing facilities required for the rotary hingeline actuation unit test program.

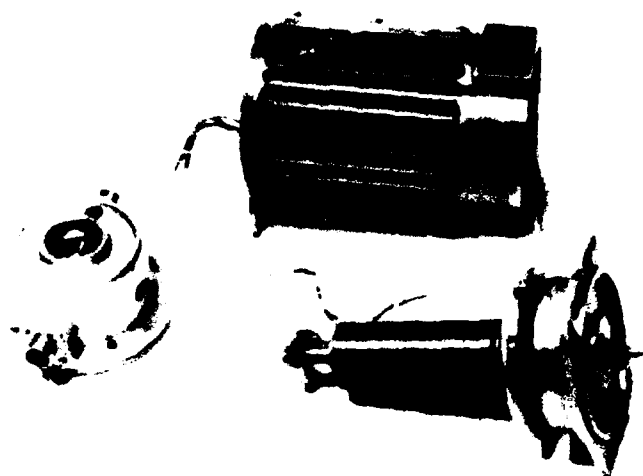
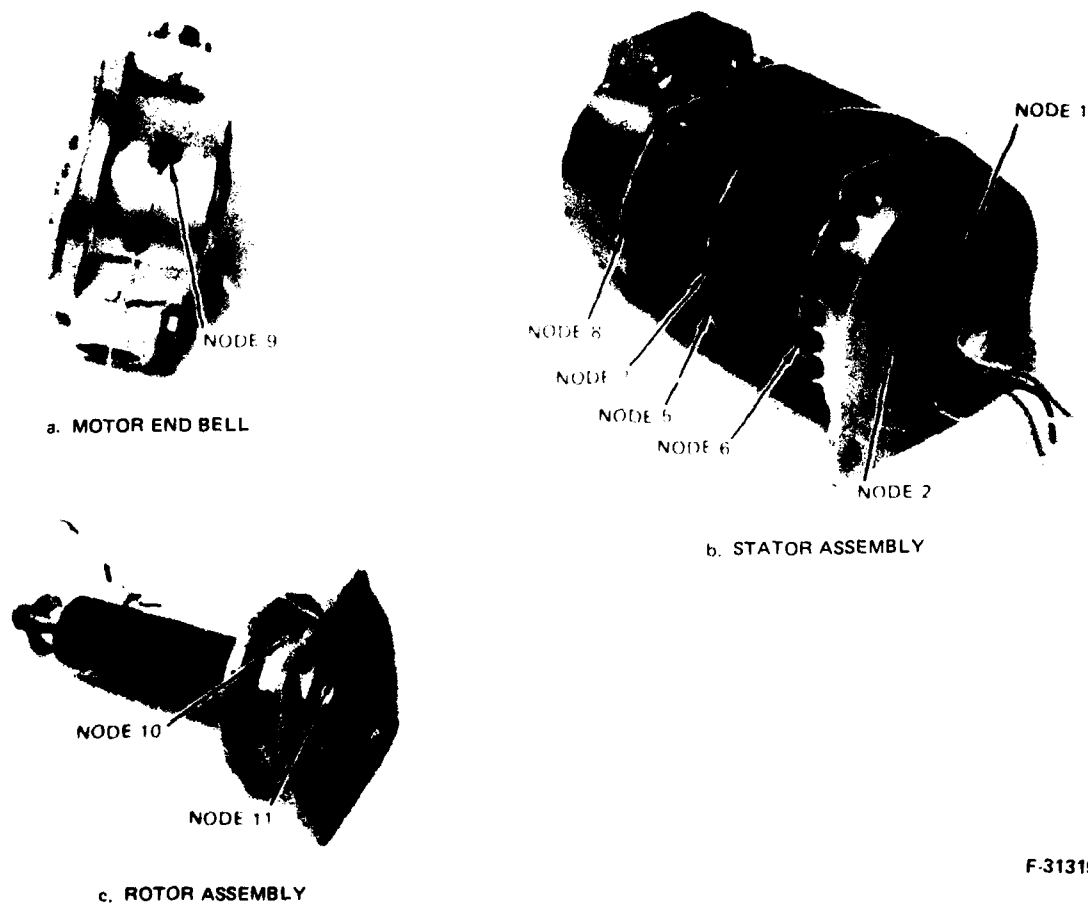


Figure 57. Thermal Instrumentation Placement



F-31315

Figure 58. Detail Placement Views

6. TESTING

This section presents the detail descriptions of each test performed for the contract amendment. Individual test briefs summarizing setup, procedures, and required data also are presented. The testing portion was divided into four specific tests as follows:

- (a) Extended temperature
- (b) Extended current limit
- (c) Power supply voltage variation
- (d) Duty cycle capability

Results of these tests are presented in Section 7 of this report.

6.1 EXTENDED TEMPERATURE TEST

The objective of this test was to demonstrate system operation at selected ambient temperatures, and to compare performance data with data gathered from room temperature tests. Frequency response tests were conducted after stabilization of the motor/actuator at ambient temperatures of -65 and +250°F. The actuation unit will then be subjected to loads of 0, 10, and 20 percent of stall torque capability. The test brief is shown in Figure 59.

The test setup is shown in Figure 60. The environmental chamber was constructed of aluminum, with foam insulation bonded to the outside. Figure 61 shows the chamber closed around the actuator and connected to the temperature conditioning unit. Temperature conditioned air is circulated by the unit through insulated ducts, to the insulated enclosure, and back to the unit for recirculation.

TEST 1
EXTENDED TEMPERATURE

Prepared by: _____
Part No. _____
Date _____

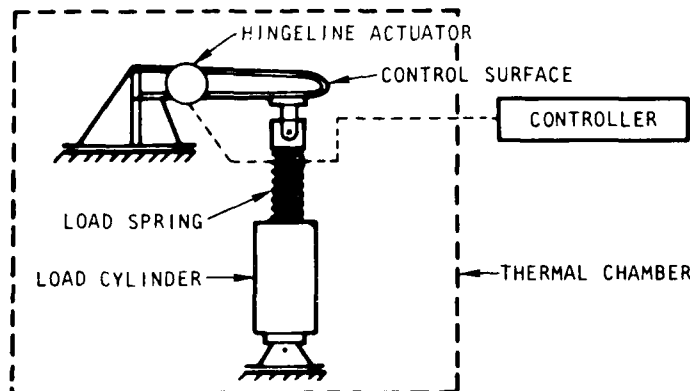
OBJECTIVE

TO DEMONSTRATE ACCEPTABLE SYSTEM PERFORMANCE AT
SELECTED AMBIENT TEMPERATURES.

FACILITY

ELECTROMECHANICAL
LABORATORY

SCHEMATIC



**EQUIPMENT AND
INSTRUMENTATION**

- 1) THERMAL CHAMBER
- 2) LOAD SYSTEM
- 3) OSCILLOGRAPH
- 4) SIGNAL GENERATOR
- 5) POSITION INDICATOR
- 6) REACTION FIXTURE

PROCEDURE

- 1) APPLY SINUSOIDAL INPUT COMMANDS OF ± 1 DEG AMPLITUDE TO THE ACTUATOR WITH LOADS OF 0, 10, AND 20 PERCENT.
- 2) SUPERIMPOSE INPUT COMMAND RATES OF 0.5, 1, 2, 4, 6, 8, AND 10 HZ.
- 3) REPEAT 1 AND 2 FOR -65 AND $+250^{\circ}\text{F}$.

REQUIRED DATA

- | | |
|------------------------|------------------------------------|
| 1) AMBIENT TEMPERATURE | 5) OUTPUT AMPLITUDE |
| 2) INPUT RATE | 6) OUTPUT LOAD |
| 3) INPUT AMPLITUDE | 7) MOTOR AND ACTUATOR TEMPERATURES |
| 4) OUTPUT RATE | |

ACCEPT/REJECT CRITERIA

TEST DEMONSTRATION ONLY

NOTES

DATA TO BE CORRELATED WITH PREDICTED MOTOR
PERFORMANCE VARIATION WITH TEMPERATURE.

S-95237

Figure 59. Extended Temperature Test

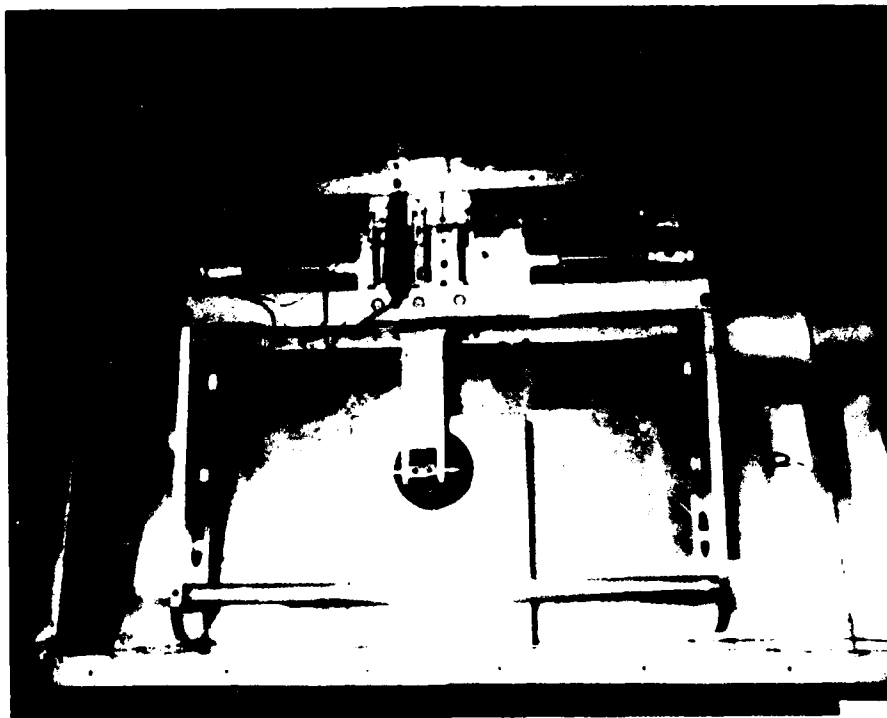


Figure 60. Actuator Installed in Environmental Enclosure



Figure 61. Actuator During Temperature Testing

F-31365

6.2 EXTENDED CURRENT LIMIT TEST

The objective of this test was to evaluate the frequency response of the actuation unit as a function of current limit setting. The peak current limit will be set at 20, 25, and 30 amp. At each current limit setting, frequency response data will be recorded at loads of 0, 10, and 20 percent. These tests will be conducted at room ambient temperature. One frequency response data run will be made at 30-amp current limit and at 250°F unloaded. The test brief is shown in Figure 62.

6.3 POWER SUPPLY VOLTAGE VARIATION TEST

The objective of this test was to evaluate the performance capability of the actuation system operating at reduced power supply voltage levels. The actuation system will be operated at 2- and 4-Hz frequencies. After each repetition of the 2- and 4-Hz frequencies, the power supply voltage level will be reduced by 15 v. This will be repeated until the power supply voltage level is 90 vdc. The test brief is shown in Figure 63.

6.4 MOTOR/ACTUATOR DUTY CYCLE CAPABILITY TEST

The objective of this test is to establish a relationship between the electrical input power and the actuation unit output. The test involves gathering input and output data over a variety of duty cycles (see Figure 64). This data will be collected while operating at room ambient temperature.

TEST 2
EXTENDED CURRENT LIMIT

Prepared by: _____
Part No.: _____
Date: _____

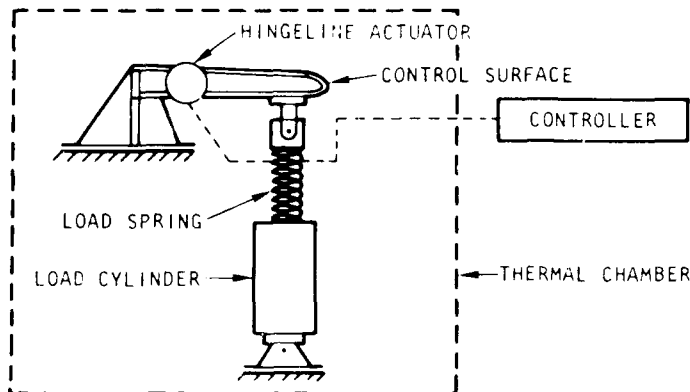
OBJECTIVE

TO EVALUATE FREQUENCY RESPONSE AS A FUNCTION OF CURRENT LIMIT.

FACILITY

ELECTROMECHANICAL
LABORATORY

SCHEMATIC



S 46619

**EQUIPMENT AND
INSTRUMENTATION**

- 1) THERMAL CHAMBER
- 2) LOAD SYSTEM
- 3) OSCILLOGRAPH
- 4) SIGNAL GENERATOR
- 5) POSITION INDICATOR
- 6) REACTION FIXTURE
- 7) ELECTRICAL INSTRUMENTATION

PROCEDURE

- 1) SUPERIMPOSE AN INPUT COMMAND RATE OF 0.5, 1, 2, 4, 6, 8, AND 10 HZ AT ± 1.0 DEG AMPLITUDE IN CONJUNCTION WITH 0 AND 10 PERCENT RATED LOAD.
- 2) REPEAT TEST FOR 10, 15, 20, 25, AND 30 AMP CURRENT LIMIT.

REQUIRED DATA

- 1) INPUT RATE
- 2) INPUT AMPLITUDE
- 3) OUTPUT POSITION
- 4) OUTPUT LOAD
- 5) MOTOR AND ACTUATOR TEMPERATURE

ACCEPT/REJECT CRITERIA

TEST DEMONSTRATION
ONLY

NOTES

- 1) ONE FREQUENCY RESPONSE TEST WILL BE CONDUCTED AT 30 AMP CURRENT LIMIT AND 250 F. ALL OTHER TESTS WILL BE RUN AT ROOM TEMPERATURE.
- 2) MONITOR MOTOR TEMPERATURE TO PREVENT OVERHEATING.

S-95237

Figure 62. Extended Current Limit Test

TEST
POWER SUPPLY VOLTAGE VARIATION

FIGURE NO. _____
DATE _____

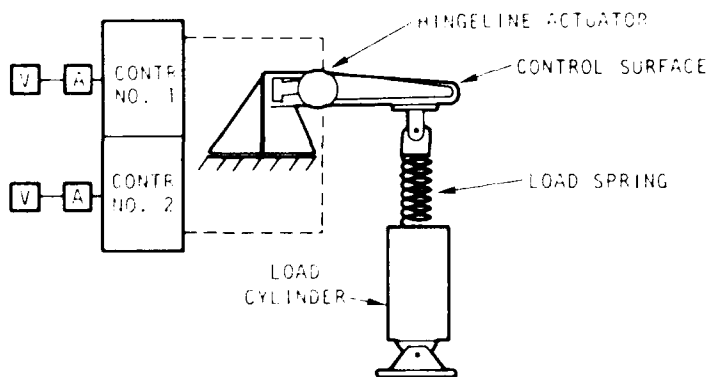
OBJECTIVE

TO DEMONSTRATE SYSTEM OPERATION FROM UNREGULATED POWER SOURCES

FACILITY

ELECTROMECHANICAL
LABORATORY

SCHEMATIC



**EQUIPMENT AND
INSTRUMENTATION**

- 1) LOAD SYSTEM
- 2) OSCILLOGRAPH
- 3) SIGNAL GENERATOR
- 4) POSITION INDICATOR
- 5) REACTION FIXTURE
- 6) ELECTRICAL INSTRUMENTATION

PROCEDURE

DRIVE ACTUATOR SYSTEM OVER PREDETERMINED DUTY CYCLE. AFTER EACH REPETITION OF THE DUTY CYCLE LOWER INPUT VOLTAGE 15 VDC. RECORD ACTUATOR OUTPUT. REPEAT PROCEDURE UNTIL THE ACTUATOR WILL NOT RESPOND TO INPUT COMMAND.

REQUIRED DATA

- | | |
|---------------------|-------------------|
| 1) INPUT AMPLITUDE | 4) OUTPUT LOAD |
| 2) TIME ELAPSED | 5) SUPPLY VOLTAGE |
| 3) OUTPUT AMPLITUDE | |

ACCEPT/REJECT CRITERIA

TEST DEMONSTRATION
ONLY

NOTES

- 1) TEST WILL BE PERFORMED AT LABORATORY AMBIENT TEMPERATURE

S-95257

Figure 63. Power Supply Voltage Variation Test

TEST 4
MOTOR/ACTUATOR DUTY
CYCLE CAPABILITY

Prepared by: _____
 Part No.: _____
 Date: _____

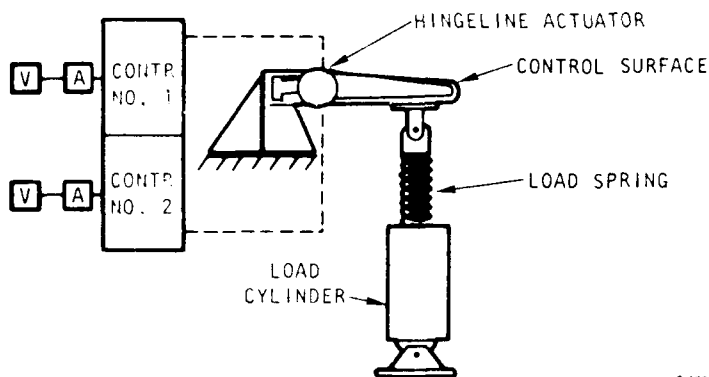
OBJECTIVE

TO DETERMINE A FIGURE OF MERIT FOR POWER UTILIZATION.

FACILITY

ELECTROMECHANICAL
 LABORATORY

SCHEMATIC



S 46621

**EQUIPMENT AND
 INSTRUMENTATION**

- 1) LOAD SYSTEM
- 2) OSCILLOGRAPH
- 3) SIGNAL GENERATOR
- 4) POSITION INDICATOR
- 5) REACTION FIXTURE
- 6) ELECTRICAL INSTRUMENTATION

PROCEDURE

- 1) DRIVE ACTUATOR SYSTEM OVER PREDETERMINED DUTY CYCLE. MEASURE INPUT POWER AND ALL OUTPUT CHARACTERISTICS.
- 2) DUTY CYCLES WILL BE DETERMINED FROM TASK 3-2.

REQUIRED DATA

- | | |
|---------------------------------|-------------------------------------------|
| 1) INPUT POWER (VOLTS AND AMPS) | 4) OUTPUT POSITION |
| 2) OUTPUT RATE | 5) OUTPUT LOAD |
| 3) ELAPSED TIME | 6) MOTOR AND ACTUATOR SURFACE TEMPERATURE |

ACCEPT/REJECT CRITERIA

TEST DEMONSTRATION
 ONLY

NOTES

ACTUATOR SYSTEM OPERATES AT ROOM TEMPERATURE.

S-95237

Figure 64. Motor/Actuator Duty Cycle Capability Test

7. TEST RESULTS

This section contains the results of tests performed on the electromechanical rotary hingeline actuator unit. The purpose of these tests was to further strengthen the evaluation data base of electromechanical actuation for aircraft primary flight control. Testing was conducted in accordance with the Air Force approved electromechanical actuation unit follow-on test plan, presented in AiResearch Report 78-15393, dated October 1, 1978. Detail test results are presented for each test previously described in Section 6.

7.1 FREQUENCY RESPONSE TEST

The results of frequency response testing at extended ambient temperatures are shown in Figures 65 through 68. In all of the frequency response plots, the input command signal was sinusoidal at a amplitude of ± 1 deg and the average current limit is 30 amp.

Figure 65 shows the actuator unit operating at full gain and compares the amplitude degradation and phase lag at -65°F , 72°F (room temperature), and $+250^{\circ}\text{F}$. There is very little variation in the amplitude degradation at these temperatures. However, the phase lag at the higher temperature is greater at higher frequencies. This result was expected because of the increased resistance in the wound stator as a function of temperature.

Figure 66 through 68 show the actuator performance when the gain in the controller is decreased by 50 percent for ambient temperatures of $+250^{\circ}\text{F}$, room temperature, and -65°F . Figure 66 is the no-load case; Figure 67 shows the 10 percent load case; and Figure 68 shows the 20 percent load response.

7.2 EXTENDED CURRENT LIMIT TEST

The results of the extended current limit test are shown on Figure 69. Figure 68 shows the actuator output response at various current limits to a ± 1 deg, sinusoidal input command signal at frequencies from 0.5 to 10 Hz.

This figure also shows the direct relationship between current limit and output performance. For a 67 percent decrease in current limit, the amplitude degradation at 10 Hz is increased by 49 percent. This relationship is the result of the decrease in torque available for acceleration of the load. In this case, the load is almost entirely the inertia of the motor rotor.

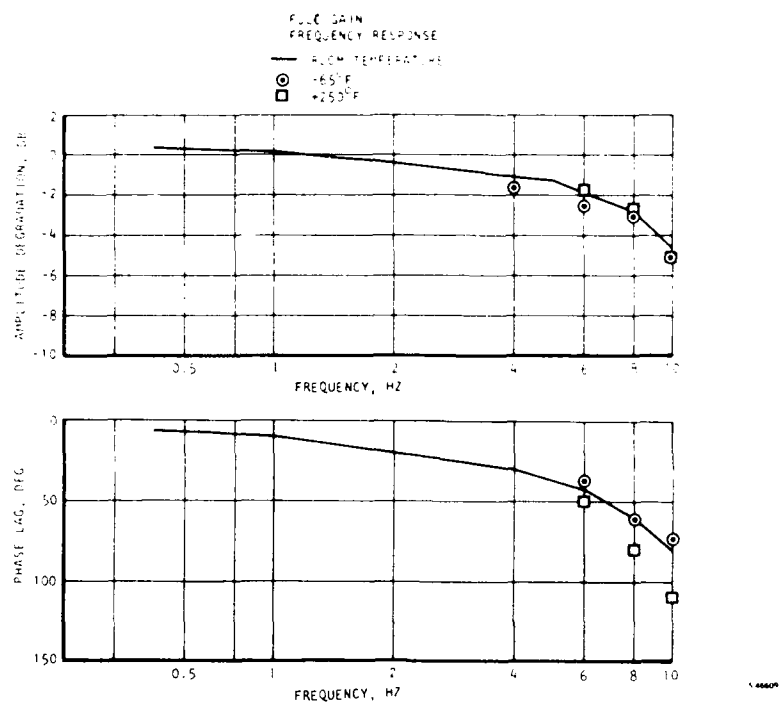


Figure 65. Frequency Response Temperature Comparison, Full Gain

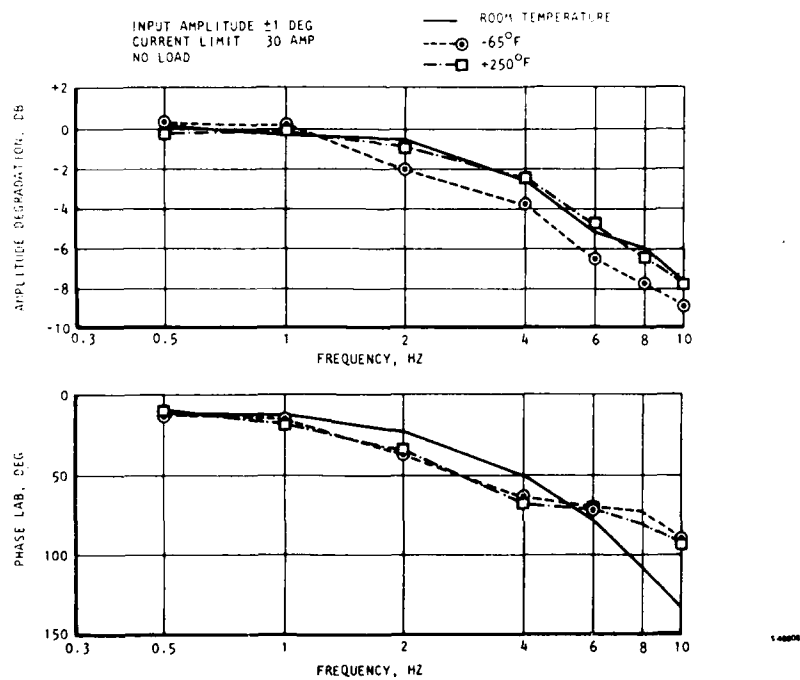


Figure 66. Frequency Response Temperature Comparison, Half Gain

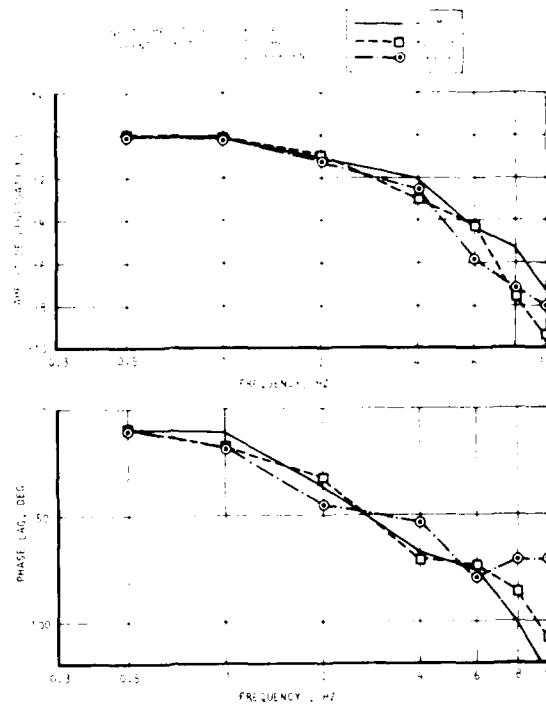


Figure 67. Frequency Response Temperature Comparison, Half Gain, 20 Percent Load

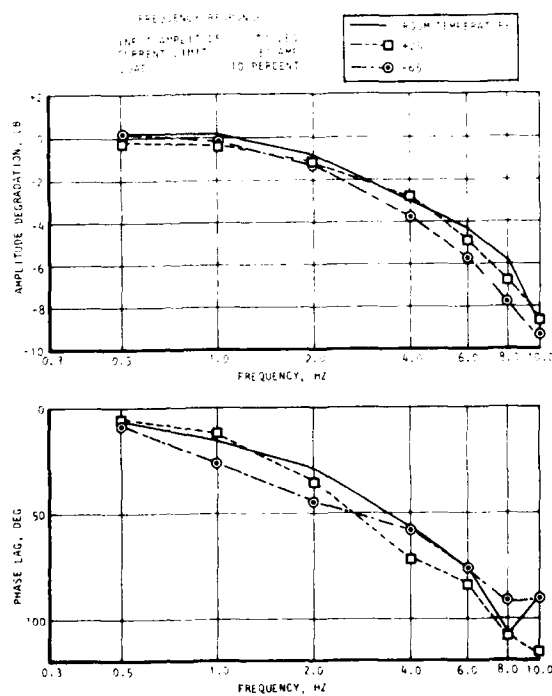


Figure 68. Frequency Response Temperature Comparison, Half Gain, 10 Percent Load

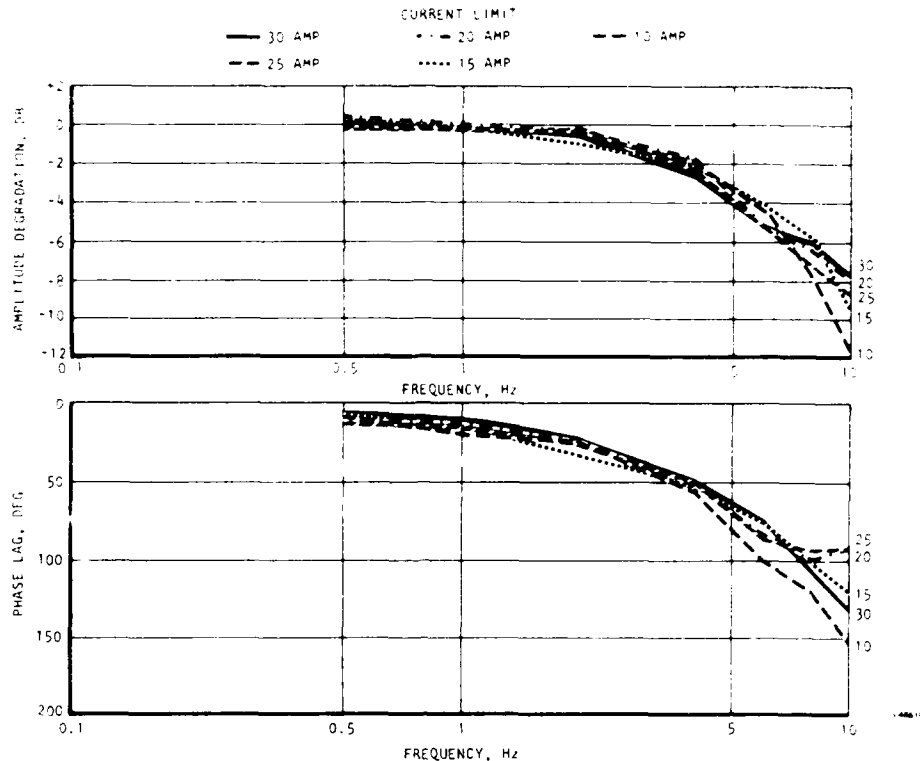


Figure 69. Frequency Response Current Limit Comparison, Half Gain, No Load

7.3 POWER SUPPLY VOLTAGE VARIATION TEST

This test demonstrated the system operation from an unregulated voltage source. The results of this test are presented in Tables 4 and 5. Table 4 summarizes the actuator response to a 2 Hz, ± 1 deg, sinusoidal input command signal. The voltage was varied from 285 vdc to 90 vdc in 15-v increments. All tests were conducted at room temperature.

Table 5 summarizes the actuator response to a 4 Hz, ± 1 deg, sinusoidal input command. The same voltage increments and ambient temperature were used.

The data of both tables show that the performance of the unit is not affected by small voltage variations at input frequencies of 4 Hz or less. This is because the controller switch duty cycle increases to provide the same average motor voltage even though the supply voltage is reduced. At the extreme low voltages when the switch duty cycle is 100 percent, the low supply voltage results in low motor speed and rate limiting occurs. For the majority of aircraft flight conditions where 2- to 4-Hz frequency response is adequate, it is clear that substantial voltage variations can be tolerated. The conclusion from this data is that the 270-vdc supply bus does not require close regulation. Indeed, direct utilization of power from engine driven generators may be entirely satisfactory and would result in major savings in power conditioning equipment weight.

TABLE 4

ACTUATOR RESPONSE SUMMARY FOR 2 Hz

Applied Input Voltage, v	Amplitude Degradation, db	Phase lag, deg
285	-.72	19.8
270	-.72	19.8
255	-.72	18
240	-.72	18
225	-.72	18
210	-.64	18
195	-.72	18
180	-.72	18
165	-.72	19.8
150	-.92	18.27
135	-.92	19.8
120	-.84	19.8
105	-.95	15.88
90	-.85	36.73

TABLE 5

ACTUATOR RESPONSE SUMMARY FOR 4 Hz

Applied Input Voltage, v	Amplitude Degradation, db	Phase lag, deg
285	-2.71	54.55
270	-2.73	54.00
255	-2.5	59.38
240	-2.80	50.40
225	-3.01	61.82
210	-2.74	61.20
195	-2.92	45.47
180	-3.14	54.68
165	-2.71	41.94
150	-3.14	47.27
135	-3.01	50.91
120	-3.30	54
105	-3.43	59.42
90	-3.70	68.40

7.4 THERMAL EVALUATION

The temperature of all nodes discussed in Section 5 was monitored during each test. The purpose of the temperature monitoring was to prevent overheating. A temperature profile of the motor winding (node 2) is shown in Figure 70. During this test, a constant load of 29 lb-in. was applied to the output of a motor. This load, when applied to the actuator output, is equivalent to 40 percent of the maximum design load (37,575 lb-in.) of the actuator. This data is compared with the predicted thermal results of Figure 71.

Temperature data gathered during high (+250°F) and low (-65°F) ambient temperatures are presented in Figure 72, Figure 73, and Table 6. Figure 72(a) and (b) shows the motor winding and motor brake coil temperature profiles during frequency response testing at +250°F ambient. Figure 73(a) and (b) shows the motor winding and motor brake coil temperature profiles during frequency response testing at -65°F ambient. This data is further supported by the temperatures given in Table 6, which presents temperatures that were recorded during the respective frequency response tests shown in Figure 72(a) and (b) and Figure 73(a) and (b). These temperatures were recorded when the highest temperatures of the windings were recorded.

Correlation between the thermal data and the thermal model results are good. These tests have confirmed the capability of electromechanical actuation performance at ambient temperatures between -65°F and +250°F.

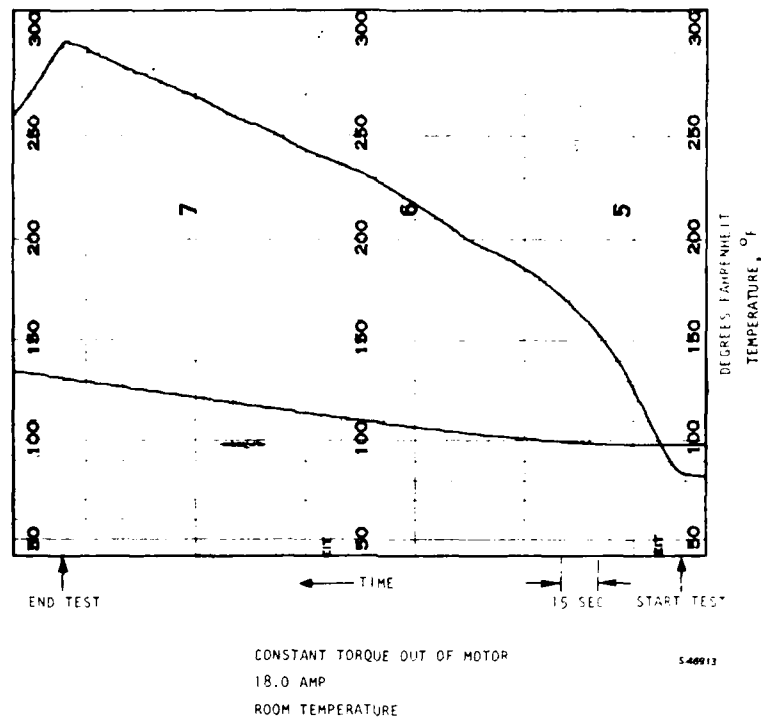


Figure 70. Temperature Profile Motor Hot Spot
TEST DATA (NO GEARBOX) AT 18 AMP

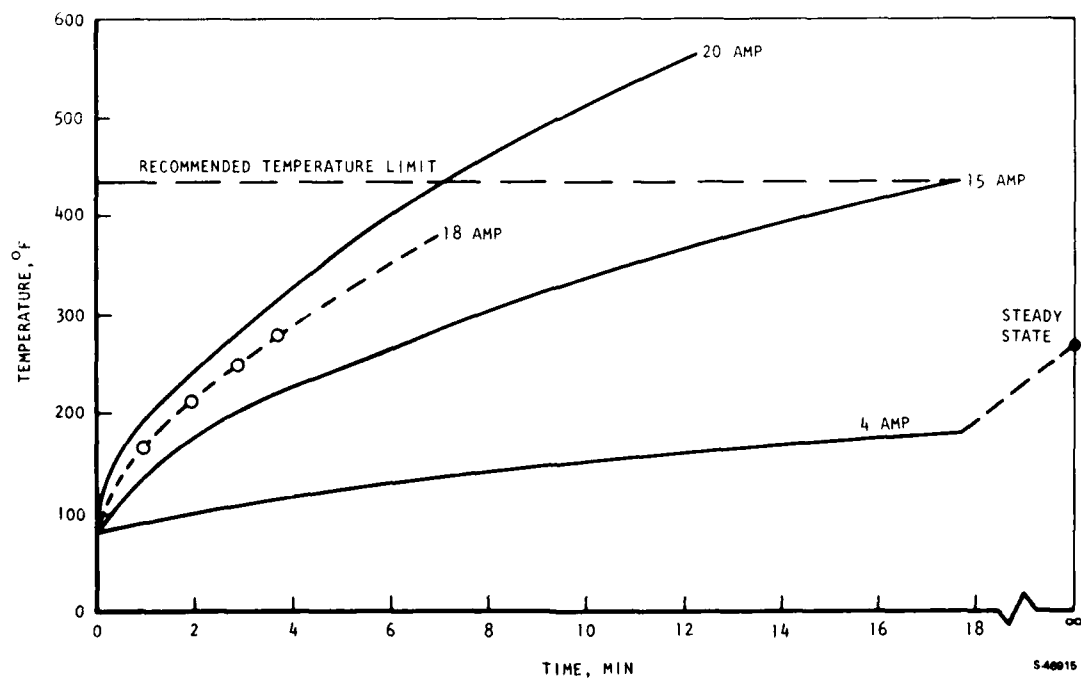
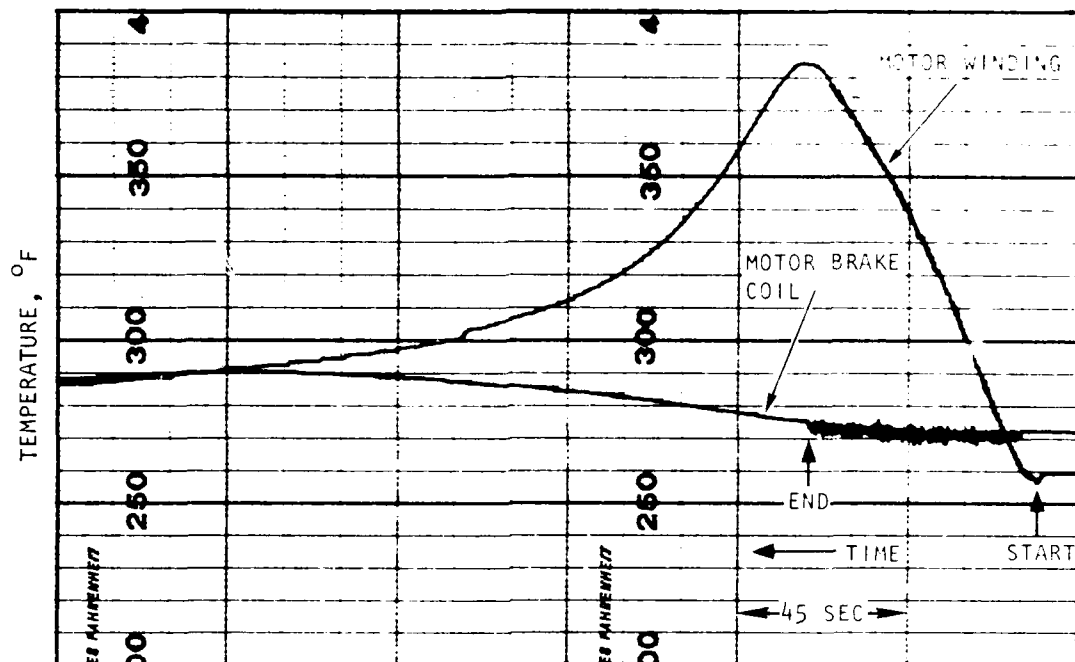
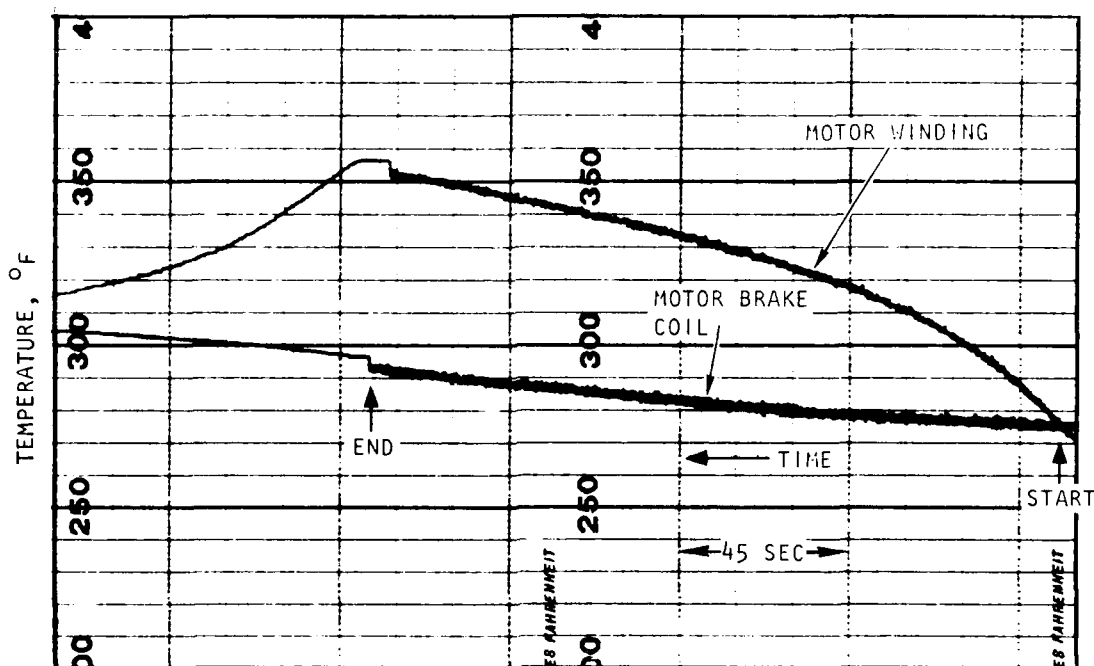


Figure 71. Data Comparison Between Predicted Hot Spot Motor Winding
Temperatures and Hingeline Actuator Motor Winding Temperatures



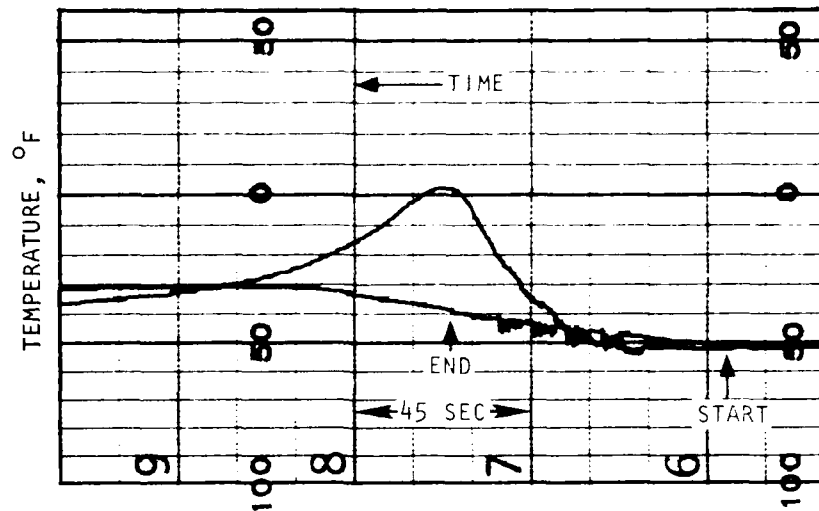
(a) TEMPERATURE PROFILE DURING 8 HZ, FULL-GAIN FREQUENCY RESPONSE TEST



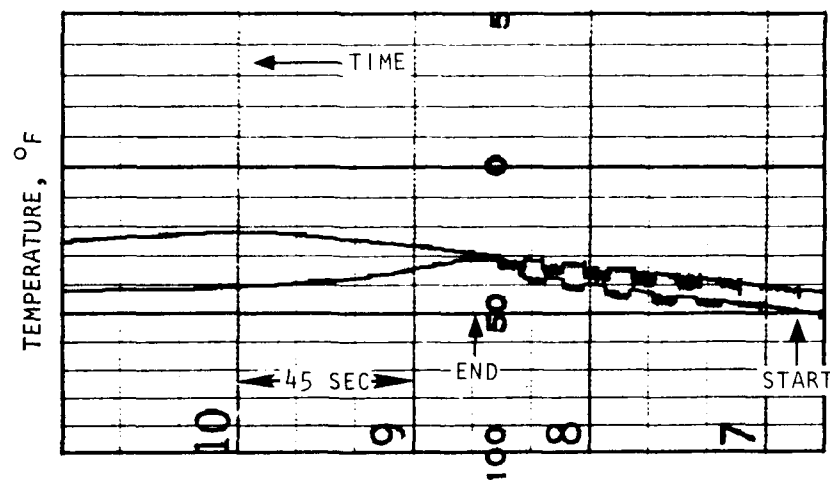
(b) TEMPERATURE PROFILE DURING 8 HZ, HALF-GAIN FREQUENCY RESPONSE TEST

S46911

Figure 72. Motor Winding and Motor Brake Coil Temperature Profile, 250°F Ambient



(a) TEMPERATURE PROFILE DURING 4 TO 10 HZ,
FULL-GAIN FREQUENCY RESPONSE TEST



(b) TEMPERATURE PROFILE DURING 0 TO 10 HZ,
HALF-GAIN FREQUENCY RESPONSE TEST

S 46912

Figure 73. Motor Winding and Motor Brake Coil
Temperature Profile, -65°F Ambient

TABLE 6
LOCAL TEMPERATURE PROFILES

Node	Temperature 250°F Ambient (See Figure 7-8a)	Temperature 250°F Ambient (See Figure 7-8b)	Temperature -65°F Ambient (See Figure 7-9a)	Temperature -65°F Ambient (See Figure 7-9b)
1	365	321	-13	-38
2	396	312	-23	-30
3	373	317	-16	-40
4	386	308	-26	-40
5	---	---	-42	-50
6	292	307	-44	-50
7	302	306	-41	-50
8	282	295	-45	-51
9	269	284	-48	-52
10	272	284	-56	-58
11	250	260	-57	-58
12	253	265	-38	-41
13	235	238	-52	-55
14	236	236	-51	-53
15	235	240	-52	-54
16	254	259	-62	-66

8. CONCLUSIONS AND RECOMMENDATIONS

AiResearch Manufacturing Company of California, under contract from WPAFB, has completed a development and testing effort that further substantiates the adaptability of electromechanical actuation to satisfy the requirement of aircraft primary flight controls.

- (a) An average current of 30 amps at 270 vdc can be controlled using transistor technology in a power servo application. Using a minor control loop with integration, the average current level is maintained nearly ripple free.
- (b) The power transistors (Westinghouse D60T) are used in a six transistor bridge circuit. The configuration provides the minimum number of solid-state switching devices required for (1) commutation of power (including reversing and regeneration) to the windings of the brushless dc, permanent magnet rotor motor, and (2) speed and torque control.
- (c) The technology of field effect transistors (FET's) is progressing rapidly into the area of high power capability. In the future, if the power capability of FET's continues to increase, they may offer significant advantages over the existing bi-polar transistors in terms of higher switching speed and lower internal losses.
- (d) The existing motor rotor position sensors could be improved, and possibly eliminated. The advantage of eliminating motor rotor position sensors (simpler motor) should be carefully considered in terms of controller complexity to implement commutation. Commutation concepts which employ use of programmed startup, and sensing of back EMF, have been studied and demonstrated by others for normal motor operation. Adopting this concept of commutation control to a fast response servo motor should be investigated.
- (e) The breadboard controller developed is not a fully redundant, two-channel configuration. Additional effort is required to provide total separation of the two servo channels. Since the actuator velocity sums the output of the two motors, cross-channel monitoring and control may be required to assure synchronization of the two independent motor drive circuits.
- (f) The technique of force summing of redundant drives should be considered instead of the velocity summing approach used in the existing design. Mechanical design studies should also include evaluation of mechanical stops to limit actuator rotation.

Additional studies of the actuator mechanical design should include the following:

- (1) The motor brakes in the present hardware are used to implement redundancy after a failure; i.e., they are passive elements in the system dynamics. An alternate design should explore the possibility of using the motor brakes as static load holding devices. This approach could significantly increase the steady-state load holding capability of the actuator by reducing the steady-state current applied to the motor.
 - (2) The study should include the feasibility of a variable gear ratio drive. The requirements for primary flight control surfaces include a high frequency response and a large steady-state load hold capability. These individual requirements are easily satisfied, but a satisfactory combination of a reliable, variable gear ratio would be a major breakthrough for electro-mechanical actuation for aircraft primary flight controls.
- (g) The final report (AFFDL-TR-78-150) evaluates and predicts the performance of the actuation system using a tachometer feedback servo configuration, which would be required for control surfaces with high inertia. This effort would require motor and controller modifications and construction of a new test fixture. The new test fixture would have an inertia similar to that of a primary flight control surface.
- (h) Lastly, but of major importance, is to update the actuation unit model to include representations of the most recent circuit improvements, and to expand the model to include the redundancy characteristics of the two-channel actuator. The modeling effort is also required to fully understand the dynamics of the velocity summed motor input and to stabilize the control surface position loop at the gain required to satisfy the frequency response requirements.

AD-A085 847

AIRESEARCH MFG CO OF CALIFORNIA TORRANCE
ELECTROMECHANICAL ACTUATION DEVELOPMENT.(U)
FEB 80 R A LEVIE, J GRAY, N E WOOD
88-16763

F/O 1/4

F33615-76-C-3043

UNCLASSIFIED

AFMIL-TR-88-3024

ML

2 of 2

AD
COMPLIST



END

DATE

FILED

8-80

DTIC

9. REFERENCES

1. Electromechanical Actuation Development, AiResearch Manufacturing Company, Report 78-15067, Air Force Contract F33615-76-C-3043, Report AFFDL-TR-78-150.
2. Electromechanical Actuation Feasibility Study, AiResearch Manufacturing Company, Report 75-12153, Air Force Contract F33615-75-C-3055, Report AFFDL-TR-76-42.
3. Bird, Daniel, "Electromechanical Flight Control Actuation Update," SAE Paper 780582 presented at SAE Committee A-6 Technical Symposium, Cherry Hill, New Jersey, April 12, 1978.
4. Bird, Daniel, "Electromechanical Flight Control Actuation," SAE Paper 771004, presented at SAE Aerospace Meeting, Los Angeles, California, Nov. 17, 1977.
5. Johnson, Tom, "Primary Flight Control Actuation with Electric Motors," Proceedings of the IEEE 1977 National Aerospace and Electronics Conference (NAECON), Dayton, Ohio, May 1977.
6. Helsey, C. W., Jr., "Power-By-Wire for Aircraft - The All-Electric Airplane," SAE Paper 771006, presented at SAE Aerospace Meeting, Los Angeles, California, Nov. 17, 1977.
7. Fitzgerald, A. E. and Charles Kingsley, Electric Machinery, 1952.
8. Sawyer, B., and J. T. Edge, "Design of Samarium Cobalt Brushless DC Motor for Electromechanical Actuator Applications," Proceedings of the IEEE 1977 National Aerospace and Electronics Conference (NAECON), Dayton, Ohio, May 1977.
9. Wood, Neal E., "Advances in Primary Flight Control Actuation Using Electromechanical Technology," Proceedings of the IEEE 1977 National Aerospace Conference (NAECON), Dayton, Ohio, May 1977.
10. Herdeg, D. F., H. W. Proctor, W. B. Spring, and G. C. Newton, Jr., Electromagnetic Harmonic Drive Low Inertia Servo Actuator, ASD-TDR-63-466 Contract AF33(567)-7731, United Shoe Machinery Corp., Beverly Mass., December 1963.
11. Parker, R. J., "Rare Earth Permanent Magnets and Energy Conversion Processes," Proceedings of the IEEE 1977 National Aerospace and Electronics Conference (NAECON), Dayton, Ohio, May 1977.

12. Brown, J. M., "Rare Earth Magnets - A New Trend in Dc Motors", Control Engineering, October 1975.
13. Parker, Rolling J. and Robert J. Strudders, Permanent Magnets and Their Application, 1962.
14. Sawyer, Bert, Barrett, A., et.al, Electromechanical Flight Control Actuator, Final Report, NASA Contract NAS9-14952, January 1978.
15. Electromechanical Flight Control Actuator, Delco Electronics, NASA Contract NAS 9-14331.
16. Brown, James, "Rare Earth Magnets - a New Trend in D.C. Motors," Control Engineering, October 1975.
17. Voight, A. A., "Electrical Flight Control Systems - Applicable Now," Proceedings of the IEEE 1977 National Aerospace and Electronics Conference (NAECON), Dayton, Ohio, May 1977.
18. Inagaki, J., Juniyoshi, M., and S. Tadakuma, "Commutators Get The Brushoff," IEEE Spectrum, June 1973, pp 52 to 58.
19. "Machine Design," Electrical and Electronics 1978 Reference Issue, Vol. 50.
20. Grau, Richard, Feasibility Investigation for Advanced Flight Control Actuation Systems; All Electric Concepts (AFCAS AE), McDonnell Douglas Electronics Company, NADC Report 76160-30.

APPENDIX

ACTUATOR DUTY CYCLE
EVALUATION ALGORITHMS

DATE 11-2-79

CALC. NO. _____ SHEET NO. 1-19

PART NO. _____

MODEL NO. _____

PREPARED BY S. ROWE

CHECKED BY _____

ACTUATOR DUTY CYCLE EVALUATION ALGORITHMS

THE PURPOSE OF THIS STUDY IS TO DETERMINE ALGORITHMS SUITABLE FOR THE EVALUATION OF ACTUATOR DUTY CYCLES. THE CURRENT REQUIRED BY AN ELECTROMECHANICAL ACTUATOR OPERATING AGAINST A LOAD IS THE PRINCIPAL RESULT.

THE FOLLOWING DERIVATIONS ARE GIVEN:

1. ACTUATOR MODEL
2. LOAD MODEL
3. EFFECTIVE INERTIAS
4. DUTY CYCLE DEFINITION
5. ACTUATOR TORQUE, MOTOR TORQUE, AND MOTOR CURRENT DEMAND

DATE 11-2-79

PART NO. _____

PREPARED BY S. LOWE

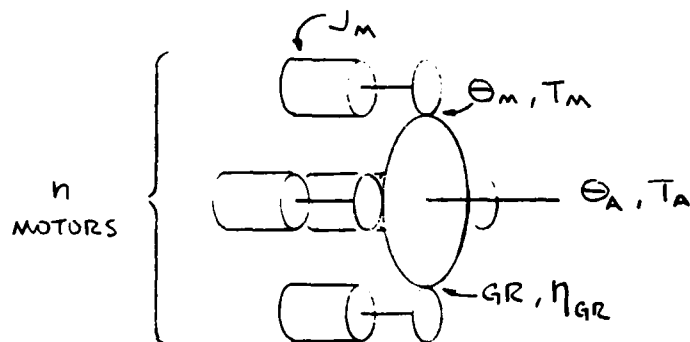
CALC. NO. _____ SHEET NO. 2-15

MODEL NO. _____

CHECKED BY _____

1.0 ACTUATOR MODEL

ASSUME THE FOLLOWING ROTORY ACTUATOR MODEL :



WHERE

θ_m	\triangleq	MOTOR POSITION
θ_A	\triangleq	ACTUATOR POSITION
T_m	\triangleq	MOTOR TORQUE
T_A	\triangleq	ACTUATOR TORQUE
J_m	\triangleq	MOTOR INERTIA
n	\triangleq	NUMBER OF MOTORS
G_R	\triangleq	GEAR RATIO
η_{GR}	\triangleq	DRIVE EFFICIENCY

DATE 11-2-79CALC. NO. _____ SHEET NO. 3-19

PART NO. _____

MODEL NO. _____

PREPARED BY S. ROWE

CHECKED BY _____

SUMMING TORQUES THROUGH THE ACTUATOR YIELDS :

$$n T_M = n J_M \ddot{\Theta}_M + \frac{1}{GR \eta_{GR}} T_A$$

THIS MAY BE ARRANGED TO ONE OF THE FOLLOWING .

$$T_M = J_M \ddot{\Theta}_M + \frac{1}{GR \eta_{GR} n} T_A \quad (1-1)$$

$$T_M = \frac{J_M}{GR} \ddot{\Theta}_A + \frac{1}{GR \eta_{GR} n} T_A \quad (1-2)$$

$$T_A = GR \eta_{GR} n T_M - J_M GR \eta_{GR} n \ddot{\Theta}_M \quad (1-3)$$

$$T_A = GR \eta_{GR} n T_M - J_M GR \eta_{GR} n \ddot{\Theta}_A \quad (1-4)$$

THESE EQUATIONS HOLD FOR THE CASE OF THE ACTUATOR DRIVING THE LOAD .

IF THE ACTUATOR IS BACKDRIVEN ,

DATE 11-2-79CALC. NO. _____ SHEET NO. 4-19

PART NO. _____

MODEL NO. _____

PREPARED BY S. ROWE

CHECKED BY _____

$$T_A = \frac{GR}{\eta'_{GR}} (nJ_M \ddot{\Theta}_M + nT_M)$$

WHERE

$$\eta'_{GR} \triangleq \text{DRIVE BACKDRIVE EFFICIENCY}$$

THIS WILL YIELD:

$$T_M = \frac{\eta'_{GR}}{GRn} T_A - J_M \ddot{\Theta}_M \quad (1-5)$$

$$T_M = \frac{\eta'_{GR}}{GRn} T_A - J_M GR \ddot{\Theta}_A \quad (1-6)$$

$$T_A = \frac{J_M GRn}{\eta'_{GR}} \ddot{\Theta}_M + \frac{GRn}{\eta'_{GR}} T_M \quad (1-7)$$

$$T_A = \frac{J_M GR^2 n}{\eta'_{GR}} \ddot{\Theta}_A + \frac{GRn}{\eta'_{GR}} T_M \quad (1-8)$$

THESE EQUATIONS HOLD FOR THE CASE OF
THE LOAD DRIVING THE ACTUATOR.

DATE 11-2-79

PART NO. _____

PREPARED BY S. ROWE

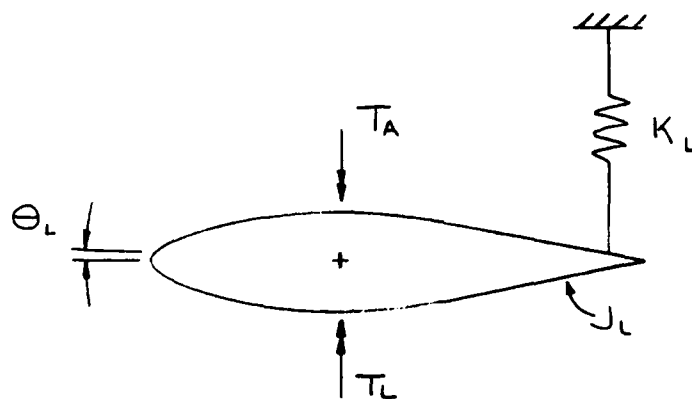
CALC. NO. _____ SHEET NO. 5-19

MODEL NO. _____

CHECKED BY _____

2.0 LOAD MODEL

ASSUME THE FOLLOWING LOAD MODEL:



WHERE

θ_L	\triangleq	LOAD POSITION
T_A	\triangleq	ACTUATOR TORQUE
T_L	\triangleq	LOAD TORQUE
J_L	\triangleq	LOAD INERTIA
K_L	\triangleq	LOAD SPRING RATE

SUMMING TORQUES THROUGH THE LOAD YIELDS:

$$T_A = T_L + K_L \theta_L + J_L \ddot{\theta}_L$$

(2-1)

DATE 11-2-79CALC. NO. _____ SHEET NO. 6-19

PART NO. _____

MODEL NO. _____

PREPARED BY _____

CHECKED BY _____

3.0 EFFECTIVE INERTIAS

CALCULATE AN EFFECTIVE INERTIA FOR THE CASE OF THE ACTUATOR OF SEC. 1.0 COUPLED TO THE LOAD OF SEC. 2.0.

3.1 ACTUATOR DRIVING LOAD

COMBINE (1-4) AND (2-1):

$$GR\eta_{GR}nT_M - J_M GR^2\eta_{GR}n\ddot{\Theta}_A = T_L + K_L\Theta_L + J_L\ddot{\Theta}_L$$

SINCE THE ACTUATOR IS COUPLED DIRECTLY TO THE LOAD:

$$\Theta_A = \Theta_L$$

AND

$$GR\eta_{GR}nT_M - J_M GR^2\eta_{GR}n\ddot{\Theta}_A = T_L + K_L\Theta_A + J_L\ddot{\Theta}_A$$

COLLECTING ALL INERTIA TERMS AND REARRANGING:

DATE 11-2-79CALC. NO. _____ SHEET NO. 7-19

PART NO. _____

MODEL NO. _____

PREPARED BY S. ROWE

CHECKED BY _____

$$\begin{aligned}
 T_M &= \frac{1}{GR\eta_{GR}n} \left[T_L + K_L \Theta_A + (J_L + J_M GR^2 \eta_{GR} n) \ddot{\Theta}_A \right] \\
 &= \frac{1}{GR\eta_{GR}n} T_L + \frac{K_L}{GR\eta_{GR}n} \Theta_A \\
 &\quad + \left(\frac{J_L}{GR\eta_{GR}n} + J_M GR \right) \ddot{\Theta}_A
 \end{aligned}$$

THUS, THE SYSTEM INERTIA REFLECTED TO THE MOTOR MAY BE WRITTEN AS:

$$J_{SM} = \left(J_L \frac{1}{GR^2 \eta_{GR} n} + J_M \right) GR \quad (3-1)$$

$$J_{SM} = J_L \frac{1}{GR\eta_{GR}n} + J_M GR \quad (3-2)$$

WHERE

$J_{SM} \triangleq$ EFFECTIVE SYSTEM INERTIA @ MOTOR

THIS PARAMETER IS VALID FOR THE CASE OF THE ACTUATOR DRIVING THE LOAD.

3.2 LOAD DRIVING ACTUATOR

COMBINE (1-8) AND (2-1) :

$$\frac{J_m GR^2 \eta}{\eta'_{GR}} \ddot{\Theta}_A + \frac{GR\eta}{\eta'_{GR}} T_m = T_L + K_L \Theta_L + J_L \ddot{\Theta}_L$$

SINCE THE ACTUATOR IS COUPLED DIRECTLY TO THE LOAD:

$$\Theta_A = \Theta_L$$

AND

$$\frac{J_m GR^2 \eta}{\eta'_{GR}} \ddot{\Theta}_A + \frac{GR\eta}{\eta'_{GR}} T_m = T_L + K_L \Theta_A + J_L \ddot{\Theta}_A$$

COLLECTING ALL INERTIA TERMS AND REARRANGING:

$$T_L = \frac{GR\eta}{\eta'_{GR}} T_m - K_L \Theta_A + \left(\frac{J_m GR^2 \eta}{\eta'_{GR}} - J_L \right) \ddot{\Theta}_A$$

THUS, THE SYSTEM INERTIA REFLECTED TO THE LOAD MAY BE WRITTEN AS:

DATE 11-2-79CALC. NO. _____ SHEET NO. 9-19

PART NO. _____

MODEL NO. _____

PREPARED BY _____

CHECKED BY _____

$$J_{SL} = \left(J_M \frac{GR\eta}{\eta'_{GR}} - J_L \frac{1}{GR} \right) GR \quad (3-3)$$

$$J_{SL} = J_M \frac{GR^2\eta}{\eta'_{GR}} - J_L \quad (3-4)$$

WHERE

 $J_{SL} \triangleq$ EFFECTIVE SYSTEM INERTIA (LOAD)

THIS PARAMETER IS VALID FOR THE CASE OF THE LOAD DRIVING THE ACTUATOR.

NOTE THAT J_{SL} INCREASES AS J_L DECREASES THIS OCCURS SINCE THE TORQUE

$$J_L \ddot{\theta}_A$$

IS AIDING IN BACKDRIVING THE ACTUATOR. THUS, REDUCING J_L REDUCES THE BACKDRIVE TORQUE, EFFECTIVELY INCREASING SYSTEM INERTIA. ALTERNATELY, INCREASING J_L DECREASES J_{SL} .

DATE 11-2-79

PART NO. _____

PREPARED BY S. ROWE

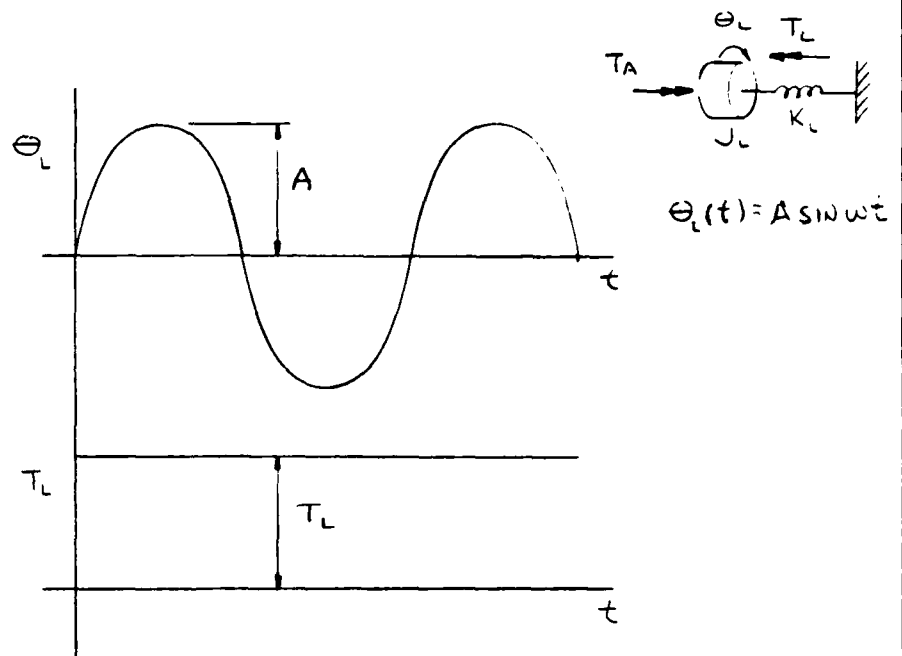
CALC. NO. _____ SHEET NO. 10-19

MODEL NO. _____

CHECKED BY _____

4.0 DUTY CYCLE DEFINITION

ASSUME THE FOLLOWING DUTY CYCLE :



SINCE THE ACTUATOR IS DRIVING THE LOAD MODEL :

$$\theta_L = \theta_A = A \sin \omega t$$

$$\ddot{\theta}_L = \ddot{\theta}_A = -A\omega^2 \sin \omega t$$

INSERTING VALUES INTO (2-1) :

DATE 11-3-79CALC. NO. _____ SHEET NO. 11-19

PART NO. _____

MODEL NO. _____

PREPARED BY S. ROWE

CHECKED BY _____

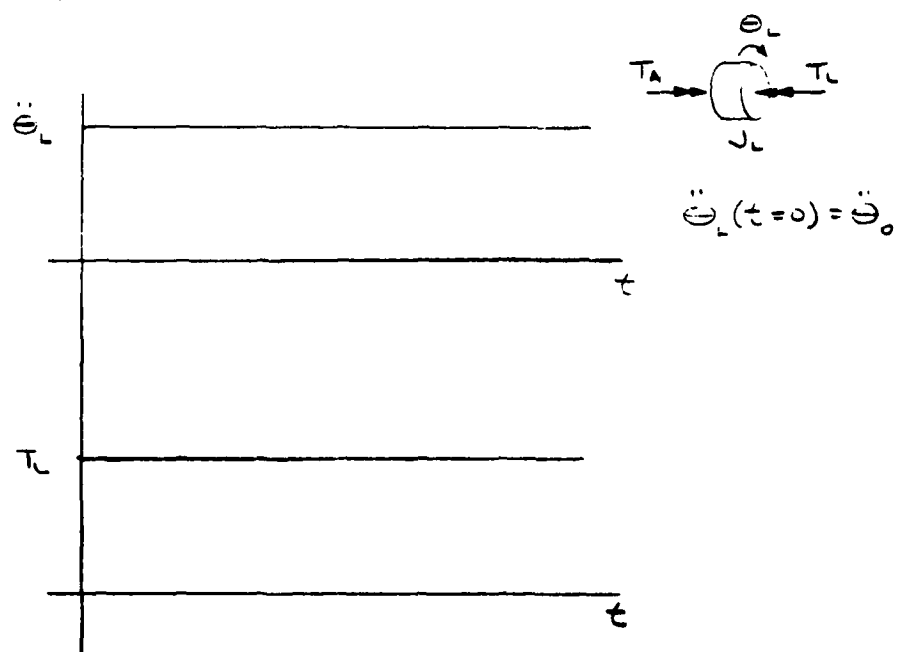
$$T_A = T_L + K_L A \sin \omega t - J_L A \omega^2 \sin \omega t$$

OR

$$T_A = T_L + [K_L - J_L \omega^2] A \sin \omega t \quad (4-1)$$

THIS EQUATION IS THE TORQUE REACTED BY THE ACTUATOR, WHEN THE ACTUATOR IS DRIVING THE LOAD AT THE DEFINED FREQUENCY AND AMPLITUDE.

FOR THE CASE OF THE LOAD BACKDRIVING THE ACTUATOR, ASSUME THE FOLLOWING:



DATE 11-3-79CALC. NO. _____ SHEET NO. 12-19

PART NO. _____

MODEL NO. _____

PREPARED BY S. ROWE

CHECKED BY _____

THUS, ACCELERATION AT THE LOAD IS CONSTANT.
THIS ALSO ASSUMES THAT THE LOAD AND ACTUATOR TORQUES
ARE CONSTANT, AND THAT THE SPRING LOAD
OF THE LOAD MODEL IS ZERO:

$$\ddot{\theta}_L = \ddot{\theta}_A$$

$$K_L = 0$$

INSERTING INTO (2-1):

$$T_A = T_L + J_L \ddot{\theta}_A \quad (4-2)$$

OR

$$\ddot{\theta}_A = \frac{1}{J_L} (T_A - T_L) \quad (4-3)$$

SO THE TORQUE TRANSMITTED TO THE ACTUATOR
IS A FUNCTION OF THE APPLIED AND INERTIAL LOADS.

EQUATIONS (4-2) AND (4-3) ARE VALID FOR THE
CASE OF THE LOAD (APPLIED TORQUE AND INERTIAL
LOAD) BACKDRIVING THE ACTUATOR (MOTOR
TORQUES AND INERTIAS).

DATE 11-3-79CALC. NO. _____ SHEET NO. 13-19

PART NO. _____

MODEL NO. _____

PREPARED BY S. ROWE

CHECKED BY _____

5.0 ACTUATOR TORQUE, MOTOR TORQUE, AND MOTOR CURRENT DEMAND

CALCULATE ACTUATOR TORQUE, MOTOR TORQUE AND MOTOR CURRENT FOR THE TWO DUTY CYCLE CASES OF SEC. 4.0.

ASSUME THAT MOTOR TORQUE IS PROPORTIONAL TO MOTOR CURRENT:

$$T_M = K_T i_M$$

WHERE

$$T_M \triangleq \text{MOTOR TORQUE}$$

$$i_M \triangleq \text{MOTOR CURRENT}$$

$$K_T \triangleq \text{MOTOR TORQUE CONSTANT}$$

FOR THE CASE OF THE ACTUATOR DRIVING THE LOAD (FIRST DUTY CYCLE CASE), EQUATE (1-4) AND (4-1):

$$GR\eta_{GR}nT_M - J_m GR^2\eta_{GR}n\ddot{\Theta}_A = T_L + [K_L - J_L\omega^2]A\sin\omega t$$

BY DEFINITION OF THE DUTY CYCLE IN SEC. 4.0:

$$\ddot{\Theta}_A = -A\omega^2\sin\omega t$$

DATE 11-3-79

PART NO. _____

PREPARED BY S. ROWECALC. NO. _____ SHEET NO. 14-19

MODEL NO. _____

CHECKED BY _____

So

$$GR\eta_{GR}nT_m - J_m GR^2\eta_{GR}n(-A\omega^2\sin\omega t) = T_L + [K_L - J_L\omega^2]A\sin\omega t$$

$$T_m = \frac{1}{GR\eta_{GR}n} \left\{ \begin{array}{l} T_L + [K_L - J_L\omega^2]A\sin\omega t \\ - J_m GR^2\eta_{GR}n A\omega^2\sin\omega t \end{array} \right\}$$

$$= \left\{ \begin{array}{l} \frac{1}{GR\eta_{GR}n} T_L + \frac{AK_L}{GR\eta_{GR}n} \sin\omega t \\ - \left(\frac{J_L}{GR\eta_{GR}n} + GRJ_m \right) A\omega^2 \sin\omega t \end{array} \right\}$$

Using (3-2):

$$T_m = \frac{1}{GR\eta_{GR}n} T_L + \left(\frac{K_L}{GR\eta_{GR}n} - J_m\omega^2 \right) A\sin\omega t \quad (5-1)$$

THEN

$$T_A = GR\eta_{GR}n T_m \quad (5-2)$$

DATE 11-3-79CALC. NO. _____ SHEET NO. 15-19

PART NO. _____

MODEL NO. _____

PREPARED BY S. ROWE

CHECKED BY _____

$$\omega_m = \frac{1}{K_T} T_m \quad (5-3)$$

FOR RMS VALUES OF T_m AND i_m

$$T_m|_{RMS} = \frac{1}{GR\eta_{GR}} + 0.707 \left(\frac{K_L}{GR\eta_{GR}} - J_{sm}\omega^2 \right) A \quad (5-4)$$

$$i_m|_{RMS} = \frac{1}{K_T} T_m|_{RMS} \quad (5-5)$$

FOR THE CASE OF THE LOAD DRIVING THE ACTUATOR
(SECOND DUTY CYCLE CASE), EQUATE (1-8) AND
(4-2):

$$\frac{J_m GR^2 \eta}{\eta'_{GR}} \ddot{\Theta}_A + \frac{GR\eta}{\eta'_{GR}} T_m = T_L + J_L \ddot{\Theta}_A$$

So

$$\ddot{\Theta}_A = \left(\frac{1}{\frac{J_m GR^2 \eta}{\eta'_{GR}} - J_L} \right) \left(T_L - \frac{GR\eta}{\eta'_{GR}} T_m \right)$$

DATE 11-3-79CALC. NO. _____ SHEET NO. 16-19

PART NO. _____

MODEL NO. _____

PREPARED BY C. ROWE

CHECKED BY _____

USING (3-4)

$$\ddot{\Theta}_A = \frac{1}{J_{SL}} \left(T_L - \frac{G R n}{\eta'_{GR}} T_M \right) \quad (5-6)$$

SINCE THE MOTOR WILL BE AT CURRENT LIMIT,

$$T_M = K_T \dot{I}_M \Big|_{\text{LIMIT}} \quad (5-7)$$

FROM (4-2)

$$T_A = T_L + J_L \ddot{\Theta}_A \quad (5-8)$$

SINCE THE TORQUES ARE CONSTANT, THESE EQUATIONS REPRESENT A STEADY-STATE CONDITION. NOTE THAT FOR

$$\ddot{\Theta}_A < 0$$

THE UNIT IS NOT BEING BACKDRIVEN. RATHER IT WOULD BE AT STALL OR DRIVING NORMALLY, IN WHICH CASE THESE EQUATIONS WOULD NO LONGER BE VALID.

DATE 11-3-79

CALC. NO. _____ SHEET NO. 17-19

PART NO. _____

MODEL NO. _____

PREPARED BY S. ROWE

CHECKED BY _____

EQUATIONS FOR SECTION 5.0 ARE SUMMARIZED
IN TABLE 5-1.

DATE 11-3-79
 PART NO. _____
 PREPARED BY C. ROWE

CALC. NO. _____ SHEET NO. 18-19
 MODEL NO. _____
 CHECKED BY _____

TABLE S-1
SUMMARY OF ACTUATOR TORQUE, MOTOR TORQUE, AND MOTOR
CURRENT EQUATIONS

ACTUATOR DRIVING LOAD:

$$T_m(t) = \frac{1}{GR\eta_{gr}n} T_L + \left(\frac{K_L}{GR\eta_{gr}n} - J_{sm}\omega^2 \right) A \sin \omega t$$

$$i_m(t) = \frac{1}{K_T} T_m(t)$$

$$T_m|_{rms} = \frac{1}{GR\eta_{gr}n} T_L + 0.707 \left(\frac{K_L}{GR\eta_{gr}n} - J_{sm}\omega^2 \right) A$$

$$i_m|_{rms} = \frac{1}{K_T} T_m|_{rms}$$

$$T_A(t) = GR\eta_{gr}n T_m(t)$$

$$J_{sm} = J_L \frac{1}{GR\eta_{gr}n} + J_m GR$$

DATE 11-3-70CALC. NO. _____ SHEET NO. 15

PART NO. _____

MODEL NO. _____

PREPARED BY S. P. JE

CHECKED BY _____

TABLE 5-1
(CONTINUED)

LOAD DRIVING ACTUATOR (NO SPRING LOAD):

$$\ddot{\Theta}_A = \frac{1}{J_{SL}} \left(T_L - \frac{GR^n}{\eta_{GR}} T_M \right) \quad (F_{SD} \quad \ddot{\Theta}_A \geq 0)$$

$$T_M = K_T \dot{\omega}_M \Big|_{LIMIT}$$

$$T_A = T_L + J_L \ddot{\Theta}_A$$

$$J_{SL} = J_M \frac{GR^{2n}}{\eta_{GR}} - J_L$$